

Chair of Hydrology  
Department of Micrometeorology  
University of Bayreuth, Germany

# Integral Turbulence Characteristics and Their Parameterisations

Diploma thesis  
in micrometeorology

by Christoph Thomas

November, 2001

---

## Contents

<i>Contents</i>	<i>II</i>
<i>Abstract</i>	<i>IV</i>
<i>Zusammenfassung</i>	<i>V</i>
<b>1 Introduction</b>	<b>1</b>
<b>2 Theoretical Background</b>	<b>4</b>
<b>2.1 Definition</b>	<b>4</b>
<b>2.2 Similarity concepts</b>	<b>6</b>
2.2.1 Monin-Obukhov similarity	6
2.2.2 Rossby-number similarity	7
<b>2.3 Turbulent Kinetic Energy budget</b>	<b>8</b>
<b>2.4 Extended application of the <math>\Pi</math>-Theorem</b>	<b>10</b>
<b>3 Dependencies and resulting parameterisations</b>	<b>12</b>
<b>3.1 Atmospheric stability</b>	<b>12</b>
<b>3.2 Pressure gradient and geographical latitude</b>	<b>17</b>
<b>3.3 Mixing layer height</b>	<b>19</b>
<b>3.4 Influence of the surface</b>	<b>22</b>
<b>4 Datasets</b>	<b>26</b>
<b>4.1 Experiments</b>	<b>26</b>
4.1.1 Tsimlyansk, 1981, USSR	27
4.1.2 FINTUREX, 1994, Antarctica	28
4.1.3 LINEX 96/2, 1996, Germany	29
4.1.4 LINEX 97/1, 1997, Germany	29
4.1.5 EBEX-2000, 2000, USA	30
4.1.6 Overview and experimental setups	31

---

<b>4.2</b>	<b>Reprocessing of the experimental data</b>	<b>33</b>
4.2.1	Calculation of statistical parameters and quality control	33
4.2.2	Spectral correction	34
<b>4.3</b>	<b>Overview over the database</b>	<b>34</b>
<b>4.4</b>	<b>Calculation of parameterisations</b>	<b>36</b>
<b>5</b>	<b><i>Calculation of additional input parameters</i></b>	<b>37</b>
<b>5.1</b>	<b>Determination of the mixing layer height</b>	<b>37</b>
5.1.1	Parcel method	38
5.1.2	Boundary layer model after Blackadar (1997)	39
<b>5.2</b>	<b>Determination of the displacement height</b>	<b>41</b>
<b>6</b>	<b><i>Results and discussion</i></b>	<b>44</b>
<b>6.1</b>	<b>Wind velocity components</b>	<b>44</b>
6.1.1	Vertical wind component	44
6.1.2	Horizontal wind component	60
<b>6.2</b>	<b>Temperature</b>	<b>68</b>
<b>6.3</b>	<b>Comparison with results from other authors</b>	<b>74</b>
<b>7</b>	<b><i>Conclusions and recommendations</i></b>	<b>79</b>
<b>8</b>	<b><i>References</i></b>	<b>81</b>
<b>9</b>	<b><i>Index of Figures</i></b>	<b>87</b>
<b>10</b>	<b><i>Index of Tables</i></b>	<b>89</b>
<b>11</b>	<b><i>Index of the used abbreviations and symbols</i></b>	<b>87</b>
<b>12</b>	<b><i>Appendix A</i></b>	<b>93</b>
<b>13</b>	<b><i>Appendix B</i></b>	<b>96</b>
<b>14</b>	<b><i>Appendix C</i></b>	<b>98</b>
	<b><i>Acknowledgements</i></b>	<b>100</b>
	<b><i>Eidesstattliche Erklärung</i></b>	<b>101</b>

## Abstract

This study presents a re-evaluation of parameterisations from literature of integral turbulence characteristics of wind velocity components and temperature in the surface layer. From this re-evaluation, recommendations for practical applications are given including a newly derived scaling factor. Integral turbulence characteristics have great importance for e.g. air pollution modelling and quality assessment of turbulence data.

The parameterisations were applied to turbulence data obtained during 5 individual experiments over homogeneous and slightly heterogeneous terrain, covering a latitudinal range from 52° North to 70° South. The parameterisations, investigated in this study, include expressions for locally influencing parameters such as atmospheric stability and surface properties, and non-local parameters such as mixing layer height and geographical latitude.

For near neutral and slightly stable conditions, integral turbulence characteristics of the vertical and horizontal wind velocities were found to be dependent on the geographical latitude. They were observed to scale best with the newly derived parameter  $z_+ f/u_*$ , stemming from the Rossby-number similarity. For unstable conditions, atmospheric stability represented by the dimensionless height  $\zeta$ , derived from the Monin-Obukhov theory, was found to be the most influencing parameter for integral turbulence characteristics of the wind components. The integral turbulence characteristic of the temperature was observed to scale with the atmospheric stability over the entire stability range. Hence, local and non-local parameters were observed to affect atmospheric turbulent flow quantities in the surface layer.

## Zusammenfassung

Die vorliegende Arbeit bietet eine Neubewertung bekannter Parametrisierungen der integralen Turbulenzcharakteristiken für die Vertikal- und Horizontalwindgeschwindigkeit und die Temperatur in der bodennahen Grenzschicht. Basierend auf den Ergebnissen der Neubewertung werden Empfehlungen für praktische Anwendungen gegeben, die einen neu abgeleiteten Parameter enthalten. Integrale Turbulenzcharakteristiken haben eine große Bedeutung für zahlreiche Anwendungen in der Meteorologie, so z.B. für die Modellierung von Luftschadstoffausbreitung oder die Qualitätsbewertung von Turbulenzdaten.

Die Datengrundlage für die durchgeführte Neubewertung der Parametrisierungen lieferten 5 Turbulenzdatensätze von verschiedenen Experimenten, die über homogenem oder nur leicht heterogenem Gelände durchgeführt worden sind. Die Experimente decken dabei einen Bereich von 52° N bis 70° S ab. Die verwendeten Parametrisierungen enthalten Abhängigkeiten sowohl von lokalen Einflussgrößen wie der atmosphärischen Stabilität und Geländeeigenschaften, als auch nicht lokaler Einflussfaktoren wie der geographischen Breite und der Mischungsschichthöhe.

Bei neutraler und leicht stabiler Schichtung zeigen die integralen Turbulenzcharakteristiken des Vertikal- und des Horizontalwindes eine deutliche Abhängigkeit von der geographischen Breite. Die besten Ergebnisse liefert eine Parametrisierung, die den Parameter  $z_+ f/u_*$  enthält, der aus der Rossbyzahl-Ähnlichkeitstheorie abgeleitet ist. Bei labiler Schichtung skalieren die integralen Charakteristiken der Windvektoren mit der atmosphärischen Stabilität, die mit Hilfe der aus der Monin-Obukhov-Ähnlichkeitstheorie abgeleiteten dimensionslosen Höhe  $\zeta$  ausgedrückt wird. Die integralen Turbulenzcharakteristiken der Temperatur zeigen unabhängig von der Schichtung eine deutliche Abhängigkeit von der atmosphärischen Stabilität. Daraus folgt, dass sowohl lokale, als auch nicht lokale Parameter einen Einfluss auf das turbulente Wind- und Temperaturfeld haben.

Не то, что мните вы, природа:  
Не слепок, не бездушный лик-  
В ней есть душа, в ней есть свобода,  
В ней есть любовь, в ней есть язык...

Федор Тютчев

## 1 Introduction

Integral turbulence characteristics are statistical measures describing atmospheric turbulence in the surface layer of our planet. They are defined for fluctuating meteorological parameters like components of the wind vectors and atmospheric scalars. The functional relationship between the integral turbulence characteristic of a meteorological parameter and an appropriate scaling factor can be described by parameterisations. Integral turbulence characteristics have been widely used in a variety of applications including standard applications like simple air pollution models, but also advanced applications like models estimating the influence of the surface on turbulent fluxes. Some detailed examples will be given below.

Integral turbulence characteristics have been investigated for a long time since the first real turbulence experiments were carried out, for example the Kansas experiment in 1968 (Haugen et al., 1971). The first semiempirical formulations based on the Kansas data, following Monin-Obukhov-similarity and the  $\Pi$ -theorem, were published by Wyngaard (1971). Since then, various authors have investigated integral turbulence characteristics, finding different expressions for the parameterisations while using different scaling factors. The important assumptions will be discussed in Chapter 3. In former experiments it was necessary to change the parameterisations of integral turbulence characteristics in order to make them match the observed data. This contradicts the idea of real universality of the obtained functions for fluctuating atmospheric variables. A reason might be that the chosen scaling factors were not appropriate. This study aims to identify statistically robust parameterisations and their appropriate scaling factors mostly influencing atmospheric turbulent flow quantities.

The main objective of this thesis is a re-evaluation of previously published parameterisations of integral turbulence characteristics by applying them to numerous datasets representing a wide range of local and non-local influencing parameters in the lower part of the atmosphere. The investigated scaling factors include parameterisations for atmospheric stability, mixing layer height and geographical latitude in terms of the pressure gradient at the surface. The influences of different surface properties will be taken into account in the discussion of integral turbulence characteristics. In a strict sense, applicability of the integral turbulence characteristics depends on the assumptions made for their scaling factors. In most cases, horizontal homogeneity, stationarity and well mixed turbulent air layers are assumed. Hence, the structure of the surface

is crucial for the general applicability of the integral turbulence characteristics over a given terrain. Based on the re-evaluation of published parameterisations, this study aims to recommend better parameterisations of integral turbulence characteristics. This work is thus expected to improve the quality of practical applications using integral turbulence characteristics.

Applications using integral turbulence characteristics cover a wide range of methods and models in the atmospheric sciences. Some examples for the application of integral turbulence characteristics will be given now. Assuming that we know the true functional relationship between integral turbulence characteristics and a scaling factor or at least the best estimates for them, we can use them as an instrument for the quality assessment of measured turbulence data. Through comparison between the observed and the predicted value one can identify if the turbulent field is fully developed or distorted at a given site. This procedure was published by Wichura and Foken (1995) and applied for example at the Weidenbrunnen site in the Fichtelgebirge mountains/Germany (Mangold, 1999), in order to characterise the influences of a complex, hilly, forested site on turbulence measurements.

Accumulation methods are commonly used for the determination of turbulent fluxes in the surface layer. They are generally based on the assumption of flux-variance similarity. Here, the flux of an observed scalar, e.g. carbon dioxide, is regarded as being proportional to the fluctuation of the vertical wind component, assuming that the vertical wind obeys the corresponding parameterisation. Turbulence characteristics can again be used for the evaluation of this assumption (Businger and Oncley, 1990). Integral turbulence characteristics can even be used to directly determine the fluxes (Wyngaard et al., 1971; Foken, 1990).

The behaviour of turbulent fluxes above and in high vegetation is not yet well understood. In these systems, integral turbulence characteristics are useful to study local atmospheric phenomena like intermittency and coherent structures.

The spreading of a pollutant plume in the atmosphere can be simulated using air pollution models such as the Monte Carlo Smoke Plume Simulation of Blackadar (1997). Deposition and release of reactive or conservative gases in an ecosystem are often calculated using coupled atmospheric chemistry/turbulence models. Instead of measured data, these models commonly use parameterisations for the fluctuation of the vertical and horizontal wind speed components and hereby involve integral turbulence characteristics.

---

The influence of surface properties on measured turbulence flux data is estimated by so-called footprint models as for example described in (Schmid, 1994). These applications based on higher-order closure terms use integral turbulence characteristics to estimate elementary input parameters of their models.

Summarising, we can state that integral turbulence characteristics provide useful information about atmospheric, turbulent motion in the surface layer. They are widely used and have great importance for a variety of practical applications. Because of the observed non-universality there is still need for further investigations. The main objective of this study is to identify their most important influencing factors and to find statistically robust parameterisations. These parameterisations should be valid for a great range of local and non-local parameters, which influence atmospheric turbulence. Thus, this study is expected to improve the quality of applications using integral turbulence characteristics.

## 2 Theoretical Background

The idea of using integral turbulence characteristics stems from considerations about turbulent atmospheric motion. This chapter will thus deal with the underlying physical theory. After defining integral turbulence characteristics in Section 2.1, we have to take a look at the fundamental concepts involved. Most of the published parameterisations use the atmospheric stability represented by the dimensionless height  $\zeta$  or the Rossby-number in order to formulate appropriate scaling factors. These scaling factors are derived from similarity concepts, which are valid only under simplifying conditions. Due to their relevance for the scaling factors and general applicability of integral turbulence characteristics, the similarity concepts will be briefly presented in Section 2.2. The mathematical relationship of integral turbulence characteristics and their parameterisations can be derived directly from the budget of turbulent kinetic energy. This derivation will be presented in Section 2.3. Buckingham's  $\Pi$ -theorem is a basic concept for the use of dimensionless parameters and is essential for both similarity concepts. In Section 2.4, it will be discussed taking all considered concepts into account.

### 2.1 Definition

Integral turbulence characteristics are defined as the normalised standard deviations of fluctuating turbulent parameters (Tillmann, 1972). Equation ( 1 ) is a general form. The word 'integral' indicates that integral turbulence characteristics represent the integral over all frequencies of the turbulent spectrum of the considered parameter.

$$\frac{\sigma_x}{X_*} = \phi_x \left( \frac{z-d}{L}, \dots \right) \quad (1)$$

where  $\sigma_x$  is the standard deviation of the fluctuating parameter  $x$ ,  $X_*$  the corresponding normalising factor,  $\phi_x$  a function of  $x$  and  $(z-d)/L$  the dimensionless height, with  $(z-d)$  being the aerodynamical height and  $L$  the Obukhov-length (see Section 2.2.1). The variable  $x$  hereby is the observed parameter and can stand for the vertical wind component  $w$ , the horizontal wind component  $u$ , the absolute temperature of the air  $T$  or the specific humidity of the air  $q$ .  $X_*$

represents the normalising factor for the variable  $x$  and is derived from its characteristic turbulent flux. The normalising factors for wind velocity components, temperature and humidity are defined by Equations ( 2 ), ( 3 ) and ( 4 ) (see e.g. Arya, 2001; Stull, 1988).

$$x = w, u: \quad X_* = u_* = \sqrt{\frac{\tau_o}{\rho}} = \sqrt{-\overline{u'w'}} \quad (2)$$

$$x = T: \quad X_* = T_* = -\frac{\overline{w'T'}}{u_*} \quad (3)$$

$$x = q: \quad X_* = q_* = -\frac{\overline{w'q'}}{u_*} \quad (4)$$

where  $\tau_o$  is the surface shear stress,  $\rho$  the mass density of air,  $u'$ ,  $w'$ ,  $T'$  and  $q'$  are the fluctuations of the horizontal and vertical wind components, temperature and specific humidity, respectively; the bar indicates the time mean of the covariance of the considered variables;  $u_*$ ,  $\overline{w'T'}$  and  $\overline{w'q'}$  denote the friction velocity, the sensible heat flux and the latent heat flux, respectively. Equations ( 2 ) – ( 4 ) imply that the dispersion of the observed variable  $x$  is made non-dimensional by dividing it through its characteristic flux. The momentum flux at the surface  $\tau_o/\rho$  is used in case of the wind components  $u$  and  $w$ . For the fluctuating scalars  $T$  and  $q$ , the standard deviations are divided by the sensible heat flux and the latent heat flux normalised by the friction velocity.

Integral turbulence characteristics are commonly defined in a non-dimensional form, making them independent of the system of units used. Additionally, the non-dimensionalised form facilitates the comparison of turbulent data measured at different sites and the identification of simple functional relationships between the scaling factor and the corresponding turbulence characteristic (Tennekes, 1982).

## 2.2 Similarity concepts

### 2.2.1 Monin-Obukhov similarity

A detailed introduction to the Monin-Obukhov similarity theory can be found in micrometeorological textbooks (Arya, 2001; Stull, 1988). Here, only the basic assumptions and the resulting equations will be presented.

The Monin-Obukhov similarity is sometimes referred to as the surface layer similarity, as it was postulated for atmospheric turbulence in the lowest layer above ground. It has provided the most acceptable semiempirical framework for organising and presenting turbulent data, as well as predicting certain micrometeorological parameters (Arya, 2001).

The similarity hypothesis was published by Monin and Obukhov (1954). It is based on three simplifying assumptions. Firstly, one assumes stationarity, which implies that the mean turbulent fluxes do not change with time. Secondly, the flow is assumed to be horizontally homogeneous and the fluxes of momentum and heat are independent of height near the surface layer. And thirdly, the influences of surface properties, boundary layer height and geostrophic winds are assumed to be fully represented by the surface shear stress parameter.

Given these assumptions, the mean surface layer wind and the temperature field depend only on four independent variables (Monin and Obukhov, 1954): the kinematic surface heat flux  $Q_H/\rho c_p$  [ $\text{Kms}^{-1}$ ], the height above ground  $z$  [m], the buoyancy parameter  $g/T$  [ $\text{mK}^{-1}\text{s}^{-2}$ ] and the surface shear stress  $\tau_o/\rho$  [ $\text{m}^2\text{s}^{-2}$ ].  $\rho$  denotes the mass density of air,  $c_p$  the specific heat at constant pressure and  $g$  the acceleration due to gravity. These four governing surface parameters involve three fundamental dimensions: length [m], temperature [K] and time [s].

According to Buckingham's  $\Pi$ -theorem,  $(n + 1)$  independent variables with  $k$  independent dimensions formulate  $(n + 1) - k$  independent dimensionless combinations of them. In our case,  $(3 + 1) - 3 = 1$  dimensionless group can be derived. As we lose one degree of freedom when deriving a new parameter,  $n$  becomes 3 (instead of 4). Traditionally, the chosen combination for this dimensionless group is the dimensionless height  $\zeta = z/L$ , where  $L$  is the Obukhov length, (Obukhov, 1946) defined as

$$L = -\frac{u_*^3}{\kappa \frac{g}{T} \frac{Q_H}{\rho c_p}} \quad (5)$$

where  $u_*$  is the friction velocity,  $\kappa$  the von-Karman constant,  $g$  the acceleration due to gravity,  $T$  the mean absolute temperature,  $Q_H/\rho c_p$  the sensible heat flux with  $\rho$  the mass density of air and  $c_p$  the specific heat at constant pressure.  $L$  has the dimension of a length [m]. The magnitude  $|L|$  represents the thickness of the layer in which shear and friction are important. The sign of  $L$  becomes negative when changing from stable to unstable conditions.

The Monin-Obukhov similarity concept predicts that any average turbulent quantity or mean flow must be a unique function of  $\zeta$  when normalised by its corresponding factors. Thus, one expects to find a functional relationship for integral turbulence characteristics by plotting them against  $\zeta$ .

### 2.2.2 Rossby-number similarity

The second basic underlying concept for atmospheric turbulence is the Rossby-number similarity. A detailed introduction to this similarity theory can be found for example in (Tennekes, 1982). Based on this reference, the basic concept will be introduced here.

The Rossby-number similarity was postulated for the conditions of a steady-state, neutrally stratified, horizontally homogeneous atmosphere.

The wind speed  $u$  in the surface boundary layer is a function of the height above ground  $z$ . Close to the surface,  $z$  is assumed to scale with surface properties, for example with the surface roughness length  $z_o$ . The influence of the geostrophic wind speed  $u_g$  is assumed to increase with increasing height and  $z$  is assumed to scale with the length scale  $u_g/f$ , where  $f$  is the Coriolis parameter. The chosen length scale  $u_g/f$  is related to the synoptic pressure gradient in the boundary layer (see Section 3.2). The surface Rossby-number  $Ro$  is defined as the ratio of both length scales ( $Ro = u_g/fz_o$ ). It is regarded as a central non-dimensional parameter in boundary layer flow.

Tennekes (1982) gives an example, which helps to understand the relationship between geostrophic and ageostrophic wind components in the atmospheric boundary layer: A balloon

drifting away from the surface follows the geostrophic wind with increasing height. The observed velocity difference ( $u_{\text{balloon}} - u_g$ ) is called the ageostrophic wind velocity and is caused by friction and decreases with height as the influence of the surface drag decreases.

The friction velocity  $u_*$  is an appropriate velocity scale for the ageostrophic wind components in the lowest 100m of the boundary layer (Tennekes and Lumley, 1972). Assuming that  $u_*$  is a function of the surface Rossby-number, as it reflects the surface shear stress  $\tau_o/\rho$ , and  $u_*$  is the appropriate velocity scale, we can construct a non-dimensional height  $zf/u_*$ . Thus, the non-dimensionalised velocity difference ( $u - u_g$ ) is expected to be a function of the constructed dimensionless height as (Tennekes, 1982)

$$\frac{(u - u_g)}{u_*} = \phi_u \left( \frac{zf}{u_*} \right) \quad (6)$$

where  $u$  is the mean horizontal wind velocity and  $u_g$  the mean horizontal geostrophic wind component.  $\phi_u$  is a function of the non-dimensional height  $zf/u_*$ . Plotting wind profiles according to Equation ( 6 ), they are found to be independent of the surface Rossby-number. This relationship is called the Rossby-number similarity of the ageostrophic wind. Thus, with the dimensionless height  $zf/u_*$  being an appropriate scaling factor for surface layer flows, one expects to find a functional relationship when plotting integral turbulence characteristics against this parameter.

### ***2.3 Turbulent Kinetic Energy budget***

In the previous sections, the scaling factors for the parameterisations have been derived from similarity concepts. The functional relationship between integral turbulence characteristics and these scaling factors, i.e. the parameterisations can be derived mathematically from the budget of turbulent kinetic energy (Högström, 1990; Wyngaard et al., 1971). This procedure will be briefly presented here.

The equation for the turbulent kinetic energy budget can be derived from the turbulent Navier-Stokes-Equation. Given stationarity, horizontal homogeneity and neutral stratification, the turbulent energy budget equals zero and becomes (Högström, 1990)

$$\overline{u'w'} \frac{\partial u}{\partial z} - \frac{g}{T} \overline{w'T'} + \frac{\partial}{\partial z} \left( \frac{\overline{w'q'^2}}{2} \right) + \frac{1}{\rho} \frac{\partial \overline{p'w'}}{\partial z} + \varepsilon = 0 \quad (7)$$

Multiplying Equation ( 7 ) with an appropriate normalising parameter, one arrives at (Högström, 1990)

$$-\frac{\kappa z}{u_*} \frac{\partial u}{\partial z} + \frac{z}{L} + \frac{\kappa z}{u_*^3} \frac{\partial}{\partial z} \left( \frac{\overline{w'q'^2}}{2} \right) + \frac{\kappa z}{u_*^3 \rho} \frac{\partial \overline{p'w'}}{\partial z} + \frac{\kappa z \varepsilon}{u_*^3} = 0 \quad (8)$$

where  $u'$  and  $w'$  are the fluctuating parts of the horizontal and vertical wind velocities respectively,  $u$  the mean horizontal wind velocity,  $z$  the height above ground,  $T$  and  $T'$  the mean and fluctuating temperature,  $q'$  the fluctuating specific humidity,  $g$  the gravity acceleration,  $u_*$  the friction velocity,  $p'$  the fluctuating pressure,  $\kappa$  the von-Karman constant,  $\rho$  the mass air density and  $\varepsilon$  the dissipation of turbulent kinetic energy; the bar indicates the time mean of the covariance of the considered variables.

The terms on the left side of Equation ( 8 ) depict from left to right: shear production, buoyancy production, turbulent transport, pressure transport and dissipation. In analogy to the turbulent kinetic energy budget, the budgets of wind stress and vertical heat flux are given by (Foken et al., 1991; Wyngaard et al., 1971)

$$\frac{\partial \overline{u'w'}}{\partial t} + \overline{w'^2} \frac{\partial u}{\partial z} - \frac{g}{T} \overline{u'T'} + \frac{\partial \overline{u'w'^2}}{\partial z} + \frac{1}{\rho} \frac{\partial \overline{w'p'}}{\partial x} + \frac{1}{\rho} \frac{\partial \overline{u'p'}}{\partial z} = 0 \quad (9)$$

$$\frac{\partial \overline{w'T'}}{\partial t} + \overline{w'^2} \frac{\partial T}{\partial z} - \frac{g}{T} \overline{T'^2} + \frac{\partial \overline{w'^2 T}}{\partial z} + \frac{1}{\rho} \frac{\partial \overline{T'p'}}{\partial z} = 0 \quad (10)$$

with the symbols being the same as in Equation ( 8 ). Equation ( 9 ) and ( 10 ) involve the dispersions of the vertical wind velocity  $\sigma_w^2$  and temperature  $\sigma_T^2$  defined as

$$\sigma_w^2 = \overline{w'^2} \quad (11)$$

$$\sigma_T^2 = \overline{T'^2} \quad (12)$$

For non-neutral stability and constant fluxes, implying that all temporal derivatives equal zero and the pressure transport term and the dissipation can be neglected due to their magnitude, from Equation ( 9 ) and ( 10 ) one can derive (Foken et al., 1991)

$$\frac{\sigma_w}{u_*} = a_1 \left( \sqrt{\frac{\kappa z}{u_*} \frac{\partial u}{\partial z}} \right)^{-1} = a_1 \frac{1}{\sqrt{\phi_m(\zeta)}} \quad (13)$$

$$\frac{\sigma_T}{T_*} = a_2 \left( \sqrt{\frac{z}{L} \frac{\kappa z}{T_*} \frac{\partial T}{\partial z}} \right)^{-1} = a_2 \frac{1}{\sqrt{\frac{z}{L} \phi_h(\zeta)}} \quad (14)$$

with the symbols being the same as in Equation ( 8 ).  $a_1$  and  $a_2$  are constants,  $\phi_m$  and  $\phi_h$  are called the dimensionless wind shear gradient and the dimensionless temperature gradient, respectively. They are the basic universal similarity functions relating the momentum flux and the sensible heat flux to the mean gradients in the surface layer (Arya, 2001). Expressions for the integral turbulence characteristics of the horizontal wind velocity  $u$  and humidity  $q$  can be derived in analogy to Equation ( 9 ) - ( 14 ). Thus, the functional relationship between integral turbulence characteristics and the dimensionless height  $\zeta$  can be derived directly from the budgets of wind stress and vertical heat flux.

#### ***2.4 Extended application of the $\Pi$ -Theorem***

The Buckingham-theorem was used in Section 2.2.1 in order to derive the dimensionless height  $\zeta$  from the surface parameters. The Monin-Obukhov similarity theory states, that the surface layer wind and the temperature field only depend on the surface heat flux  $Q_H/\rho c_p$ , the height above ground  $z$ , the buoyancy parameter  $g/T$  and the surface shear stress  $\tau_o/\rho$ , giving three characteristic scaling parameters  $u_*$ ,  $T_*$  and  $z$ . The Rossby-number similarity theory on the other

---

hand, finds the constructed non-dimensional scaling factor  $zf/u^*$  to be appropriate for surface layer flows. This scaling factor introduces one new independent variable: the Coriolis parameter  $f$ . In Section 3.3, another independent parameter comes into play when discussing the parameterisations of integral turbulence characteristics: the mixing layer height  $z_i$ . Peltier et al. (1996) introduce this parameter through the dimensionless term  $z/z_i$ .

Hence, the total number of independent variables increases to 6. In contrast, no further fundamental dimension is involved, as the Coriolis parameter has the dimension of time [ $s^{-1}$ ] and the mixing layer of length [m]. Now we can apply Buckingham's  $\Pi$ -theorem to the extended number of variables. From the expression  $n + 1 - k$  follows that 3 dimensionless groups can be derived. These groups can be  $z/L = \zeta$ ,  $zf/u^*$  and  $z/z_i$ . Thus, the use of these three dimensionless scaling parameters for the discussion of possible dependencies of integral turbulence characteristics in this study is in accordance with Buckingham's theorem.

### 3 Dependencies and resulting parameterisations

Integral turbulence characteristics were found to scale with a variety of parameters. These scaling parameters are called dependencies of integral turbulence characteristics. They can be divided into two different groups:

The first group represents local parameters or local conditions of the surface boundary layer such as atmospheric stability and surface properties. Atmospheric stability, expressed in terms of  $\zeta$ , has been used by many authors to formulate parameterisations for the integral turbulence characteristic. The dependence on stability and resulting parameterisations will be presented in Section 3.1. The influence of surface properties on aerodynamics and turbulent fluxes will be discussed in Section 3.4.

The second group contains non-local influencing parameters such as the geographical latitude and height of the mixed atmospheric boundary layer. In most publications, the non-local parameters were regarded as having no direct influence on turbulence in the surface layer and therefore neglected. However, Högström (1990) and Smedman (1991) derive parameterisations containing the geographical latitude, represented by the Coriolis parameter. This dependence and the corresponding scaling factors will be introduced in Section 3.2. The possible dependence of integral turbulence characteristics on the mixing layer height was introduced by Panofsky et al. (1977) and Peltier et al. (1996), and will be presented in Section 3.3.

#### 3.1 *Atmospheric stability*

The derivation of the atmospheric stability in terms of  $\zeta$  as a scaling factor for integral turbulence characteristics has already been presented in Section 2.3. Thus, only the parameterisations given by various authors will be introduced here.

Many authors found atmospheric stability to be the most appropriate scale for the integral turbulence characteristics of the vertical and horizontal wind velocities, temperature and humidity (e.g. Wyngaard et al., 1971; Wesely, 1988; Panofsky et al., 1977; Foken et al., 1991; Foken et al., 1997a; Tillmann, 1972). In accordance with the Monin-Obukhov similarity concept (Section 2.2.1), the stability condition of the atmosphere is represented by the dimensionless height  $\zeta$ .

Various parameterisations are used by different authors. Wyngaard et al. (1971), Foken et al. (1991) and Wesely (1988) use the parameterisation given in Equation ( 15 ). A survey of the coefficients  $C_1$  and  $C_2$  in Equation ( 15 ) was given by Foken et al. (1997a) and is presented in an expanded form in Table 1.

$$\frac{\sigma_x}{X_*} = \phi_x \left( \frac{z}{L} \right) = C_1 \left( \left| \frac{z}{L} \right| \right)^{C_2} \quad (15)$$

where  $\sigma_x/X_*$  depicts the integral turbulence characteristics of the variable  $x$  (see Section 2.1) and  $\phi_x$  its corresponding function.  $C_1$  and  $C_2$  are constants given in Table 1.

**Table 1: Coefficients used in Equation ( 15 ) as given by various authors**

variable x	stability $\zeta$	$C_1$	$C_2$	authors	in figures referred to as
w	$\geq -0.4$	1.4	0	Wyngaard et al. (1971)	(1) Wyngaard 71
	$\leq -0.4$	1.9	1/3		
	$\geq -0.0625$	1.41	0	Foken et al. (1991)	(2) Foken 91
	$-0.0625 > \zeta > -1$	2	1/8		
	$< -1$	2	1/6		
	$0 > \zeta > -0.0319$	1.3	0		
	$< -0.0319$	2	1/8	Foken et al. (1997a)	(12) Foken 97
	$> 0.0319$	2	1/8		
	$0.0319 > \zeta > -0.0319$	1.3	0		
	$< -0.0319$	2	1/8		
u	$0 > \zeta > -0.0319$	2.7	0	Foken et al. (1997a)	(14) Foken 97
	$< -0.0319$	4.15	1/8		
T	$\geq -0.31$	1.85	0	Wesely (1988)	(3) Wesely 88
	$\leq -0.31$	1.25	-1/3		
	$< -0.05$	0.95	-1/3	Wyngaard et al. (1971)	--
	$\geq -0.0625$	0.5	-1/2	Foken et al. (1991)	(4) Foken 91
	$-0.0625 > \zeta > -1$	1	-1/4		
	$< -1$	1	-1/3		

Another parameterisation, empirically found by Panofsky et al. (1977) and Wesely (1988) to reflect the dependency on stratification, is given in Equation ( 16 ). This formula was obtained compiling many aircraft and tower data over various surfaces. Arya (2001) recommends the formula after Panofsky et al. (1977) with slightly different coefficients for unstable conditions (see Table 2). Tillmann (1972) uses a slightly different parameterisation given in Equation ( 17 ).

A survey of coefficients  $C_1$ ,  $C_2$  and  $C_3$  can be found in Foken et al. (1997a) and is given in an expanded form in Table 2.

$$\frac{\sigma_x}{X_*} = \Phi_x \left( \frac{z}{L} \right) = C_1 \left( 1 - C_3 \frac{z}{L} \right)^{C_2} \quad (16)$$

$$\frac{\sigma_x}{X_*} = \Phi_x \left( \frac{z}{L} \right) = C_1 \left( C_3 - \frac{z}{L} \right)^{C_2} \quad (17)$$

with symbols used in Equation ( 15 ).  $C_1$ ,  $C_2$  and  $C_3$  are constants shown in Table 2.

**Table 2:** Coefficients used in Equation ( 16 ) and ( 17 ) as given by various authors

variable x	stability $\zeta$	$C_1$	$C_2$	$C_3$	authors	in figures referred to as
w	$\geq 0$	1.3	0	1	Panofsky et al. (1977),	(5) Panofsky 77
Equation (16)	$< 0$	1.3	1/3	2	Wesely (1988)	
	$< 0$	1.25	1/3	3	Panofsky and Dutton (1984)	(15) Panofsky 84
T	$-0.055 \geq \zeta \geq -60$	0.95	-1/3	-0.055	Tillmann (1972)	(6) Tillmann 72
Equation (17)	$0 > \zeta > -0.055$	2.5	0	1		

Due to the use of the universal functions proposed by Skeib (1980), Foken et al. (1991) subdivide the entire stability range into different intervals: the first spans the stable and near neutral ranges with  $\zeta > -0.0625$ , where turbulent eddies are assumed to be generated only mechanically by shear stress and  $\sigma_w/u_*$  is assumed to be constant. Within the second range,  $-0.0625 > \zeta > -1$ , turbulence is assumed to be both induced thermally by buoyancy and mechanically by shear stress. The last range with  $\zeta < -1$  reflects conditions, where shear production is negligible and turbulence is generated only by buoyancy. In this range, turbulence is supposed to obey the laws of free convection. Later, Foken et al. (1997a) shifted the border of only mechanically induced turbulence towards neutrality ( $0 > \zeta > -0.0319$ ) and found  $\sigma_w/u_*$  and  $\sigma_u/u_*$  approaching a 1/8 power law (see Table 1) for the entire unstable range. Interpreting the

values given in Table 1 and Table 2, most authors observe the integral turbulence characteristic of the vertical and horizontal wind velocity to be constant under stable and near neutral conditions when plotted against  $\zeta$ . This constant value was found to be  $\sim 1.4$  consistently (Foken et al., 1991; Wyngaard et al., 1971). In contrast, Foken (*pers.comm.*) suggests to use the same power laws of  $\zeta$  for the integral characteristic of the vertical wind velocity under stable and unstable conditions. Thus,  $\sigma_w/u_*$  is assumed to be again a function of  $\zeta$  for  $\zeta > 0.0319$ , remaining the near neutral range constant. With increasing instability on the other hand, all authors predict the integral turbulence characteristics of the vertical wind velocity to be non-constant with increasing instability obeying power laws of  $\zeta$  varying from  $1/3$  to  $1/8$ .

It is important to note at this point that the integral turbulence characteristic of the horizontal wind velocity can directly be derived from the integral characteristic of the vertical wind velocity, using the transformation  $2\sigma_w^2 \approx \sigma_u^2$  (Wyngaard and Clifford, 1978). This simple relation implies that all parameterisations for  $\sigma_w/u_*$  can be used in order to predict  $\sigma_u/u_*$  using a transformation coefficient.

According to Panofsky et al. (1977), Wesely (1988) and Tillmann (1972), at neutral stratification the integral turbulence characteristic of the temperature approaches a constant value ranging from 1.3 to 2.5. In addition, Wesely (1988) predicts  $\sigma_T/T_*$  to remain constant for stable conditions. Again, the findings of Foken et al. (1991) contradict this so far widely accepted notion. They did not find  $\sigma_T/T_*$  to approach a constant value at neutral conditions. Referring to the coefficients shown in Table 2, these authors predict the integral turbulence characteristic of the temperature to be a function of  $\zeta$  over the entire stability range, following different power laws and exhibiting a maximum at  $\zeta = 0$ . All authors agree that the integral turbulence characteristic of the temperature is expected to obey a  $-1/3$  power law with increasing instability.

Summarising, we can state that many authors have been investigating integral turbulence characteristics as a function of the atmospheric stability. The majority of them, except those mentioned above, found them to be constant when approaching neutrality and remaining constant for the entire stable range. Under the conditions of unstable stratification, all authors predict the integral turbulence characteristics to be related to  $\zeta$ , following different power laws.

### 3.2 *Pressure gradient and geographical latitude*

In this section, the derivation of the geographical latitude as a scaling factor for integral turbulence characteristics will be introduced (Högström, 1990; Tennekes, 1982; Yaglom, 1979).

The Coriolis parameter  $f$  is a non-local parameter, depending only on the geographical latitude  $\phi$  (Equation (18)). As the Coriolis force influences the wind direction (e.g. Stull, 2000),  $f$  appears wherever the wind's magnitude or direction is calculated.

$$f = 2\Omega \sin \phi \quad (18)$$

where  $\Omega$  is the rotational speed of the earth and  $\phi$  the geographical latitude. Högström (1990) states that the surface atmospheric pressure gradient  $dp/dx$  (used for synoptic purposes) is related to the Coriolis parameter as

$$\left(\frac{1}{\rho}\right)\left(\frac{\partial p}{\partial x}\right) = fv_g \quad (19)$$

where  $dp/dx$  is the longitudinal pressure gradient,  $\rho$  the mass density of air,  $f$  the Coriolis parameter and  $v_g$  the y-geostrophic wind component. Yaglom (1979) introduced a length scale for laboratory studies, where the pressure gradient  $dp/dx$  is made nonzero with respect to real atmospheric conditions. This so-called pressure gradient length scale  $\delta_p$  is given by

$$\delta_p = u_*^2 \left(\frac{1}{\rho} \frac{\partial p}{\partial x}\right)^{-1} \quad (20)$$

Combining Equation (19) and (20), one yields

$$\delta_p = \frac{u_*^2}{fv_g} \quad (21)$$

From the Rossby-number similarity theory (Section 2.2.2), it can be obtained that  $v_g$  is proportional to  $u_*$ . Thus, for  $v_g = (B/\kappa) u_*$  one can write

$$\delta_p = \frac{\kappa u_*}{B f} = C_{Dg} \frac{u_*}{f} \quad (22)$$

where  $\kappa$  is the von-Karman constant,  $B$  a proportionality factor ( $\approx 5$ ; Tennekes, 1982),  $C_{Dg}$  is the geostrophic drag coefficient and found to be  $\approx 0.08$ . Högström (1990) plotted near neutral  $\sigma_w/u_*$  data against  $\ln[(z - d)/u_*]$ . This expression includes the pressure gradient length scale derived above, which coincides with the non-dimensional height  $zf/u_*$  obtained from the Rossby-number similarity. The geometrical height  $z$  was replaced by the expression  $(z - d)$  following the concept of the aerodynamical height (Stull, 1988), where  $d$  depicts the displacement height (see Section 5.2). Through linear regression of all individual datapoints plotted against  $\ln[(z - d)/u_*]$ , Högström (1990) obtained Equation ( 23 ) with coefficients shown in Table 3 as the best fit.

$$\frac{\sigma_x}{X_*} = C_1 \ln \left[ \frac{(z - d)f}{u_*} \right] + C_2 \quad (23)$$

Smedman (1991) supported this parameterisation with slightly different coefficients (Table 3), interpreting data obtained over homogeneous and slightly heterogeneous terrain from several sites in Sweden. Additionally, she derived an equation for the integral turbulence characteristic of the horizontal wind velocity in agreement with Equation ( 23 ) with coefficients given in Table 3.

**Table 3: Coefficients used in Equation ( 23 ) as given by various authors**

variable x	$z/L = \zeta$	$C_1$	$C_2$	authors	in figures referred to as
w	$0.1 > \zeta > -0.2$	0.12	2	Högström (1990)	(9) Hoegstr. 90
	$0.1 > \zeta > -0.2$	0.1	1.8	Smedman (1991)	(10) Smedman 91
u	$0.1 > \zeta > -0.2$	-0.05	2.4	Smedman (1991)	(11) Smedman 91

Högström (1990) and Smedman (1991) found the integral turbulence characteristics of the vertical and horizontal wind velocities not to be constant when plotted against  $\ln[(z - d)/u_*]$ . Equation ( 23 ) implies that  $\sigma_w/u_*$  and  $\sigma_u/u_*$  vary linearly with this scale, the slope being given by coefficient  $C_1$  in Table 3. The validity of the parameterisations presented above is limited to the near neutral range with  $0.1 > \zeta > -0.2$  due to the underlying concept of the Rossby-number similarity theory. Smedman (1991) predicts  $\sigma_u/u_*$  to decrease with increasing stability due to the negative value of the corresponding slope.

### 3.3 *Mixing layer height*

The mixing layer height represents the second non-local parameter of the atmospheric boundary layer entering the discussion of possible dependencies of integral turbulence characteristics. Some authors found parameterisations containing terms with the mixing layer height  $z_i$  involved. Before presenting these equations, a short introduction into the dynamics of the atmospheric boundary layer height will be given (Arya, 2001; Kaimal and Finnigan, 1994).

The atmospheric boundary layer is the lower part of the troposphere. It has been observed to obey a diurnal variation, predominantly caused by the variation of incoming solar radiation (Figure 1). The nocturnal boundary layer is characterised by stable stratification and nocturnal inversions both inhibiting turbulent exchange. Stable conditions imply that buoyancy equals zero and thus turbulence can only be caused by strong wind shear, so called forced convection (Businger, 1982). If present at all, nocturnal turbulence does not occur permanently, but has an intermittent character. As the sun rises, the lower nocturnal inversions are progressively eroded due to the sensible heat flux coupled to the incoming solar radiation, leading to positive (upward directed) buoyancy. Consequently, the upward exchange of sensible and latent heat intensifies in

the lower layer of the atmosphere. Thus, the stable nocturnal boundary layer is replaced by an unstable stratified or convectively mixed boundary layer. All properties are rather well-mixed over most of the convective boundary layer.

The nocturnal surface inversion shifts upwards when the convective mixed layer arises and acts as its capping layer, reaching heights of 1-2 km. The average height of this capping inversion is one possible definition of the mixing layer height (see Section 5.1).

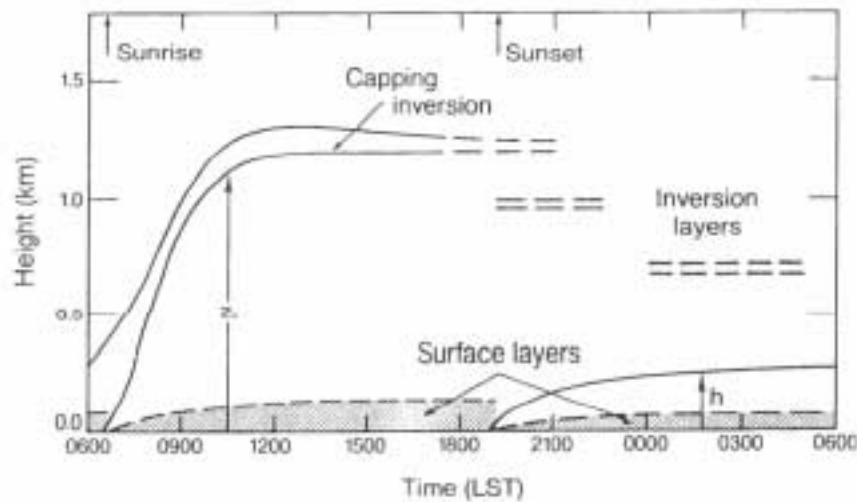


**Figure 1:** Dynamics of the stable nocturnal boundary layer and convectively mixed boundary layer due to cooling and heating processes at the surface. The time indicated is Local Standard Time (Kaimal and Finnigan, 1994).

During daytime and above the unstable surface layer, convective large-scale motion dominates beginning from a level of  $\sim 0.1z_i$ , and the flow is insensitive to the surface. Now, the surface heat flux  $Q_H/\rho c_p$  and the mixing layer depth  $z_i$  are the appropriate scaling parameters (Kaimal and Finnigan, 1994). Hence, scaling laws should differ from those in the surface layer. In Equations ( 24 ) and ( 25 ) they are formulated for velocity and temperature respectively (Willis and Deardorff, 1974), where  $w_*$  is called the Deardorff-velocity.

$$w_* = \sqrt[3]{\frac{g}{T} \frac{Q_H}{\rho c_p} z_i} = \sqrt[3]{\frac{g}{T} \overline{w'T'} z_i} \quad (24)$$

$$T_{*f} = \frac{Q_H}{\rho c_p w_*} = \frac{\overline{w'T'}}{w_*} \quad (25)$$

However, some authors proposed parameterisations for integral characteristics of wind velocity components, which contain  $z_i$  and use the characteristic velocity and temperature scales of the surface layer. Panofsky et al. (1977) proposed a prediction for the integral turbulence characteristic of the horizontal wind velocity as given in Equation ( 26 ) with parameters shown in

Table 4.

$$\frac{\sigma_x}{X_*} = C_1 \left( \frac{z_i}{L} \right)^{C_2} + C_3 \quad (26)$$

**Table 4:** Coefficients used in Equation ( 26 )

variable x	stability $\zeta$	$C_1$	$C_2$	$C_3$	authors	in figures referred to as
u	< -1	0.77	1/3	2	Panofsky et al. (1977)	(16) Panofsky 77

Equation ( 26 ) is valid only under conditions of free convection ( $\zeta < -1$ ). Here,  $\sigma_u/u_*$  is supposed to be a function of the dimensionless scaling parameter  $z_i/L$ . The use of a further dimensionless group, additionally to  $\zeta$ ,  $z_f/u_*$  and  $z/z_i$ , does not contradict the idea of Buckingham's  $\Pi$ -theorem (Section 2.4), as it can be derived directly from the other scaling parameters replacing one of them.

Peltier et al. (1996) derived an expression for the integral turbulence characteristics of the vertical wind velocity (Equation ( 27 )). Here, both relevant velocity scales of the atmospheric boundary layer are taken into account:  $u_*$  at neutral and slightly unstable stratification following

Monin-Obukhov similarity, and  $w_*$  in free convection. Johansson et al. (1999) supported this parameterisation, but found slightly modified coefficients after regression analysis.

$$\frac{\sigma_x}{X_*} = \sqrt{C_1 + C_2 \left( \frac{z}{L} \right)^{2/3} - 46 \left( \frac{z}{z_i} \right)^{4/3} \left( \frac{z}{L} \right)^{2/3}} \quad (27)$$

**Table 5:** Coefficients used in Equation ( 27 ) as given by various authors

variable x	$z/L = \zeta$	$C_1$	$C_2$	authors	in figures referred to as
w	< -0.2	1.6	3.7	Peltier et al. (1996)	(7) Peltier 96
	< -0.2	0.6	3.44	Johansson et al. (1999)	(8) Johansson 99

The minimising effect of  $z/z_i$  in Equation ( 27 ) vanishes with the growing height of the convectively mixed atmospheric boundary layer approaching  $(C_1 + C_2|\zeta|^{2/3})^{1/2}$ .

Summarising, we can state that some authors predict the integral turbulence characteristics of the wind velocities to scale with the mixing layer height  $z_i$ . These parameterisations are limited to the range of increasing instability with  $\zeta < -0.2$ .

### 3.4 Influence of the surface

The distribution of aerodynamical obstacles and varying surface parameters like canopy height and texture have a considerable effect on turbulent fluxes, and therefore on integral turbulence characteristics (DeBruin et al., 1991).

Large inhomogeneities in the order of 10-50 km affect the atmospheric boundary layer, whereas small scale irregularities in the order of 100 m to 1 km are assumed to influence only the surface layer and its quantities (DeBruin et al., 1991).

On a small scale, the surface roughness  $z_0$  is expected to influence atmospheric turbulence (see Section 2.2.2). The roughness length  $z_0$  can be derived graphically by extrapolating neutral wind profiles to a level where the wind speed equals zero (e.g. Stull, 1988). Empirical estimates of the

roughness length can be grouped by the type of terrain (Figure 2) or the average height of the roughness elements (Arya, 2001). However, Högström (1990) plotted near neutral  $\sigma_w/u_*$  data obtained at the fairly homogeneous Lövsta site as a function of  $\ln[(z - d)/z_0]$ . He found that the dimensionless height  $(z - d) / z_0$  is not the right scaling length for the integral turbulence characteristics of the vertical wind velocity.

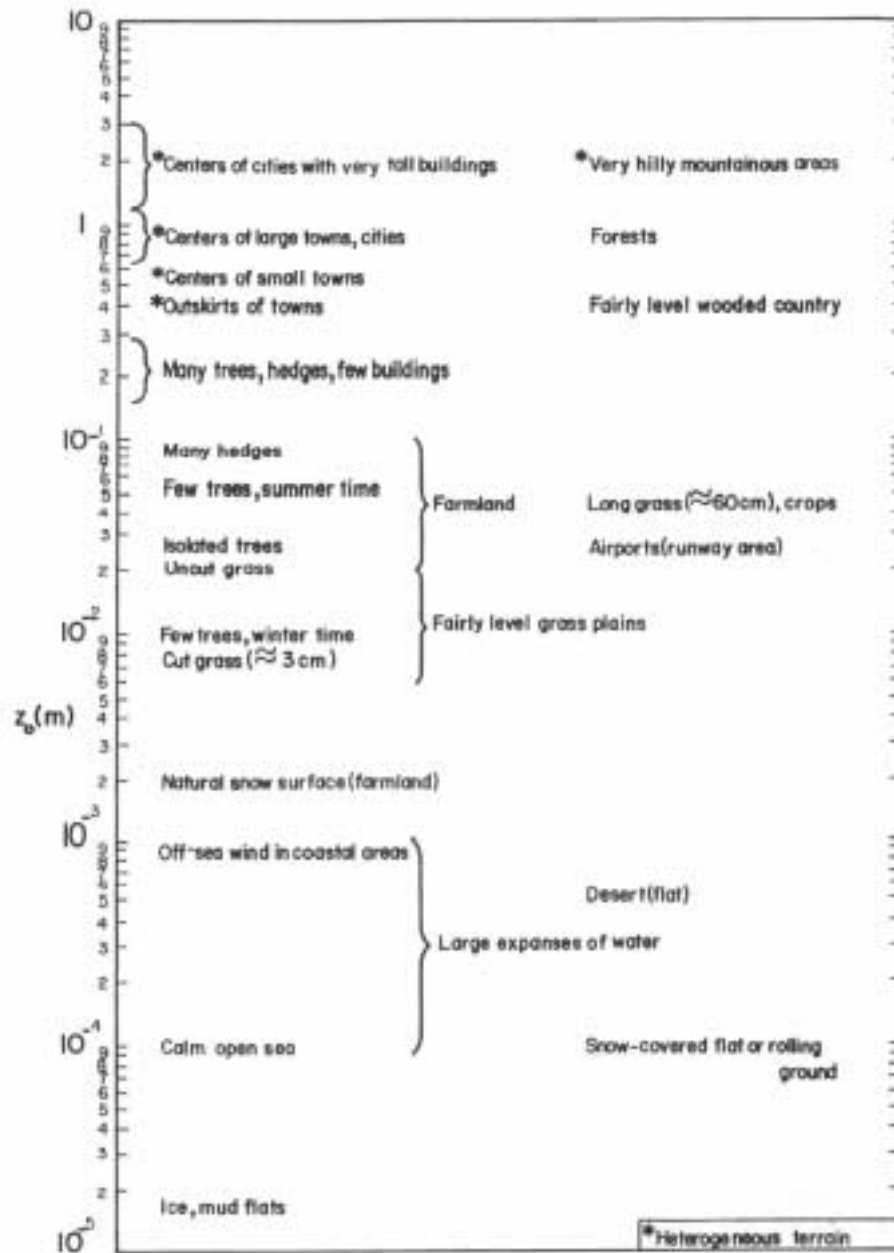


Figure 2: Typical values of the surface roughness  $z_0$  according to different types of terrain [From Tables by the Royal Aeronautical Society (1972), cited by Arya (2001)].

Based on turbulence data derived over uniform and non-uniform terrain at various sites in the Netherlands and France, DeBruin et al. (1991) came up with a way to estimate the effect of the surface on turbulent flow quantities. This concept neither involves concrete parameterisations nor suggests appropriate scaling factors. Nonetheless, it is crucial for the general applicability of integral turbulence characteristics and thus will be introduced below.

Among surfaces that are non-homogeneous on small scales, two different types can be distinguished according to DeBruin et al. (1991): *Type A* is characterised by a constant surface roughness, whereas the terrain consists of patches with different thermal properties. An example for a terrain of this type is an irrigated grassland field surrounded by dry land. A comparison between turbulent fluxes derived from eddy-covariance technique on one hand and using integral turbulence characteristics on the other hand yields that the integral turbulence characteristics method overestimates the sensible and latent heat fluxes over irrigated patches. The momentum flux however was not significantly distorted. Thus, terrain of type A seems to affect the temperature and humidity field but not the wind field. Strictly speaking, integral turbulence characteristics should therefore not be used to estimate the sensible and latent heat fluxes over such a terrain (Wichura and Foken, 1995). Hence, the  $\sigma_T/T^*$  and  $\sigma_q/q^*$  predictions are invalid. The terrain of *type B* is uniform, but covered with isolated aerodynamical obstacles. The typical Dutch landscape, consisting of meadows and obstacles like cows and isolated trees, serves as an example for this type. Here, the comparison of results obtained using eddy-covariance technique on one hand and integral turbulence characteristics on the other hand shows, that only the wind field was disturbed but not the temperature or humidity field. However, the applied integral turbulence characteristics method is still valid over terrain of type B (DeBruin et al., 1991). Thus, this concept provides a useful tool for estimating the effect of surface properties on integral turbulence characteristics and their general applicability.

Another concept that accounts for different surface properties is the aerodynamical height. Here, the geometrical height above ground  $z$  is replaced by the expression  $(z - d)$ , where  $d$  denotes the so-called displacement height. Assuming that the individual roughness elements are very close to each other, their top acts like a displaced surface. Thus, using  $(z - d)$  instead of  $z$ , the surface is virtually displaced upward by the magnitude of  $d$ . It is important to note that  $d$  is not equal to  $z_0$  as the wind velocity is expected to equal zero at the level  $(d + z_0)$ . In the surface layer one can distinguish between two parts: the roughness sublayer, where flow is distorted by roughness elements, and the inertial sublayer, where equilibrium theory is assumed to be valid (e.g. Rotach,

---

1993). Within the roughness sublayer, the displacement height can be interpreted as the level of mean momentum absorption (Thom, 1971). Several methods exist to estimate the displacement height using either turbulence measurements (Rotach, 1992) or the canopy height (Stull, 1988). Details will be given in Section 5.2.

Summarising, we can state that the surface has an effect on turbulent flow quantities (DeBruin et al., 1991; Högström, 1990; Rotach, 1992) and therefore on the general applicability of integral turbulence characteristics (DeBruin et al., 1991; Wichura and Foken, 1995).

## 4 Datasets

The main objective of this thesis is the re-evaluation of parameterisations and their scaling factors for integral turbulence characteristics derived by various authors. The parameterisations should be applied to datasets spanning a great range of possibly influencing parameters. Thus, statistically robust parameterisations of integral turbulence characteristics can be derived. Five datasets from different experiments were therefore selected, which were provided by the Department of Micrometeorology of the University of Bayreuth, the German Weather Service DWD and the Meteorological Service of the former GDR. The individual experiments will be characterised briefly in Sections 4.1.1 to 4.1.5, an overview over basic variables and experimental setups will then be given in Section 4.1.6. All datasets were obtained ensuring high data quality through careful quality control and using devices approved for micrometeorological research. Calculation of statistical parameters, filtering and correction were performed using the methods described in Section 4.2. An overview over the total amount of data will be presented in Section 4.3. The parameterisations were calculated using a self-written programme, which will be introduced briefly in Section 4.4.

### 4.1 Experiments

The experiments were carried out at different geographical latitudes (Figure 3), spanning from 52° North to 70° South. Surface properties varied from snow without any vegetation to cotton plantation with a slightly heterogeneous canopy layer of about 1m height. The sites were climatically classified using the climate index of Köppen (e.g. Hupfer, 1996). The climate types covered by this study are subtropical (C), tempered (D) and polar (F) climate in different specifications.

None of the experiments was especially designed for investigating integral turbulence characteristics; nevertheless they all provide useful datasets for this purpose.

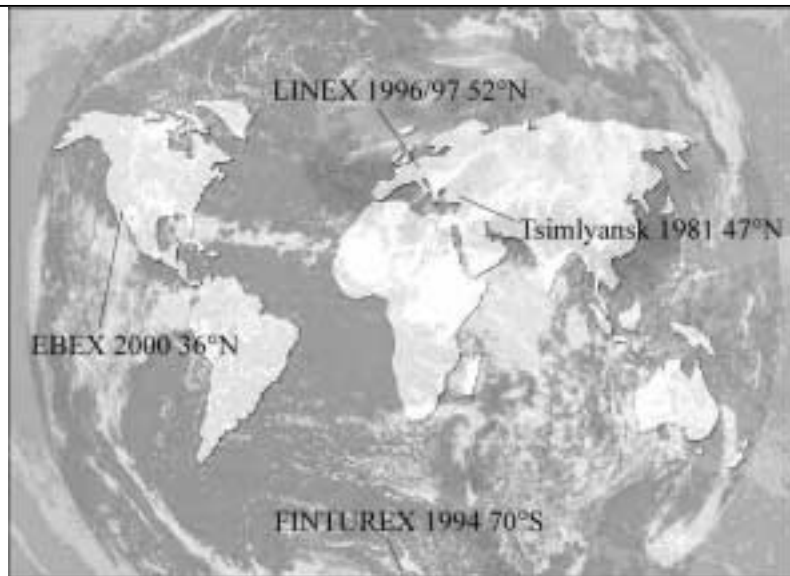


**Figure 3:** Geographical position and latitude of the experiments providing data basis for the re-evaluation.

#### 4.1.1 Tsimlyansk, 1981, USSR

The 4<sup>th</sup> International Turbulence Comparison Expedition (ITCE) was carried out near the village of Tsimlyansk in the former USSR in summer of 1981. This site is located at  $\sim 47^\circ$  North. The results of this experiment were published by Tsvang et al. (1985) and Foken and Haake (1984). The main objective of the expedition was to improve knowledge about the atmosphere-surface interaction in general and for applications like air pollution models and numerical weather predictions. Scientists from the USSR, CSSR, Poland, GDR and Bulgaria took part in this international expedition.

Meteorological measurements were performed using ultrasonic, hot-wire, cup and propeller type anemometers and different thermometer types as well as SODAR and aircraft-based devices within the atmospheric boundary layer, focussing especially on the surface layer.

When turbulence data were obtained, the weather was characterised by high summer temperatures of about  $30^\circ$  Celsius and low cloudiness under anticyclonic conditions. Easterly and north-easterly winds prevailed, with wind speeds of about  $4$  to  $7 \text{ ms}^{-1}$  in the surface layer. In mid-July, however, the weather in Tsimlyansk was temporarily influenced by cold fronts resulting in strong northerly to north-easterly winds, high cloudiness, nocturnal precipitation and temperatures of about  $18^\circ$  Celsius.

The surface was covered by vegetation with a fairly homogeneous spatial distribution, classified as non-irrigated short grass steppe with an average canopy height of 0.4 m. Thus, individual patches of vegetation were expected not to differ in thermal properties. According to the concept of estimating the influence of the surface (Section 3.4), the site belongs to type B, but with uniform dynamical properties. Hence, integral turbulence characteristics are assumed to be undistorted and should therefore to be suitable for re-evaluating their parameterisations and scaling factors.

#### **4.1.2 FINTUREX, 1994, Antarctica**

The experiment FINTUREX (Foken, 2002; Foken and Baum, 1994) was carried out at the Neumayer-Station in Antarctica from January until March 1994. The site is located at 70° South.

Data were obtained using ultrasonic anemometers and towers equipped with meteorological standard devices like cup anemometers and psychrometers. Observations were supplemented by radiosondes.

During the campaign, the meteorological conditions of the surface layer were dominated by mean wind velocities of  $\sim 6 \text{ ms}^{-1}$  with peaks up to  $14 \text{ ms}^{-1}$  at a height of 2 m. The strong winds temporarily lead to heavy snow drift. Snowfall was observed on 4 days during the measuring period. The stratification of the surface layer was often found to be stable even during daytime.

The surface was covered with loose snow. The shape of the snow was constantly changed due to snow drift and snow fall. The displacement height was determined to equal zero. According to the concept of the influencing effect of the surface, the site belongs to type B with also uniform dynamical properties, providing ideal conditions for turbulence measurements. However, the turbulence measurements were often affected by high wind velocities and stable stratification.

### **4.1.3 LINEX 96/2, 1996, Germany**

The LINEX 96/2 experiment (Foken et al., 1997a; Foken et al., 1996) was carried out at the site ‘Gemeinsames Messfeld’ of the Meteorological Observatory Lindenberg, Germany at 52° North. The main objective of this campaign was to determine the surface properties of the given site according to DeBruins concept (DeBruin et al., 1991; Wichura and Foken, 1995), with special focus on internal boundary layers (Jegade and Foken, 1999). Additionally, intercomparison studies for different types of sonic anemometers and fast response sensors for temperature and humidity fluctuations were performed.

The turbulence measurement complexes consisted of sonic anemometers and fast response humidity and temperature probes. Towers, equipped with slow response devices like cup anemometers and psychrometers, were used to obtain mean meteorological parameters. Observations were supplemented by radiosondes and tethered balloon sonde measurements.

The synoptical conditions during the field campaign were rather unstable. Frequently changing cyclonic and anticyclonic fronts lead to alternating cloudiness and changing mean air temperatures.

The measurement site was covered by homogeneously distributed grass of about 0.7 m height during the period of measurements. The Leaf Area Index was estimated to about 2. The site was surrounded by corn fields with an average height of 0.4 m during the considered period of time. Foken et al. (1997a) classified the measurement site as a non-homogeneous terrain of type A. The momentum flux was assumed to not be affected by these inhomogeneities. Hence, the acquired turbulence data is considered as to be suitable for investigating the integral turbulence characteristic of the vertical and horizontal wind velocities.

### **4.1.4 LINEX 97/1, 1997, Germany**

The LINEX 97/1 experiment (Foken, 1998; Foken et al., 1997b) was carried out in May/June, 1997 as a follow-up study of LINEX 96/2. For geographical position and general information see the previous section. The micrometeorological instrumentation described above was complemented by a SODAR device and the Helipod technique.

In the first half of June, the weather was dominated by an anticyclone without precipitation, with winds coming from East to South. The maximum air temperature was about 22° Celsius. After the passage of a thunderstorm front from 11 June until 13 June, cyclonic conditions prevailed until the end of the measurements. Thus, high cloudiness and precipitation were observed, leading to decreased maximum air temperatures of about 15° Celsius. The synoptical situation was characterised by instationarities and was therefore disadvantageous for micrometeorological measurements.

In contrast to the LINEX 96/2 experiment, the surface of the measurement site was covered by short grass of about 0.3 m height. The Leaf Area Index was estimated to about 2.5. The site was surrounded by wheat fields of about 1 m height. Foken et al. (1997a) classified the measurement site as a non-homogeneous terrain of type A.

#### **4.1.5 EBEX-2000, 2000, USA**

The Energy Balance Experiment was carried out in July/August, 2000 (Oncley et al., 2000; Bruckmeier et al., 2001). The site is located in California, between Hanford and Kettleman City at 36° North. The main objectives of this international experiment were the exact determination of all terms of the energy balance with respect to the energy balance closure problem, intercomparison of different turbulence measurement devices and intercomparison of different data processing methods.

The turbulence data were obtained using sonic anemometers in conjunction with fast response temperature and humidity probes. Mean values of meteorological parameters were obtained at towers equipped with cup anemometers and aspiration psychrometers. The tower measurements were supplemented by SODAR measurements.

During the whole measuring period of 1 month, the weather was hot and humid. No precipitation events were recorded. Little or no clouds were observed, with cloudiness ranging from 1/8 to 3/8. The prevailing anticyclone resulted in high mean air temperatures of about 35° Celsius. The mean wind speed during daytime at 4.7 m above ground was recorded as 2.5 ms<sup>-1</sup> with peaks up to 5 ms<sup>-1</sup>. Wind directions were mainly north-westerly, northerly and north-easterly. During night, however, winds were persistently coming from the west.

The surface was covered with irrigated cotton fields of about 1 m canopy height. The site can be classified as a non-homogeneous terrain of type A, but with homogeneous thermal conditions of

the underlying surface due to the fact that all fields were irrigated. Referring to DeBruin et al. (1991), the heat fluxes over heterogeneous, patchy terrain would only be distorted due to differing thermal properties of the patches. Thus, we can assume the heat fluxes of EBEX-2000 to be undistorted. The momentum flux of type A terrain was not found to be influenced by the heterogeneity of the canopy layer (Section 3.4). Hence, the data obtained at this site are suited for investigations of integral turbulence characteristics.

#### **4.1.6 Overview and experimental setups**

In this section, an overview of the essential parameters of all experiments will be given. Table 6 contains general information about the experiments, the geographical positions, surface properties and the measuring devices used. The displacement heights  $d$  in Table 6 were calculated using methods described in Section 5.2. The surface roughness parameters  $z_0$  were determined graphically as described in Section 3.4 or estimated from Figure 2.

**Table 6: Overview of basic parameters of the experiments providing the database for this thesis**

<b>Experiment</b>	<b>Tsimlyansk</b>	<b>FINTUREX</b>	<b>LINEX 96/2</b>	<b>LINEX 97/1</b>	<b>EBEX-2000</b>
year	1981	1994	1996	1997	2000
country	USSR	Antarctica	Germany	Germany	USA
latitude	47° N	70° 39' S	52° 10' N	52° 10' N	36° 06' N
longitude	42.5° E	08° 15' W	14° 07' E	14° 07' E	119° 56' W
altitude above sea level [m]	~ 50	40	73.1	73.1	67
climate after Köppen (Hupfer, 1996)	Dc	Ft	Do	Do	Cs
measurement period	30/06/81 – 24/07/81	21/01/94 – 19/02/94	16/06/96 – 24/06/96	02/06/97 – 24/06/97	08/08/00 – 24/08/00
surface cover	grass	snow	long grass	short grass	cotton
canopy height [m]	0.4	-	0.7	0.3	1
mean displacement height d [m]	0.25	0	0.48	0.23	0.65
roughness length $z_0$ [m]	0.03	0.0005	0.02	0.005	0.1
Leaf Area Index	2	0	2	2.5	2.5
surface type (DeBruin et al., 1991)	B uniform in $u^*$	B uniform in $u^*$	A	A	A
measuring height of turbulence complex above ground [m]	4.5/4/4.2/2.2	1.9/1.8/1.75 1.7/1.65	2.1	2.05	4.1
sonic anemometer	Kaijo Denki DAT- 300 A-Probe	Kaijo Denki DAT- 310 A-Probe	Kaijo Denki DAT- 310 A-Probe	Kaijo Denki DAT- 310 A-Probe	Campbell CSAT 3

## ***4.2 Reprocessing of the experimental data***

The raw turbulent data were obtained from the turbulence measurement complexes and devices presented in Table 6. The turbulent fluxes of momentum, sensible heat and latent heat were calculated according to Equations ( 2 ), ( 3 ) and ( 4 ) respectively.

The turbulence measurements were carried out in high frequency sampling mode with sampling rates of 20 Hz, the CSAT 3 was operated in an oversampling mode at 60 Hz with subsequent averaging to 20 Hz data. The process of calculating statistical parameters and quality control was done by various software tools. Further processing of the data obtained during FINTUREX, the LINEX experiments and EBEX-2000 was performed by a program, which will be introduced in Section 4.2.1. After calculation of the covariances for a 30 min-interval, a spectral correction after Moore (1986) was applied (Section 4.2.2).

### **4.2.1 Calculation of statistical parameters and quality control**

Turbulent fluctuations of wind velocities were measured at high-frequent sampling rates. The 20 Hz data was recorded by loggers. The following calculation of the needed covariances (Equation ( 2 ), ( 3 ) and ( 4 )) was done by software tools. Due to new developments and increasing computing power during the period between Tsimlyansk 1981 and EBEX-2000, no uniform tool was applied. In the case of FINTUREX, the LINEX experiments and EBEX-2000 calculation of statistical parameters was performed using the TXX-software. A special version of this software tool was applied to each experiment. The output consists of 5-min means of the desired data. The further reprocessing was done using the software ‘Der Bayreuther Turbulenzknecht’ (Foken, 1999). This programme provides calculation routines and a quality control programme.

The programme ‘Der Bayreuther Turbulenzknecht’ includes a quality control tool based on three routines, namely tests of stationarity, integral turbulence characteristics and inclination/orientation of the sonic anemometer (Foken and Wichura, 1996). Based on these test routines, a quality flag is calculated. Quality flags are calculated for the friction velocity and turbulent fluxes of sensible and latent heat. In general, the data classified by quality flags ranging from 1 to 3 are suited for micrometeorological research purposes (Foken, 1999). The test of integral turbulence characteristics implements the parameterisations presented in Equation ( 15 ) with coefficients after Foken et al. (1996) and Foken et al. (1997). The use of these test routines in

order to filter data for investigating integral characteristics appears to be questionable, because it might be that data is removed only due to invalid, non-universal parameterisations. However, a quality flag of 3 indicates that only steady-state conditions have to be fulfilled, implying that the test of integral turbulence characteristics does not affect the selection of data. This test method comes into play when the quality flag is greater than 3. Where quality flag data were available, data with quality flags from 1 to 3 were selected. Due to the high wind velocities during FINTUREX, resulting in distorted measurements through snow drift, the dataset was selected for horizontal wind velocities below  $5 \text{ ms}^{-1}$ .

### 4.2.2 Spectral correction

The spectral correction method after Moore (1986) was applied to the turbulence data. The underlying theory is that so-called ‘spectral losses’ occur during measuring and reprocessing atmospheric turbulence as a result of losses caused by instruments and processing software. These spectral losses are differences between the measured and the theoretical energy density spectra (Moore, 1986). Thus, they result in underestimated flux data and have to be compensated. The spectral correction after Moore (1986) was found to be essential for turbulence data (e.g. Foken, 1990). This correction method was therefore applied to the data of all experiments.

### 4.3 Overview over the database

Table 7 gives an overview over the amount of data in each dataset. The individual integral turbulence characteristics data were split into four classes of atmospheric stability: the stable range for  $\zeta > 0.1$ , the near neutral range for  $0.1 > \zeta > -0.2$ , the unstable range for  $-0.2 > \zeta > -1$  and the range of free convection for  $\zeta < -1$ . The borders of these stability classes were defined in dependence on the total amount and distribution of data within a dataset of all five experiments and in some respect to the critical stability values representing different turbulence regimes (Skeib, 1980). Quality filter methods could only be used for the datasets of LINEX 97/1 and EBEX-2000 due to quality flag data availability.

Most of the data lie in the near neutral and slightly stable range with  $\zeta > -0.2$ . The amount of data in the unstable range with  $-1 < \zeta < -0.2$  is small compared to the amount of data with  $\zeta > -0.2$ . Under conditions of free convection with  $\zeta < -1$ , only few  $\sigma_w/u^*$ ,  $\sigma_u/u^*$  and  $\sigma_T/T^*$  data

are available. As we can see from the LINEX 97/1 and EBEX-2000 values, filtering of data with quality flags ranging from 1 to 3 removes about 35 % of the total amount of available raw data series.

**Table 7: Overview of the datasets before and after filtering and application of spectral correction as a function of atmospheric stability classes**

Experiment	Tsimlyansk	FINTUREX	LINEX 96/2	LINEX 97/1	EBEX-2000	$\Sigma$
averaging period [min]	34	30	30	30	30	-
amount of data series	69	183	405	316	705	1678
amount of filtered $\sigma_{w,u}/u^*$ series	69	183	405	207	430	1294
$\zeta > 0.1$	0	65	93	46	110	314
$0.1 > \zeta > -0.2$	59	103	293	148	250	853
$-0.2 > \zeta > -1$	9	11	9	10	57	96
$-1 > \zeta$	1	4	10	3	13	31
amount of filtered $\sigma_T/T^*$ series	69	183	405	100	145	902
$\zeta > 0.1$	0	65	93	14	43	215
$0.1 > \zeta > -0.2$	59	103	293	78	78	611
$-0.2 > \zeta > -1$	9	11	9	6	23	58
$-1 > \zeta$	1	4	10	2	1	18

#### ***4.4 Calculation of parameterisations***

The parameterisations of integral turbulence characteristics described in Chapter 3 were calculated using a self-written Fortran-programme called ‘parameterisierungen’. The programme requires the geographical latitude, displacement height and source data file name of the experiment as input before calculating the parameterisations. The format of these source data files is based on the XZYYTTzu.NNd output file of the programme ‘Der Bayreuther Turbulenzknecht’ (see Foken, 1999) with additional columns for required parameters. The source data file contains the measured values of the turbulent fluxes and their assigned quality flags, integral turbulence characteristics, atmospheric stability, measuring height, wind direction, horizontal wind velocity and the computed values of the mixing layer height with a resolution of 30 minutes. The programme output was recorded in output-files, which contain the measured integral turbulence characteristics, atmospheric stability as well as the predicted values and scaling factors. Additionally, a stability flag is assigned to each predicted value, providing information about the turbulent regime as a function of the atmospheric stability.

## 5 Calculation of additional input parameters

Integral turbulence characteristics are assumed to scale with various local and non-local parameters, as laid out in Chapter 3. The following variables are needed in order to calculate the described integral turbulence characteristics predictions: the height above ground  $z$ , the Obukhov length  $L$ , the mixing layer height  $z_i$ , the friction velocity  $u_*$ , the displacement height  $d$  and the geographical latitude  $\phi$ .

The height above ground is derived from the experimental setup, the geographical latitude is defined by the geographical position of the site. The friction velocity and the Obukhov length are obtained through eddy covariance method using Equations ( 2 ) and ( 5 ). Thus, the mixing layer height and the displacement height remain to be determined.

The definition of the mixing layer height, its determination and the technique applied in this thesis will be presented in Section 5.1. The applied methods for the determination of the displacement height are given in Section 5.2.

### 5.1 Determination of the mixing layer height

A short introduction into mixing layer height determination, its definitions will be given now (Seibert et al., 1998). Several definitions exist for  $z_i$  depending on the purpose it is needed for. The diurnal dynamics of the atmospheric boundary layer were introduced in Section 3.3. According to Figure 1, firstly, the height of the capping inversion, limiting the exchange of momentum and matter to an upper boundary, is referred to as the height of the convective boundary layer  $z_i$  (e.g. Arya, 2001). Secondly, Seibert et al. (1998) defined  $z_i$  as the height of the layer over which any constituent emitted within the convective boundary layer or entrained into it becomes vertically dispersed by convection or mechanical turbulence. As there is no distinct boundary between well-mixed and stably stratified layers in the atmosphere, the mixing height cannot be determined exactly under real atmospheric conditions. Rather, a so-called entrainment layer is introduced above the convective boundary layer. It represents the transition zone between the well-mixed conditions below and the stably stratified capping inversion above. High energy thermals can penetrate through this layer into the inversion from below and its dry and warm air can in turn entrain downward into the well-mixed layer. Thus, thirdly, the mixing layer height is practically defined as the average height of this entrainment layer.

$z_i$  can be either estimated from meteorological data or calculated by computer routines. If meteorological data from radiosoundings, tethered balloons, masts, aircrafts, SODAR, LIDAR, Radar or wind profilers is available in a sufficient temporal resolution, this methods must be preferred for estimating the mixing layer height (Seibert et al., 1998). In absence of such meteorological data,  $z_i$  can be estimated using calculation methods such as meteorological preprocessors, methods based on Richardson numbers or the so-called parcel method. The parcel method, introduced in Section 5.1.1, is the most reliable method under convective conditions (Seibert et al., 1998). The boundary layer model by Blackadar (1997) (section 5.1.2) provides estimates of the mixing layer height using the parcel method and was therefore used in this study.

### 5.1.1 Parcel method

The parcel method is briefly presented in this section (Seibert et al., 1998). The mixing layer height is calculated as the equilibrium level of an air parcel, hypothetically released at the ground and rising through the convective boundary layer. Various methods differ in defining the thermodynamical equilibrium level and determining the temperature of the air parcel.

The simple parcel method was first published by Holzworth (1964). The considered air parcel is assumed to have the virtual potential temperature at the ground level derived from a radiosounding. The mixing height is determined as the equilibrium level with the same temperature as the air parcel.

The advanced parcel method is based on Beljaars and Betts (1992), who assume that the air parcel has the temperature of the ground level plus an excess temperature  $\delta\Theta_v$ . The excess temperature is calculated by (Holtslag et al., 1990; Troen and Mahrt, 1986).

$$\delta\Theta_v = \frac{C_1 \overline{w'\Theta'_v}}{\sqrt[3]{u_*^3 + C_2 w_*^3}} \quad (28)$$

where  $\Theta'_v$  is the fluctuation of the virtual potential temperature defined as  $\Theta_v = \Theta (1 + 0.61 q)$  with  $q$  denoting the specific humidity of air and  $w_*$  as defined in Equation ( 24 );  $C_1$  and  $C_2$  are

constants with  $C_1 = 20$  and  $C_2 = 0.6$  (Seibert et al., 2000). Figure 4 illustrates the determination of the mixing layer height corresponding to both methods.

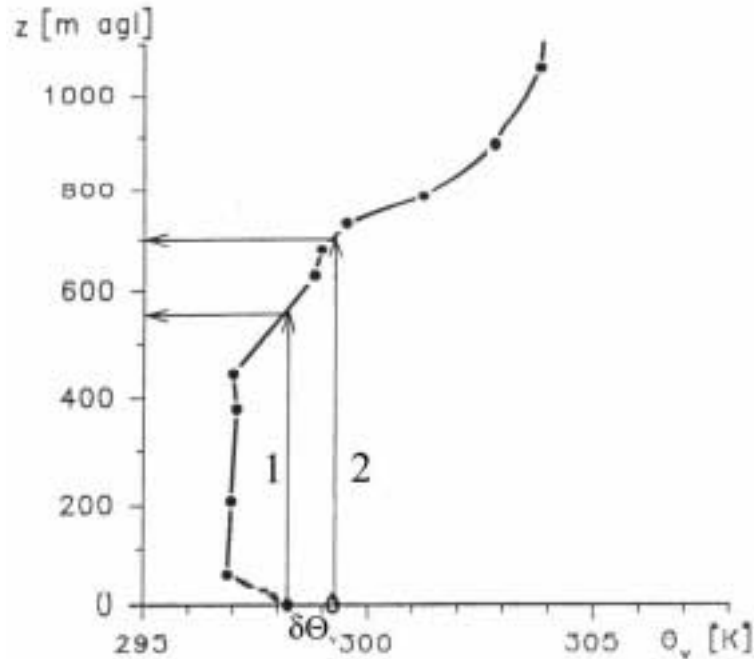


**Figure 4:** Illustration of the simple (1) and the advanced (2) parcel method used to derive the mixing layer height  $z_i$  (Seibert et al., 1998, changed).

### 5.1.2 Boundary layer model after Blackadar (1997)

The boundary layer model by Blackadar (1997) was used in this study to calculate the mixing layer height as an additional input parameter for the integral turbulence characteristics predictions described in Section 3.3.

The model is a one-dimensional, time-dependent model simulation of the planetary boundary layer. Existing three-dimensional versions are used in the Penn State–NCAR mesoscale model and the U.S. National Acid Deposition Model. The model consists of 30 layers  $n_i$ , with a thickness of 100 m each, starting at 10 m above ground. For each layer midpoint, located at  $(n_i + 10)$  m, the budgets of internal energy, specific humidity, liquid water content and horizontal momentum are kept while simulating. The turbulent fluxes and their generating parameters are calculated for all interfaces between the individual layers at every 2-min time step. In absence of free convection, a K-closure parameterisation is used, with K depending on the wind shear and

the Richardson number. The K-parameters are the turbulent exchange coefficients for momentum, heat and moisture (Kaimal and Finnigan, 1994). If the ratio  $w^*/u^*$  exceeds 1/3, the model switches to a free-convection simulation based on the concept of the parcel method and starts to compute the mixing layer height.  $z_i$  is determined using the entrainment layer concept mentioned above. Below the lowest layer, the model assumes a 10 m thick surface layer obeying the Monin-Obukhov similarity. Additionally, a vegetation layer is placed into this surface layer, interacting with radiation and the air of the surface layer. Under the surface layer lies the ground surface, receiving the radiation from the overlying vegetation and radiating upwards as a black body. Interaction with the surface layer and the layers above is realised through the backscatter of the incoming short-wave radiation as defined by the albedo.

The model calculates profiles of temperature, dew point and wind speed as a function of height up to 2000 m above ground. In addition to these basic parameters, the mixing layer height and potential cloud formation is calculated every 10 minutes. The computed surface temperatures and the mixing layer height are recorded in an output file, whereas the profiles are displayed as graphs.

The initial values for the individual runs are read from data files, selected before starting the model. This input file includes among other variables: meteorological surface layer parameters such as wind speed, temperature and humidity; basic surface properties like albedo, roughness length and fraction of surface covered with vegetation; geostrophic wind components; information about the site and time of the year, i.e. geographical latitude and declination of the sun; synoptical data like cloudiness. In addition to the surface data, the initial values of wind speed, mixing ratio and temperature for all midpoints of the 30 layers have to be given. Appendix A gives a detailed list of all variables needed for input.

The input files were adapted for all experiments, one for each day. Initial data for the surface layer was obtained from turbulence or tower measurements, while initial values for the layers up to a height of 3000 m were derived from available radiosonde data. In case of the experiment EBEX-2000, only SODAR data up to a height of ~ 500 m were available. The starting time of the model was set to the starting time of the radiosonde or to 05:00 Standard Local Time, in the case of continuous SODAR data.

**Table 8: Overview of the initial input data files used for the boundary layer model by Blackadar (1997). Starting time is indicated in Standard Local Time.**

<b>Experiment</b>	<b>Tsimlyansk</b>	<b>FINTUREX</b>	<b>LINEX 96/2</b>	<b>LINEX 97/1</b>	<b>EBEX-2000</b>
amount of initial input data files	-	19	11	10	17
starting time [SLT]	-	12:00	06:00	06:00	05:00
source of initial profiles	-	radiosondes	radiosondes	radiosondes	SODAR
source of initial surface data	-	turbulence complex/ tower	turbulence complex/ tower	turbulence complex/ tower	turbulence complex/ tower

Wherever input data was missing, they were added using the best matching standard input file provided with the boundary layer program. For the Tsimlyansk experiment, neither radiosonde nor Doppler SODAR data were available. Here, a daily standard development of the mixing layer height as a function of local time was assumed (Appendix A). The mean of three subsequent model runs was taken as the value of the mixing layer height for the calculation of integral turbulence characteristics parameterisations.

## ***5.2 Determination of the displacement height***

The displacement height  $d$  is needed for the calculation of the term  $(z - d)$  in Equation ( 23 ). The expression  $(z - d)$  is called the aerodynamical height (Section 3.4). In this study, two possible methods for the determination of  $d$  were selected. Firstly, the concept given by Rotach (1992) was used, which was recommended by Wichura and Foken (1995) and applied in this study to datasets obtained over terrain of type A. Secondly, a more general and simple concept for estimating  $d$  was used for the datasets where the first method did not yield reliable results.

The method by Rotach (1992) involves integral turbulence characteristics in order to determine  $d$ . Assuming that the shape of  $\sigma_T/T^*$  can be well predicted by an arbitrary parameterisation of the

corresponding integral turbulence characteristic, the root-mean-square difference between the measured and the predicted value can be used for the calculation of  $d$  (Equation ( 29 )). When plotting the calculated root-mean-square difference against assumed values of  $d$ , the displacement height can be identified as the value for  $d$  at the graph's minimum.

$$\text{rmsd} = \sqrt{\frac{1}{N-1} \sum \left[ \left( \frac{\sigma_T}{T_*} \right)_{\text{measured}} - \left( \frac{\sigma_T}{T_*} \right)_{d^*, \text{predicted}} \right]^2} \quad (29)$$

where rmsd is the root-mean-square difference and  $N$  the amount of data used for the calculation.  $(\sigma_T/T^*)_{d^*, \text{predicted}}$  depicts the integral turbulence characteristic prediction with different values assumed for  $d$ . In the parameterisation,  $z$  is replaced by  $(z - d)$ , while  $d$  is denoted by  $d^*$  and varied from the largest possible value (i.e. the canopy height) downwards. Here, the predicted values of  $\sigma_T/T^*$  were computed using the universal function after Skeib (1980) with coefficients after Foken et al. (1991).  $d$  has to be determined as a function of the wind direction (Rotach, 1992). Hence the  $\sigma_T/T^*$  data were subdivided into 8 wind direction sectors of  $45^\circ$  each, starting clockwise from  $1^\circ$ .

The result for the sector  $1 - 45^\circ$  is given in Figure 5. For the other sectors ( $46 - 360^\circ$ ), the method did not yield reliable results mainly due to small amounts of data. For the EBEX-2000 site, the displacement height was determined as 0.65 m.

The more simple method for estimating the displacement height is given in Equation ( 30 ) (e.g. Kaimal and Finnigan, 1994). Here,  $d$  is assumed as  $2/3$  of the average canopy height  $h_c$ . The results derived for the displacement height of each experimental site are given in Table 6. As the displacement height  $d$  increases with increasing canopy height  $h_c$  during an experiment, the values listed in Table 6 represent mean  $d$  values for the total duration of the experiments.

$$d = \frac{2}{3} h_c \quad (30)$$

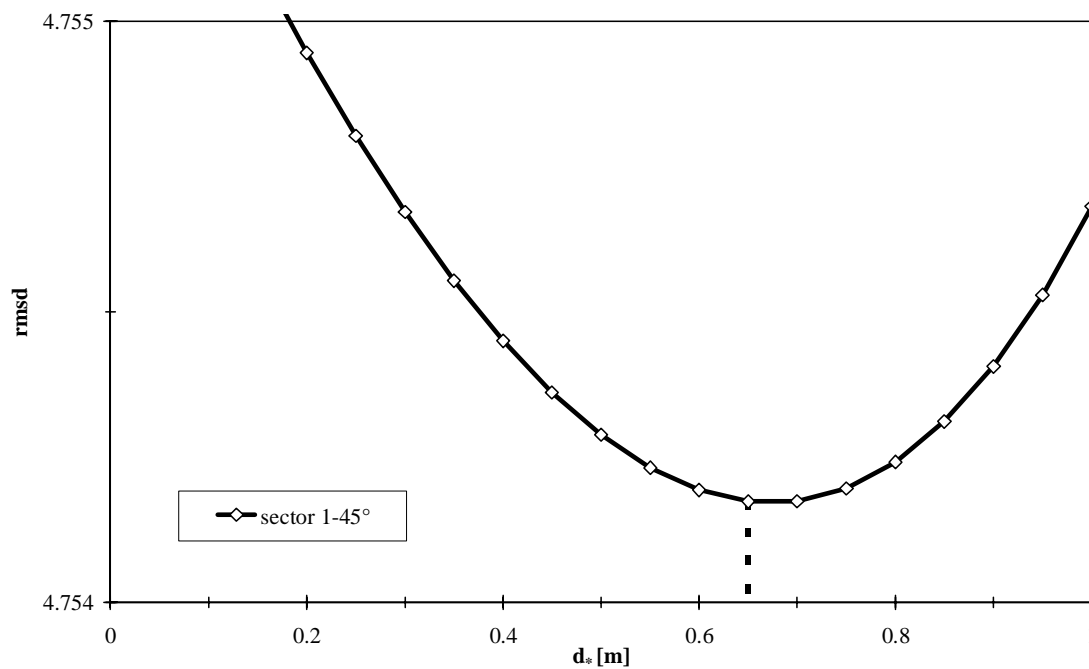


**Figure 5:** Root-mean-square difference as a function of the assumed value of the displacement height  $d_*$  for EBEX-2000, wind direction sector 1 - 45°. The amount of data for this sector is 41.

## 6 Results and discussion

In this chapter, the results of the re-evaluation of the parameterisations of integral turbulence characteristics will be presented and a new scaling factor will be derived. The integral turbulence characteristics of the wind velocity components are presented and discussed in Section 6.1, those of the temperature in Section 6.2. A comparison between the findings of this study with the results derived by other authors will be presented in Section 6.3.

The results will be presented in figures, where the x-axis depicts the chosen scaling factor and the y-axis the measured and/or predicted value of the corresponding integral turbulence characteristic

### 6.1 Wind velocity components

In the following sections, the measured data of  $\sigma_w/u_*$  and  $\sigma_u/u_*$  and the corresponding predicted integral turbulence characteristics will be discussed. According to Chapter 3, the results will be presented as a function of  $\zeta$  and  $\ln[f(z-d)/u_*]$ , representing the atmospheric stability and the pressure gradient length scale involving the geographical latitude, respectively. The parameterisations including  $z/z_i$  and  $\zeta$  terms will be presented as a function of  $\zeta$ . The discussions will first deal with the stable and near neutral data, before analysing the unstable data.

#### 6.1.1 Vertical wind component

The observed  $\sigma_w/u_*$  data of all experiments are shown in Figure 6 as a function of  $\zeta$  with  $\zeta$  ranging from -1 to 0.5. The chosen axis intercepts will be the same in nearly all figures, to ensure the comparability of the presented results. According to Table 7, most of the experimental data lies in the near neutral range of approximately  $-0.2 < \zeta < 0.1$ . The unstable data for  $\zeta < -0.2$  were mostly obtained at EBEX-2000, FINTUREX and LINEX 97/1. The stable range  $\zeta > 0.1$  contains data from all experiments except the Tsimlyansk data. This is due to the fact that only unstable, daytime data were available from the Tsimlyansk experiment. Most of the measured values of  $\sigma_w/u_*$  vary between about 0.5 and 2.5, concentrating in the range from 1 to 2. However, a distinct group of data with  $\sigma_w/u_* < 1.1$  does not match this general pattern. These data were recorded during EBEX-2000 and FINTUREX and were excluded from further analysis for reasons discussed below.

The scatter of data within the near neutral range is large, and it is difficult to get a clear picture of the behaviour of  $\sigma_w/u_*$  within this range. The unstable data show slightly, but systematically decreasing values towards neutrality. This trend seems to be non-linear, following a power law. The stable data show differing trends among various experiments: the EBEX-2000 data remain constant at values for  $\sigma_w/u_*$  of about 1.3 with increasing stability. In contrast, the LINEX 96/2 and LINEX 97/1 data increase non-linearly with increasing stability, becoming constant only at  $\zeta \approx 0.4$ . The FINTUREX data on the other hand do not show a clear dependence on  $\zeta$  under stable conditions.

Figure 7 plots the near neutral data against  $\ln[f(z - d)/u_*]$ . The picture obtained this way is obviously very different from Figure 6: here all experimental data seem to fit a trend without large scatter when the  $\sigma_w/u_*$  data group below 1.1 is excluded. Now the values of  $\sigma_w/u_*$ , representing different geographical positions, follow a clear general pattern. Choosing  $\ln[f(z - d)/u_*]$  instead of  $\zeta$  as the scaling factor for integral turbulence characteristics thus seems to remove systematical differences among the datasets in the considered stability range. From Figure 7 we have the indication that the expression including the geographical latitude is the appropriate scaling factor for near neutral data. This intuitive statement must be confirmed by further statistical examination and will be illustrated using the LINEX 96/2 data (Figure 8 and Figure 9).

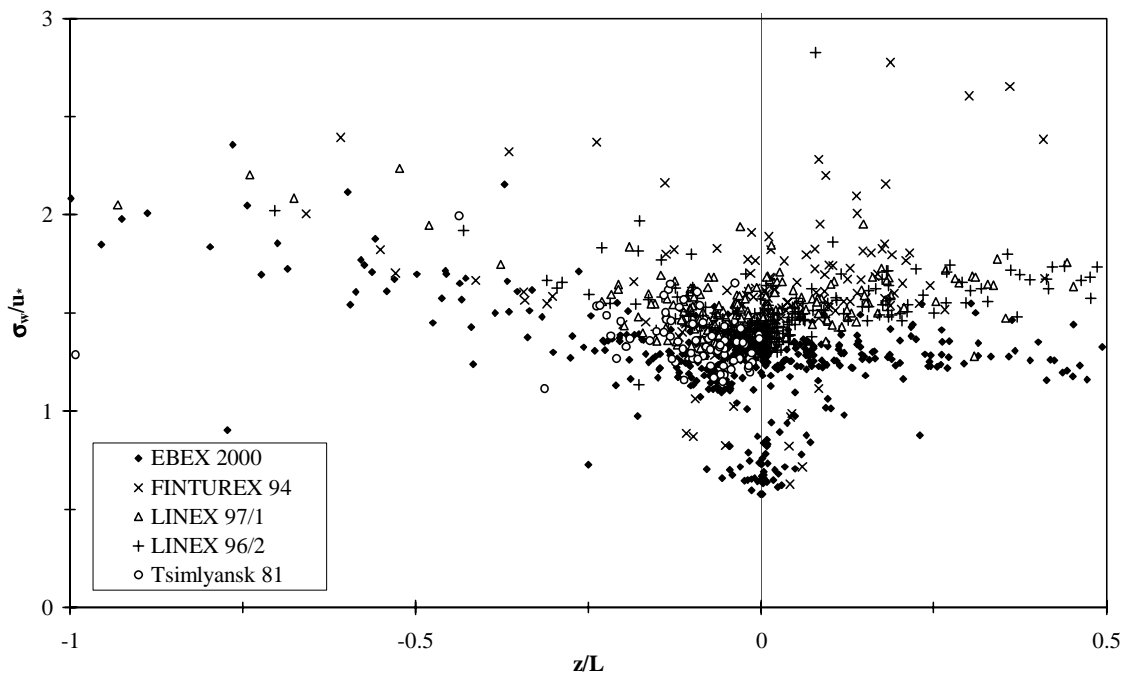


**Figure 6:** Measured  $\sigma_w/u_*$  data as a function of  $\zeta$ . The Figure contains data of all experiments with  $\zeta$  ranging from -1 to 0.5.

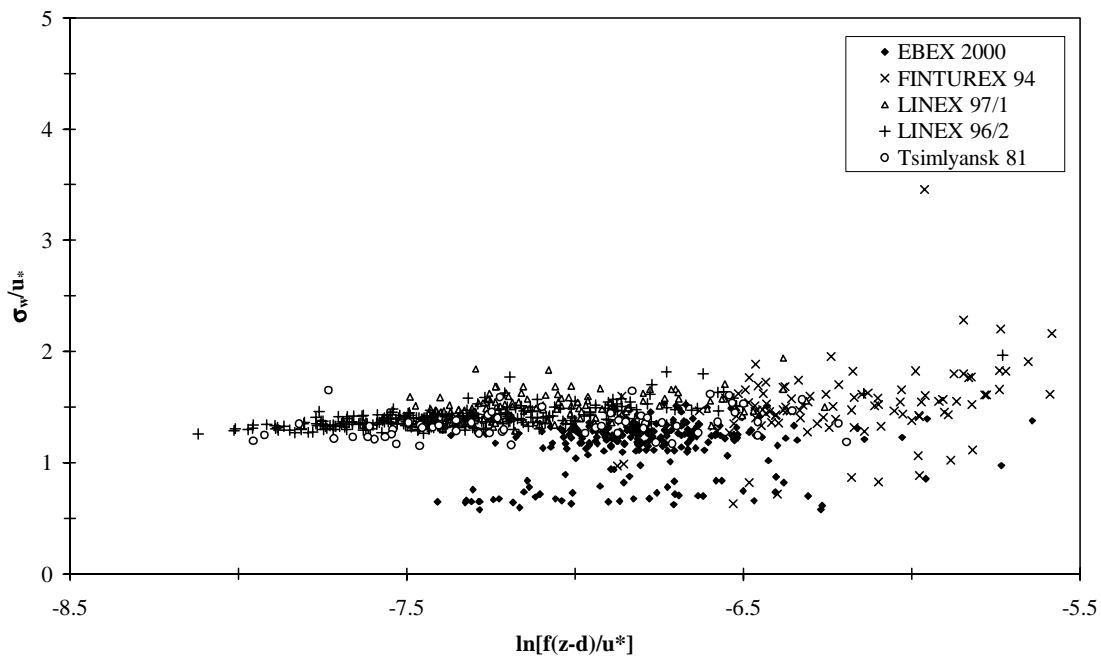


**Figure 7:** Measured  $\sigma_w/u_*$  data as a function of  $\ln[f(z-d)/u_*]$ . The Figure illustrates data of all experiments selected by  $-0.2 < \zeta < 0.1$ .

No uniform behaviour of  $\sigma_w/u_*$  can be derived using the  $\zeta$  scaling factor (Figure 8). The values decrease with decreasing instability, around neutral no clear picture can be observed, and in the stable range the values seem to increase with increasing stability. The proposed parameterisations only partly follow the observed data. When plotting the data as a function of  $\ln[f(z - d)/u_*]$ , the data look much more uniform and show a linear trend (Figure 9). The parameterisations seem to systematically underestimate the observed  $\sigma_w/u_*$  data, but match their overall shape. Performing correlation analysis for all experiments and predictions, one can find the following results:

**Table 9: Results of the correlation analysis between the predicted values derived from parameterisations illustrated in Figure 8 and 9 and the observed experimental data of the corresponding experiment. Data were selected for  $-0.2 < \zeta < 0.1$ . A dash denotes that no correlation coefficient R could be determined.**

scaling factor	parameterisation	correlation coefficient R				
		Tsimly-ansk	FINT-UREX 94	LINEX 96/2	LINEX 97/1	EBEX-2000
$\zeta$	(1) Wyngaard 71	-	-	-	-	-
	(2) Foken 91	0.41	<0.00	0.35	<0.00	<0.00
	(5) Panofsky 77	0.37	<0.00	0.26	<0.00	0.35
	(12) Foken 97	0.37	<0.00	0.48	<0.00	0.46
	(13) Foken unpubl.	0.37	<0.00	0.48	<0.00	0.46
	(15) Panofsky 84	0.37	<0.00	0.26	<0.00	0.35
$\ln[f(z - d)/u_*]$	(9) Hoegstroem 90	0.35	0.33	0.70	0.37	0.20
	(10) Johansson 91	0.35	0.33	0.70	0.37	0.20

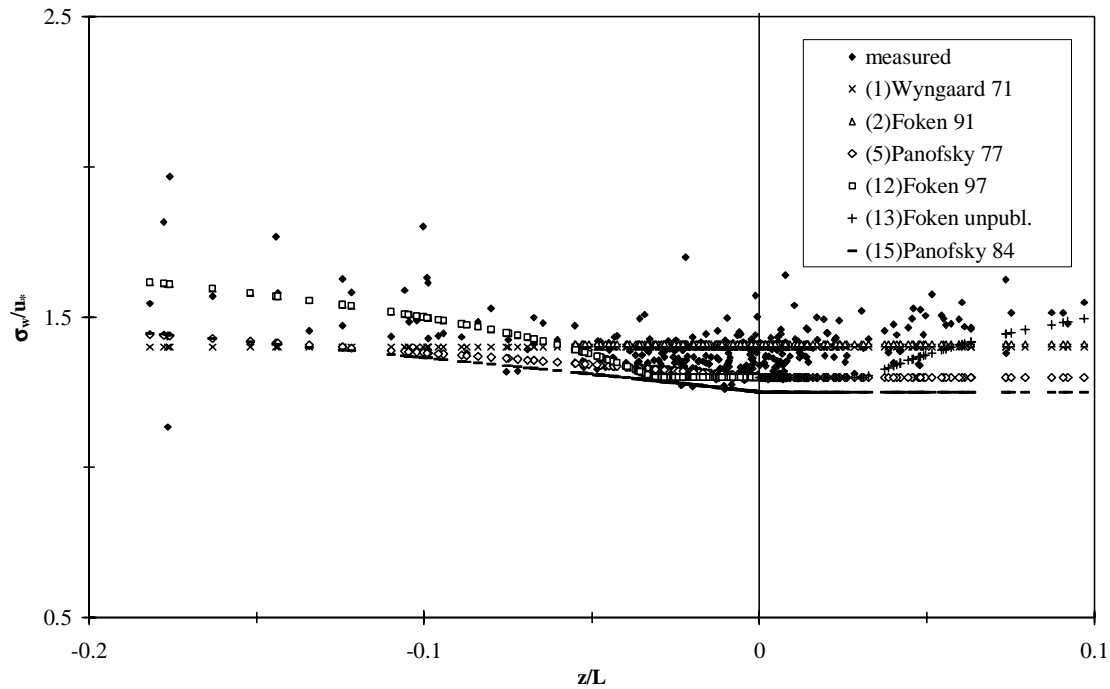


**Figure 8:** The nondimensional vertical velocity standard deviation of the LINEX 96/2 experiment as a function of  $\zeta$  with  $-0.2 < \zeta < 0.1$ . The coloured curves are predicted values of  $\sigma_w/u_*$  according to parameterisations by various authors (see Section 3.1).

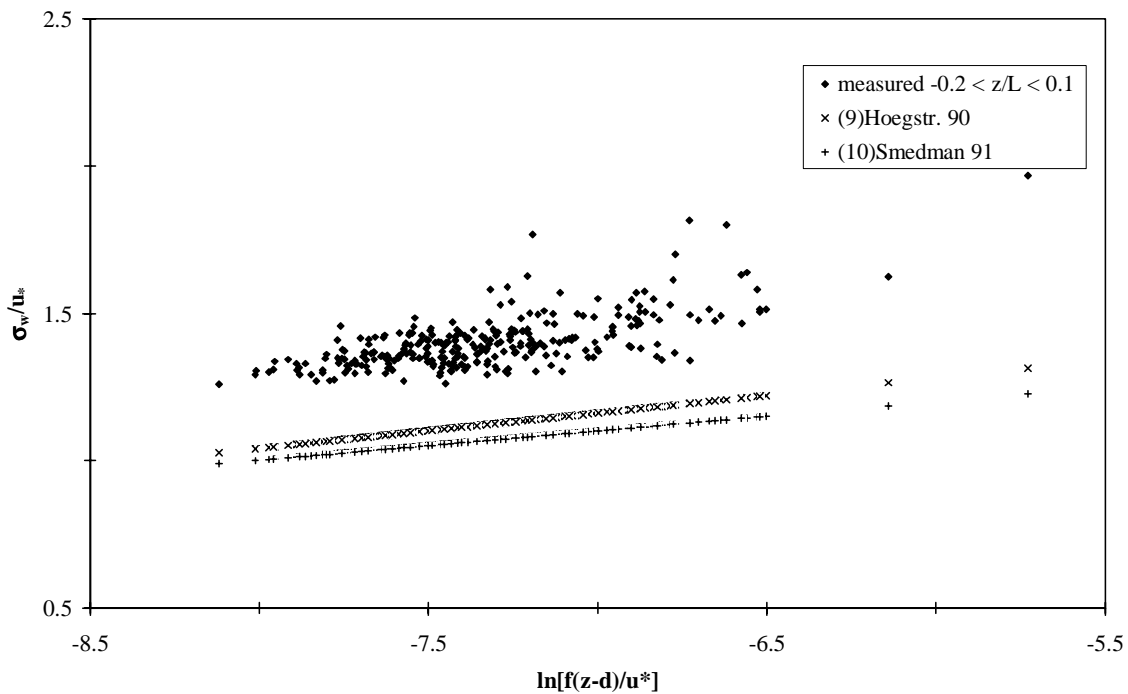


**Figure 9:** The nondimensional vertical velocity standard deviation of the LINEX 96/2 experiment as a function of  $\ln[f(z-d)/u_*]$ . The coloured lines depict the predictions of  $\sigma_w/u_*$  given by various authors. For details of the parameterisations see Section 3.1.

The parameterisation of Wyngaard et al. (1971) predicts  $\sigma_w/u_*$  to be constant in the range  $-0.2 < \zeta < 0.1$ . Hence, no correlation coefficient could be calculated. Correlation coefficients are generally low, but all significantly different from zero (see Appendix C). An exception are the data from the LINEX 96/2 experiment. Scaling them against  $\ln[f(z - d)/u_*]$ , about 50% of the variance of data given in Figure 8 and Figure 9 can be explained. In contrast, only 15% of the scatter is explained when using  $\zeta$  as the scaling factor. The parameterisations using the  $\ln[f(z - d)/u_*]$  term in order to predict  $\sigma_w/u_*$  within the interval  $-0.2 < \zeta < 0.1$  show better correlation with the observed data for the FINTUREX, the LINEX 96/2 and the LINEX 97/1 experiments, but no difference could be found for the Tsimlyansk data. In contrast, the parameterisations scaling with  $\zeta$  yield a better overall correlation for the EBEX-2000 data. The applied parameterisations include coefficients which were fit to match completely different data, and no new regression analysis has been performed so far to adjust the coefficients to our data. Thus, despite the low average correlation coefficients, we can conclude that the dimensionless scaling factor derived from the pressure gradient length scale  $\ln[f(z - d)/u_*]$  yields better results than scaling against  $\zeta$  for near neutral nondimensional vertical velocity standard deviations, i.e. the integral turbulence characteristics of the vertical wind velocity. Furthermore, the non-uniform behaviour of  $\sigma_w/u_*$  from different datasets with increasing stability cannot be explained satisfactorily when scaling with  $\zeta$ .

The application of  $\ln[f(z - d)/u_*]$  as an appropriate scaling factor for  $\sigma_w/u_*$  has already been proposed by Högström (1990), who restricted its validity to the near neutral range (Section 2.2.2). The basic concept of this dimensionless expression is the Rossby-number similarity, which was established for neutral conditions. Figure 10 and Figure 11 illustrate data obtained during EBEX-2000 and LINEX 97/1 over the entire stability range, segregated into three stability classes: unstable ( $\zeta < -0.2$ ), near neutral ( $-0.2 < \zeta < 0.1$ ) and stable ( $\zeta > 0.1$ ).

The data of all three stability intervals show a uniform behaviour in both figures: the stable data seem to continue the trend observed for the near neutral data with slightly increasing scatter. On the other hand, the unstable data do not match the pattern of the near neutral and stable data but increase distinctly with increasing instability. When plotting the  $\sigma_w/u_*$  data of the other three experiments over the entire stability range against  $\ln[f(z - d)/u_*]$ , they support these findings. Due to the fact that the stable data seem to continue the trend observed for the near neutral  $\sigma_w/u_*$ , further analysis of this group is performed.

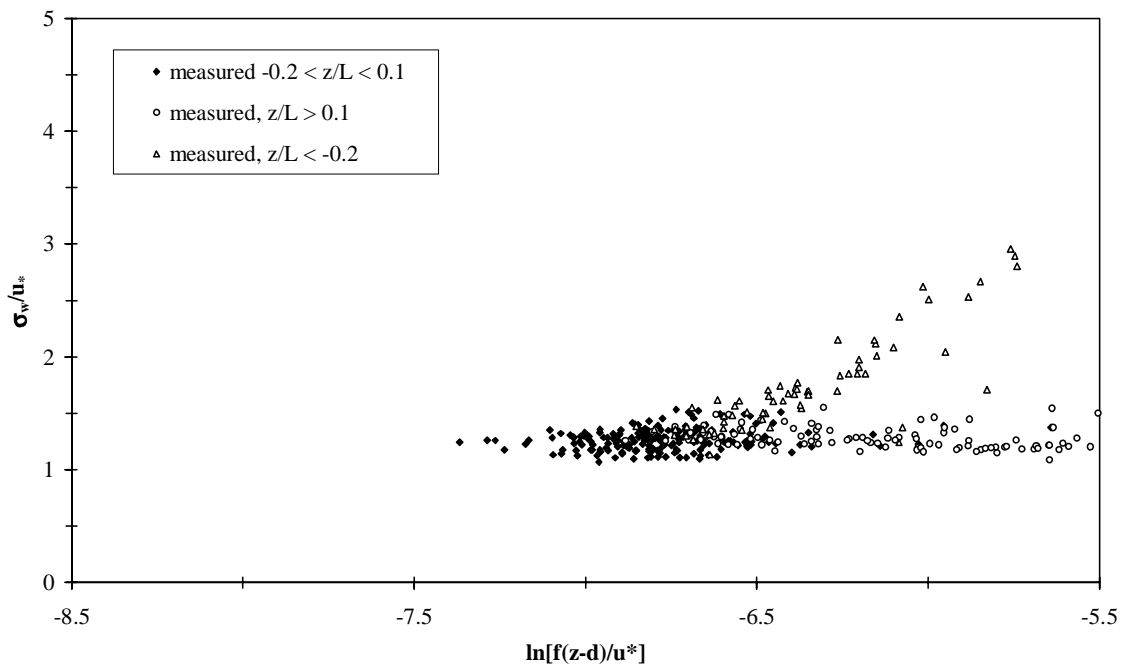


**Figure 10:** The nondimensional vertical velocity standard deviation over the entire stability range observed during EBEX-2000 plotted against  $\ln[f(z-d)/u_*]$ .

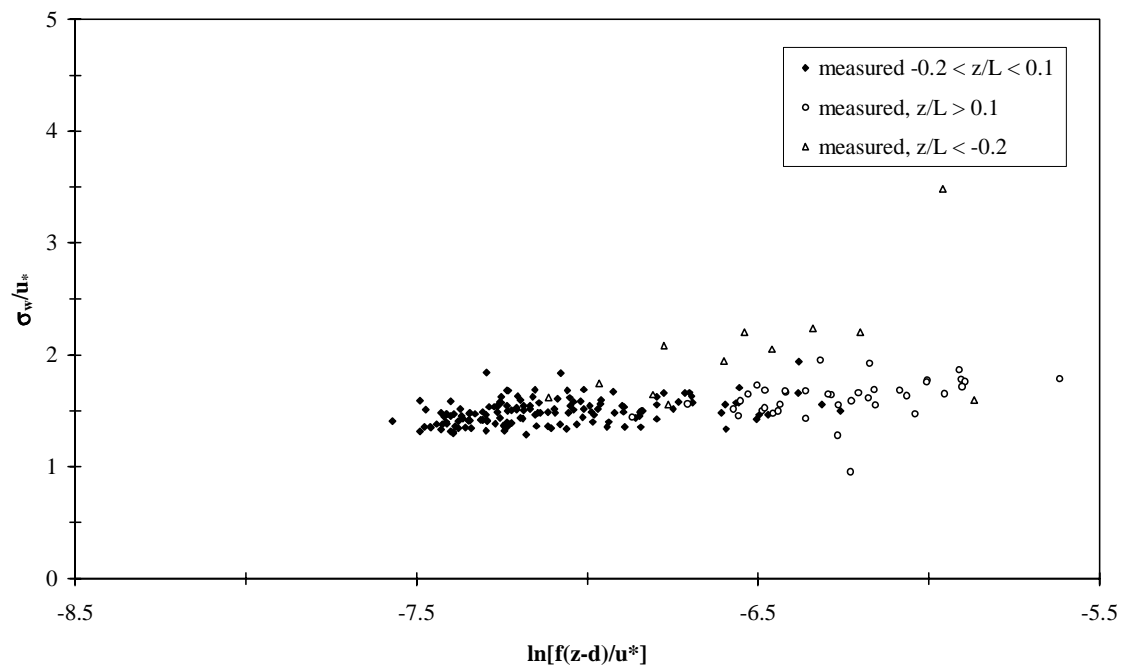


**Figure 11:** The nondimensional vertical velocity standard deviation over the entire stability range observed during LINEX 97/1 plotted against  $\ln[f(z-d)/u_*]$ .

The scatter of the stable data was found to increase with increasing stability (Figure 10, Figure 11). After careful analysis of all individual stable data, it became obvious that most of the scatter commences only at  $\zeta > 0.4$ . Hence, based on these empirical findings, it seems acceptable to expand the validity of the  $\ln[f(z - d)/u_*]$  scale to  $-0.2 < \zeta < 0.4$ .

Concluding from the results for the near neutral and stable range, we can state that the  $\ln[f(z - d)/u_*]$  scaling factor shows a better correlation to the observed data for  $-0.2 < \zeta < 0.1$  than  $\zeta$ , and that there are reasons to expand the validity of  $\ln[f(z - d)/u_*]$  towards stable conditions up to  $\zeta = 0.4$ .

These findings require a detailed discussion of the  $\ln[f(z - d)/u_*]$  scaling factor in order to assess the contributing effect of each individual variable involved. Performing a mathematical decomposition of the considered scaling factor using the logarithm laws, one can derive

$$\ln \left[ \frac{(z - d)f}{u_*} \right] = -\ln[u_*] + \ln[(z - d)] + \ln[f] \quad (31)$$

The decomposed form of the scaling factor allows to exactly analyse the contribution of each term. Interpreting the three terms on the right hand of Equation ( 31 ), one can subdivide them into a dynamical and a static class. The former consists only of  $-\ln[u_*]$ , as this is the only variable showing highly frequent turbulent fluctuations during measurements. The second class, representing more static variables, includes  $\ln[(z - d)]$  and  $\ln[f]$ . Neglecting changes of the measuring height and the displacement height at the measuring site, the aerodynamical height  $(z - d)$  can be assumed to remain constant, resulting in a constant value of  $\ln[(z - d)]$ . The Coriolis parameter, and thus the natural logarithm of it, is also constant at a given site, as it only depends on the geographical position.

The question arises, what is the effect for the  $\sigma_w/u_*$  data plotted against  $\ln[f(z - d)/u_*]$ ? Within a dataset, as the other variables are constant, the position of a point in relation to all others only depends on the natural logarithm of the friction velocity. The static terms only become important when different datasets are considered, involving different aerodynamical heights and different geographical positions. The differences in  $(z - d)$  and  $f$  shift the  $\sigma_w/u_*$  data of the different datasets along the abscissa, causing them to either diverge or merge.

Having realised this relationship, one can now arbitrarily combine the terms and apply them to the data of this study. The underlying hypothesis is that the best results, as shown by the highest correlation coefficients, should be obtained for those combinations, which include the most influencing terms, i.e. the most appropriate factors. This will be illustrated below. The various combinations of terms from Equation ( 31 ) yield 7 different scales. However, as we can assume that atmospheric turbulence depends not only on parameters of the static class, only 4 of them will be discussed further. Hence, the expressions  $\ln[z - d]$ ,  $\ln[f]$  and  $\ln[(z - d)f]$  can be excluded. The considered scaling factors will be  $-\ln[u_*]$ ,  $\ln[f/u_*]$ ,  $\ln[(z - d)/u_*]$  and  $\ln[f(z - d)/u_*]$ . Figure 12 and Figure 13 illustrate the results of plotting the nondimensional vertical velocity standard deviation of all experiments with  $-0.2 < \zeta < 0.4$  against  $\ln[f/u_*]$  and  $\ln[(z - d)/u_*]$ , respectively. The figures representing the  $-\ln[u_*]$  and  $\ln[f(z - d)/u_*]$  scaling factors are given in Appendix B.

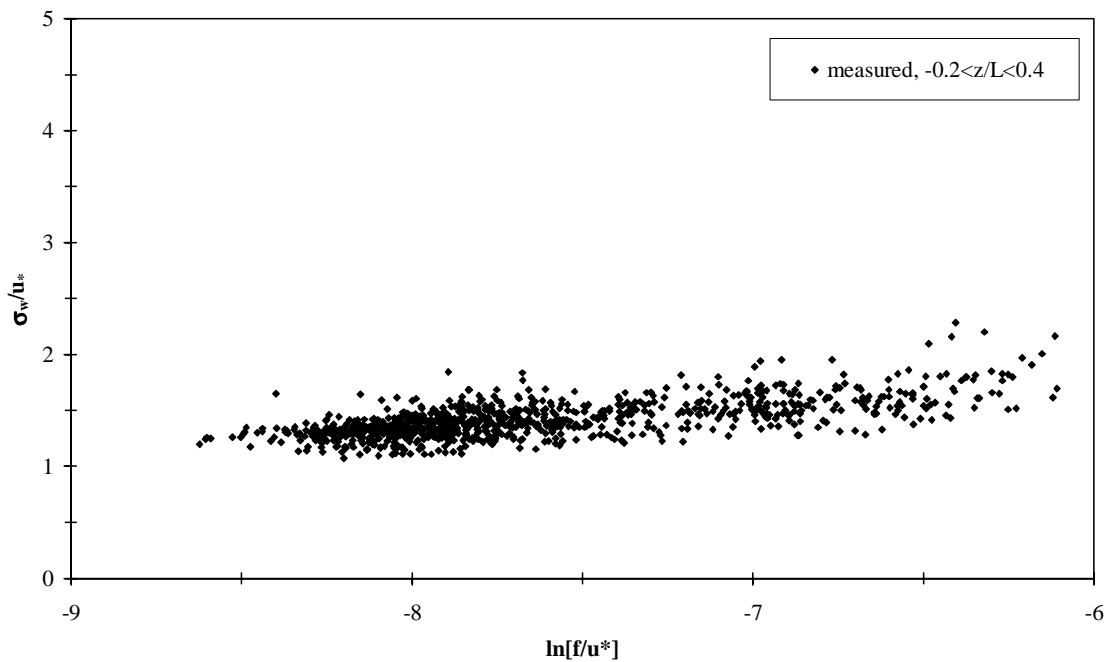


**Figure 12:** The nondimensional vertical velocity standard deviations of all experiments plotted against  $\ln[f/u_*]$ . Data was selected with  $-0.2 < \zeta < 0.4$ .

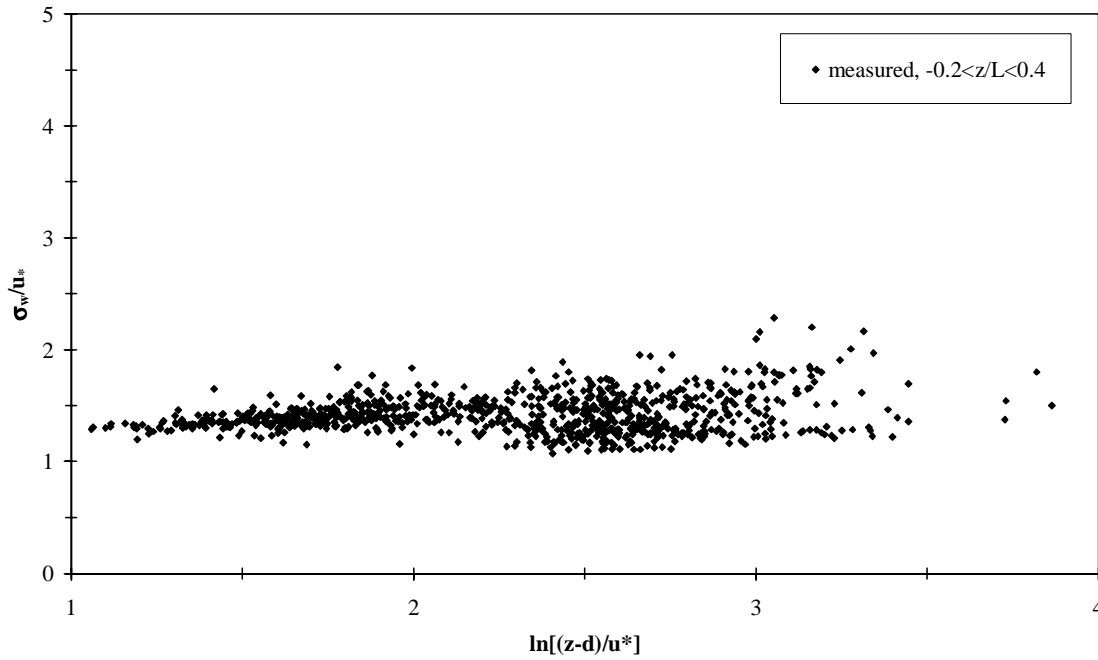


**Figure 13:** The nondimensional vertical velocity standard deviations of all experiments plotted against  $\ln[(z - d)/u_*]$ . Data was selected with  $-0.2 < \zeta < 0.4$ .

A linear regression using the least squares method and involving all 946 individual data points was performed. Subsequently, the real data was correlated to the predicted values calculated by the equations resulting from the regression analysis (Table 10). It is worth to mention that the results of the linear regression given in Table 10 reflect the mean values of both possible regression lines, which can be derived by standard regression analysis.

**Table 10:** Results of the linear regression using the least squares method and correlation analysis for the measured  $\sigma_w/u_*$  data of all experiments shown in Figure 12, Figure 13 and Appendix C. Data was selected with  $-0.2 < \zeta < 0.4$ .

scaling factor <sup>1</sup>	linear regression $f(x) = ax + b$		correlation coefficient
x	a	b	R
$-\ln[u_*]$	0.21	1.1	0.60
$\ln[f/u_*]$	0.21	3.1	0.69
$\ln[(z - d)/u_*]$	0.07	1.3	0.25
$\ln[f(z - d)/u_*]$	0.14	2.4	0.42

<sup>1</sup>: Resulting units:  $u_* = [\text{ms}^{-1}]$ ,  $f/u_* = [\text{m}^{-1}]$ ,  $(z-d)/u_* = [\text{s}]$ ,  $f(z-d)/u_* = [1]$

The best correlation coefficient to the observed values yields the equation  $\sigma_w/u_* = 0.21\ln[f/u_*] + 3.1$ . The prediction using the  $-\ln[u_*]$  scaling factor can explain 36% of the observed variance, the equation scaling with  $[f(z-d)/u_*]$  explains 18% of the observed scatter. The lowest R value is derived from the linear equation using  $\ln[(z-d)/u_*]$ .

Applying the  $\ln[f/u_*]$  relationship found here to the datasets of the individual experiments yields correlation coefficients of 0.28 (EBEX-2000), 0.33 (Tsimlyansk), 0.50 (FINTUREX, LINEX 97/1) and 0.76 (LINEX 96/2, Figure 14). Hence, data of all experiments show a significant correlation to the prediction by the equation  $0.21\ln[f/u_*] + 3.1$ .

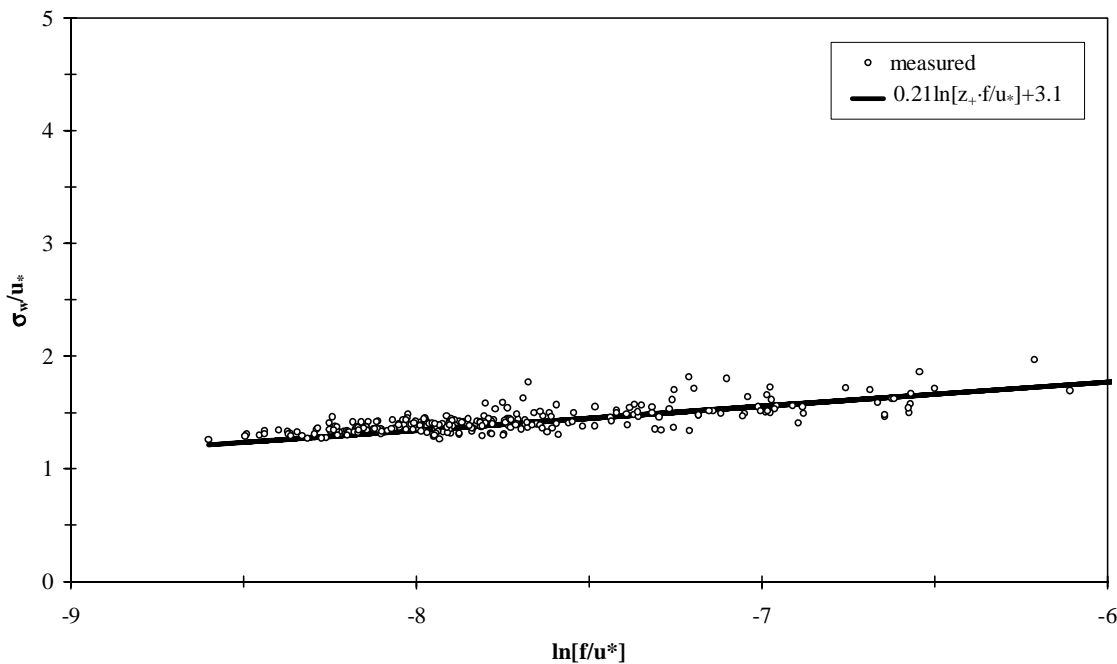


**Figure 14:** The nondimensional vertical velocity standard deviation observed during LINEX 96/2 plotted against  $\ln[f/u_*]$ . The solid line represents  $0.21\ln[z_+ f/u_*] + 3.1$  with  $R = 0.76$ .

Three conclusions can be drawn: firstly, the suggested ratio of the Coriolis parameter and the friction velocity seems to be the most suitable scaling factor for the integral turbulence characteristic of the vertical wind velocity under near neutral and slightly stable conditions, and thus to have an influence on atmospheric turbulence. As discussed in Chapter 3, most authors found integral turbulence characteristics only to be dependent on local parameters such as atmospheric stability or surface properties. However, the findings of this thesis support the conclusions of some authors (Section 3.2, 3.3) that the normalised fluctuation of the vertical

wind depends on local as well as on non-local parameters. As the ratio  $f/u_*$  has the dimension of a length, it is not dimensionless as required by turbulence theory. Scaling the observed  $\sigma_w/u_*$  data against the scaling factor  $z_0 \cdot f/u_*$  did not yield satisfying results. For mathematical convention, at this point a coefficient  $z_+$  is introduced, setting  $z_+ = 1$  m. The resulting scaling factor  $z_+ \cdot f/u_*$  thus is dimensionless.

Secondly, the data obtained during the EBEX-2000 experiment do not follow the behaviour of the data obtained during the other experiments. So far, no obvious reason could be found to explain this discrepancy. The EBEX-2000 data is influenced strongly by mesoscale effects, which could be possible reasons for the observed discrepancies (Foken, *pers.comm.*).

Thirdly, given that the  $\ln[z_+ \cdot f/u_*]$  scaling factor is found to yield the best overall correlation of the discussed scaling factors,  $\sigma_w/u_*$  does not seem to depend on the measuring height above ground  $z$  or the displacement height  $d$ . The integral turbulence characteristic of the vertical wind velocity is thus assumed to be invariable with height. As the friction velocity was found to be the appropriate velocity scale in the lowest 100m of the atmospheric boundary layer, the underlying Rossby-number similarity restricts this finding to this part of the atmosphere.

This hypothesis can be strengthened using the FINTUREX data. During this experiment, three independent measuring complexes were operated at different heights. Figure 15 illustrates the observed normalised fluctuations of the vertical wind velocity at 2 m, 4 m and 12 m. No statistically significant difference or systematical dependence on height could be observed among the individual data or their calculated group mean values for the different heights above ground. It should be mentioned, however, that the amount of data is small at 12 m height (only 14 values). This finding is restricted to data obtained over homogeneous surfaces, as the FINTUREX data represent fairly homogeneous surface conditions ( $z_0 = 0.0005$  m) without vegetation. Högström (1990) found the nondimensional vertical velocity standard deviation increasing with increasing measuring height. The observed independence on height contradicts these results (see Section 6.3).

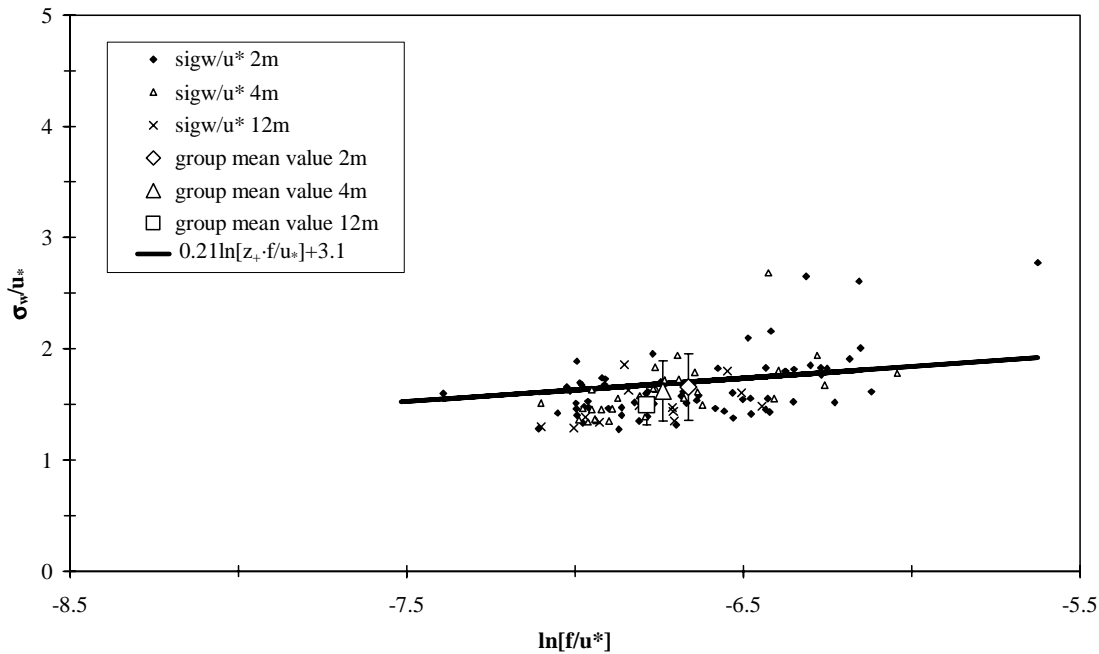


**Figure 15:** The nondimensional vertical velocity standard deviations observed during FINTUREX at three different measuring heights: 2m, 4m and 12m. The individual data and the group mean values are displayed.

So far, only the near neutral and stable ranges have been discussed. Now we can proceed with the unstable interval with  $\zeta < -0.2$ . The atmospheric stability  $\zeta$  and the dimensionless term  $z/z_i$  were proposed to be possible scaling factors within this stability interval (Chapter 3). According to the underlying Rossby-number similarity, the pressure gradient length scale is not valid in this stability interval. Nevertheless, analysis of data with  $\zeta < -0.2$  plotted against the pressure gradient length scale was performed (Figure 35 in Appendix B). The results support turbulence theory predicting  $\ln[f(z - d)/u_*]$  to be invalid as scaling factor for integral turbulence characteristics of the wind velocities.

The  $\zeta$  and the  $z/z_i$  dependencies will be discussed now. In Figure 6, the unstable data was observed to increase non-linearly with increasing instability. Figure 16 shows the combined data of all experiments with  $-3 < \zeta < -0.2$  and the corresponding suggested parameterisations. This plot seems to support the trend observed before for  $\sigma_w/u_*$  with  $\zeta < -0.2$ . All graphs seem to underestimate the real data, the difference increasing with increasing instability. One should take into account that the amount of data with  $\zeta < -1$ , which represent the conditions of free convection, is small compared to the amount of data with  $-1 < \zeta < -0.2$  and thus these data are

not expected to have large influence on the quality of the correlation. Correlation analysis was performed including all 107 observed data. (Table 11).

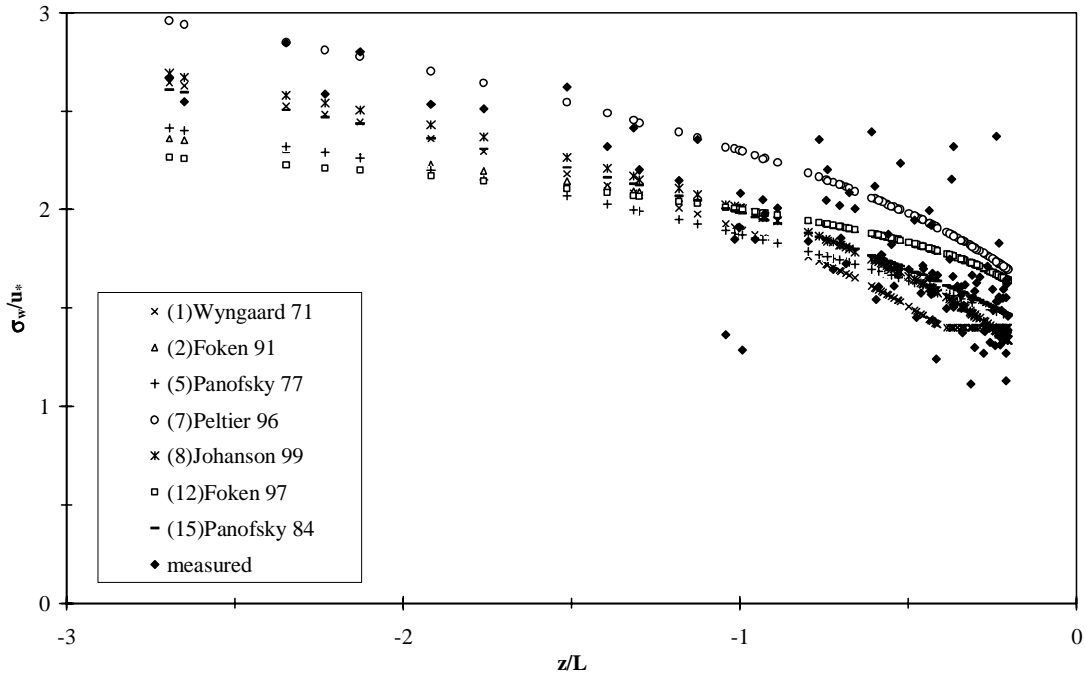


**Figure 16:** The nondimensional vertical velocity standard deviations of all experiments observed with  $-3 < \zeta < -0.2$ . The coloured lines depict the predictions according to various authors (see Chapter 3).

**Table 11:** Results of the correlation analysis between the observed data of all experiments and the predictions according to various authors with  $-3 < \zeta < -0.2$ . The total amount of data is 107.

scaling factor	parameterisation	correlation coefficient R
$\zeta$	(1) Wyngaard 71	0.77
	(2) Foken 91	0.79
	(5) Panofsky 77	0.84
	(12) Foken 97	0.79
	(15) Panofsky 84	0.79
$\zeta, z/z_1$	(7) Peltier 96	0.79
	(8) Johansson 99	0.79

The derived R values span from 0.77 to 0.84. The parameterisation after Panofsky et al. (1977) yields the highest correlation coefficient 0.84 and can explain 70% of the observed variance. All other predictions yield slightly lower R values and explain about 62 % of the observed scatter. However, the correlation coefficient of the prediction by Panofsky et al. (1977) is not significantly different. Fitting the coefficients did not improve the correlation coefficients any further. The predictions after Peltier et al. (1996) and Johansson et al. (1999) include the scaling factor of atmospheric stability as well as the mixing layer height. However, the goodness of fit of these parameterisations is not different than of the ones only based on  $\zeta$ . We can therefore conclude that the mixing layer height does not significantly influence atmospheric turbulence in the surface layer in the stability interval of  $-3 < \zeta < -0.2$  under the surface conditions of the experiments used in this study presented in Chapter 4.

Concluding the findings presented above, we can state that no significant difference could be found between the various predictions for the nondimensional vertical velocity standard deviation depending on the atmospheric stability. Including terms which involve the mixing layer height as done by Peltier et al. (1996) does not seem to give better results for the prediction of the integral turbulence characteristic of the vertical wind velocity. Generally, the parameterisations valid within the unstable range seem to fit the observed data better than those restricted to the near neutral and slightly stable ranges. The stability range below  $\zeta = -3$  must remain excluded from the discussion due to very few available data. In this range, parameterisations involving the height of the convectively mixed layer are expected to yield better results due to increasing contribution of free convection and increased influence of  $z_i$ .

The group of data, characterised by  $\sigma_w/u_* < 1.1$ , was observed to differ from the general pattern, independently of the scaling factor used. These data were recorded during EBEX-2000 and FINTUREX. Analysing the EBEX-2000 data with  $\sigma_w/u_* < 1.1$  around neutral, one finds that all values were recorded between 09:00 and 13:30 UTC, i.e. 02:00 and 06:30 local time (Figure 17). All data obtained within this period of time show a comparatively low fluctuation of the vertical wind velocity. Thus, the nocturnal local wind field was more homogeneous than the wind field prevailing during daytime.

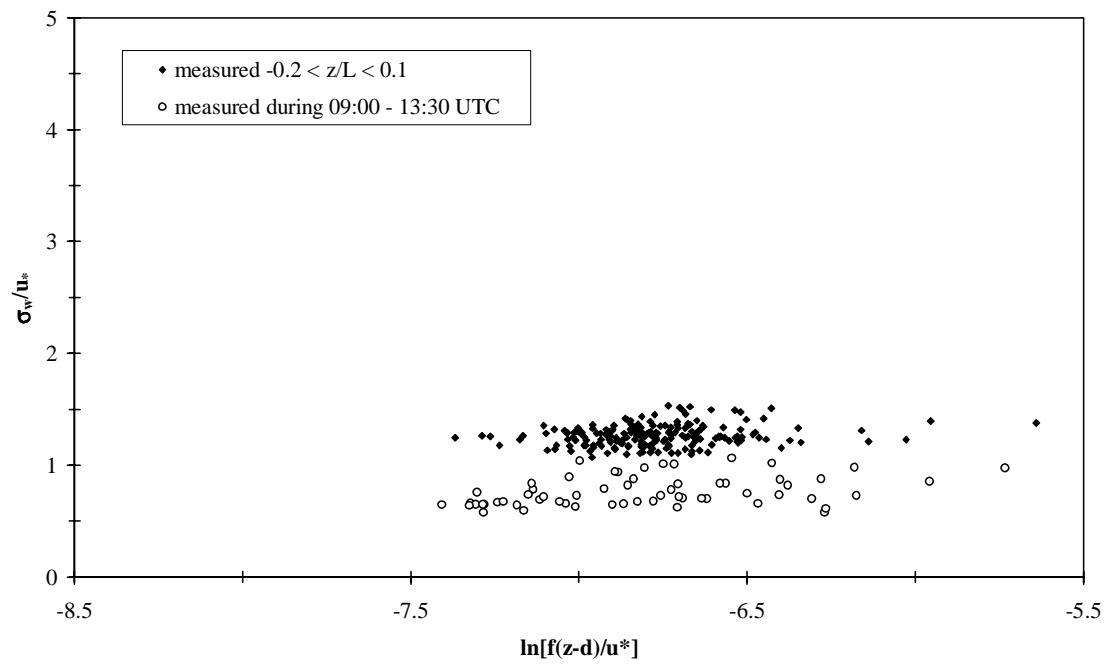


Figure 17:  $\sigma_w/u_*$  data of EBEX-2000 selected by  $-0.2 < \zeta < 0.1$  as a function of  $\ln[f(z-d)/u_*]$ .

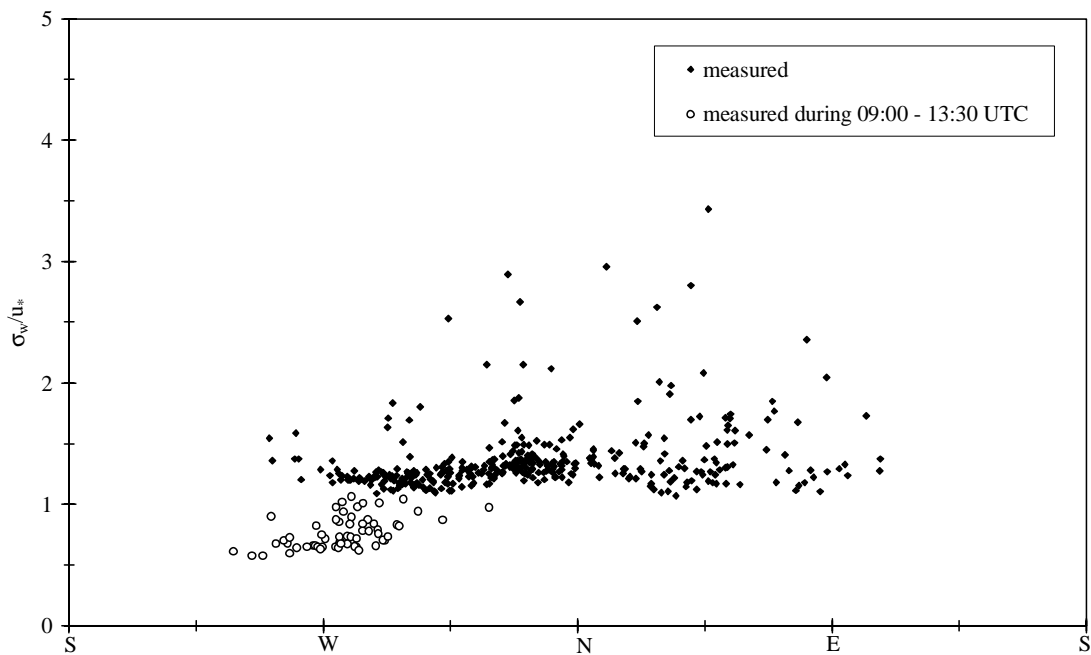


Figure 18:  $\sigma_w/u_*$  data of EBEX-2000 selected by  $-0.2 < \zeta < 0.1$  as a function of the observed wind direction.

The considered data with  $\sigma_w/u_* < 1.1$  were always connected to constant, westerly winds (Figure 18). Lehner (2001) analysed the wind profiles, continuously recorded by a SODAR system during EBEX-2000, and found a local, mesoscale wind from the Kettleman Hills developed in the near-surface layer during night-time, resulting in wind directions from  $280^\circ$  to  $330^\circ$ . The nocturnal wind was observed to be decoupled from the wind field during daytime. This observation can explain the differences within the dataset and thus the near neutral, nocturnal data was excluded from further analysis. Thus it appears that additional measurements using SODAR technique or other sounding methods can provide useful information to detect distorted integral turbulence characteristics and thus prevent misinterpretation of such data.

A closer look at the FINTUREX data with  $\sigma_w/u_* < 1.1$  gives the following result: these data were recorded during the first days of the campaign, between Jan, 21. 04:30 and Jan, 22. 03:00 UTC. During this period of time, the drag coefficient  $u_*/u$  was observed to scatter significantly. This observation indicates a changing adaptation of the snow covered surface to a changed approaching flow of the wind field. During Jan, 21. 04:30 and Jan, 22. 03:00 UTC, the mean air temperature (ranging from  $-20^\circ$  to  $-11^\circ$  Celsius) was low compared to the mean air temperature observed during the other days ( $\sim -5^\circ$  Celsius). Both observations presented above point to a change in the synoptic situation during the campaign. The data with  $\sigma_w/u_* < 1.1$  are thus assumed to represent a different wind field than the one observed during the other days and were therefore also excluded from analysis.

### 6.1.2 Horizontal wind component

In this section, the results for the horizontal wind velocity component will be discussed analogously to the previous section. The discussion of the stable and near neutral data will follow now.

Most of the  $\sigma_u/u_*$  data fall into the stability range from  $-0.25$  to  $0.25$  (Figure 19). The  $\sigma_u/u_*$  values concentrate in the range between about 2 and 4. The unstable data for  $\zeta < -0.25$  were mostly obtained at EBEX-2000, FINTUREX and LINEX 97/1 experiments only contribute few data in this range. The stable range  $\zeta > 0.25$  contains data from all experiments except those from Tsimlyansk due to the fact that only daytime measurements were performed providing no stable data from this campaign.

The used y-axis intercept indicates that the dispersion of the horizontal wind velocity is much larger than the scatter observed for the  $\sigma_w/u_*$  data (Figure 6). It is very hard to get a clear picture

of the behaviour of  $\sigma_u/u_*$  in this stability interval. The unstable and near neutral data with  $-1 < \zeta < 0.1$  do not show any clear pattern. However, on one hand the stable values of LINEX 96/2, LINEX 97/1 and EBEX-2000 with  $\zeta > 0.1$  seem to remain constant with increasing stability at values of about 2.75. The data from FINTUREX on the other hand do not show a clear dependency on  $\zeta$ .

Figure 20 plots the near neutral  $\sigma_u/u_*$  data of all experiments against the expression  $\ln[f(z - d)/u_*]$  derived from the pressure gradient length scale. The data with  $\sigma_u/u_* < 2.15$  separate from the general pattern. As discussed for the vertical wind component, these values are assumed to represent different wind fields and were therefore excluded from further analysis. The  $\sigma_u/u_*$  data do not show a uniform trend (Figure 20). The large scatter observed in Figure 19, where data are plotted against the atmospheric stability, does not vanish as it did in case of the vertical wind velocity when plotting against  $\ln[f(z - d)/u_*]$ . However, the observed near neutral nondimensional horizontal velocity standard deviation of all experiments seems to remain constant or to increase slightly with increasing stability as a function of the pressure gradient length scale.

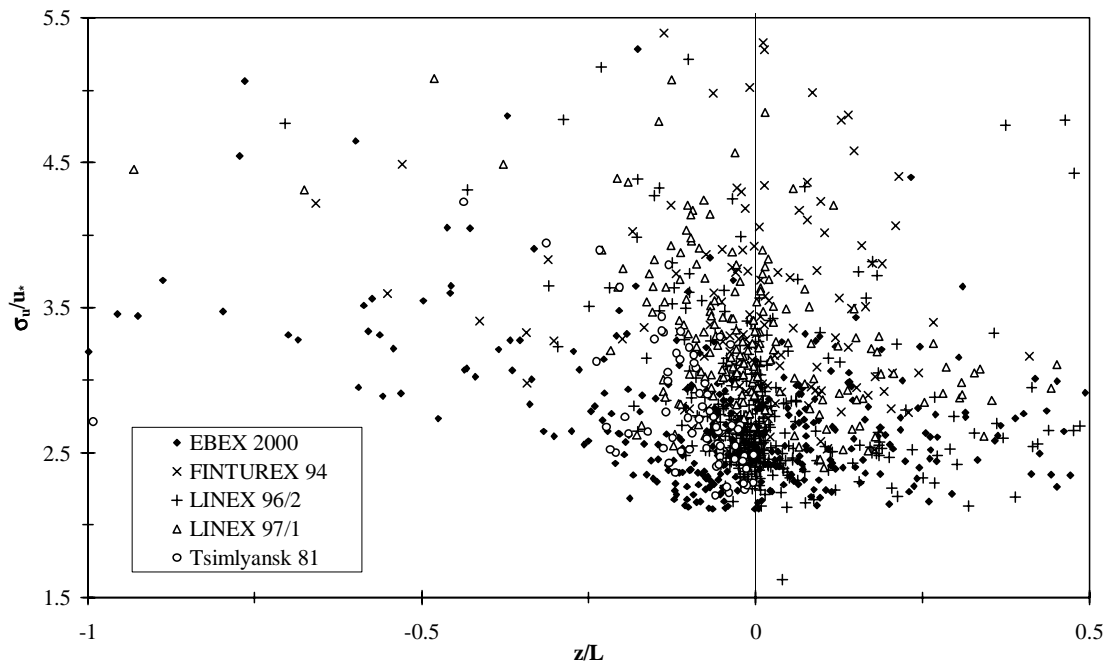


**Figure 19:** The observed nondimensional horizontal velocity standard deviation of all experiments plotted against  $\zeta$  with  $-1 < \zeta < 0.5$ .

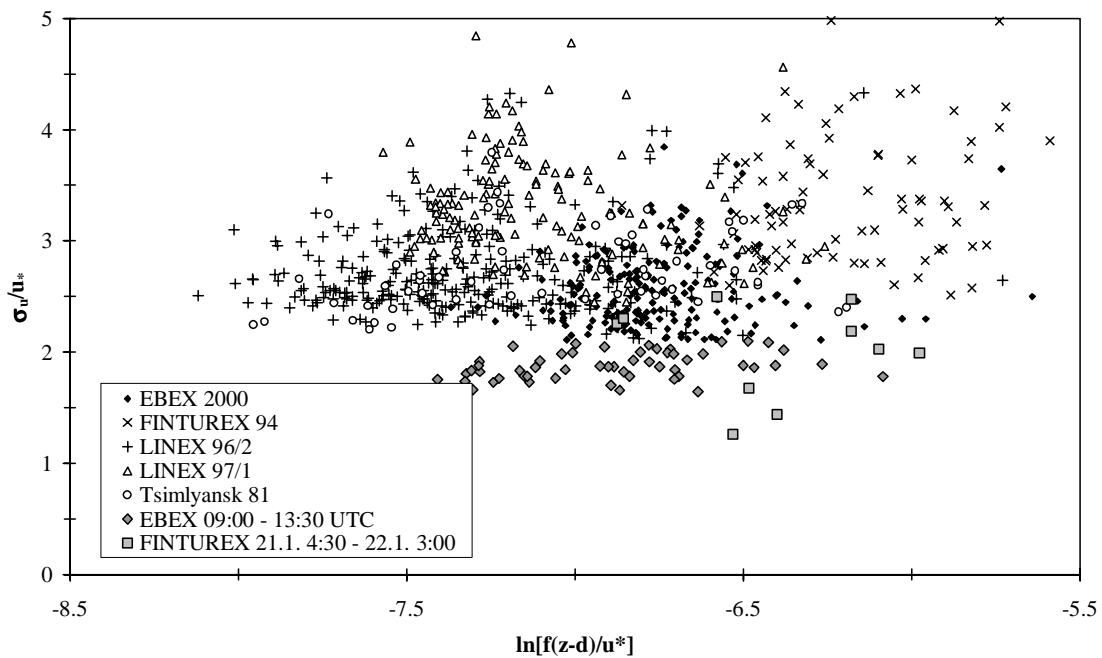


**Figure 20:** The observed nondimensional horizontal velocity standard deviation of all experiments plotted against  $\ln[(z-d)/u_*]$ . Data were selected for  $-0.2 < \zeta < 0.1$ .

Figure 21 and Figure 22 illustrate the measured  $\sigma_w/u^*$  values of LINEX 96/2 as well as the predicted data according to parameterisations by various authors as a function of the atmospheric stability and the pressure gradient length scale, respectively. According to Section 3.1, the parameterisations for  $\sigma_w/u^*$  can be used in order to predict  $\sigma_w/u^*$  using a transformation coefficient. The predictions for  $\sigma_w/u^*$  will be discussed exemplarily using the parameterisations shown in Figure 21 and Figure 22.

No uniform picture of the behaviour of  $\sigma_w/u^*$  can be observed plotted against  $\zeta$  (Figure 21). The prediction by Foken et al. (1997a) is restricted to the unstable range. The  $R^2$  value for this prediction to the observed data is 0.3. On the other hand, plotting the considered data against  $\ln[f(z-d)/u^*]$  does not seem to improve the quality of correlation between the observed values and the predicted ones. The parameterisation by Smedman (1991) can explain 22% of the observed variance (Figure 22). A correlation analysis without fitting of coefficients and involving all experimental and predicted data yields the results presented in Table 12.

**Table 12: Results of the correlation analysis between the predicted values derived from parameterisations illustrated in Figure 21 and Figure 22 and the observed experimental data of the corresponding experiment. Data were selected for  $-0.2 < \zeta < 0.1$ .**

scaling factor	parameterisation	correlation coefficient R				
		Tsimly- ansk 81	FINT- UREX 94	LINEX 96/2	LINEX 97/1	EBEX- 2000
$\zeta$	(14) Foken 97	0.52	0.10	0.55	0.32	0.10
$\ln[f(z-d)/u^*]$	(11) Smedman 91	0.26	0.28	0.47	0.14	0.20

Correlation coefficients below 0.18 indicate that no significant correlation between the observed and predicted  $\sigma_w/u^*$  data could be found (see Appendix C). The determined correlation coefficients are generally low (Table 12). On one hand, scaling the  $\sigma_w/u^*$  data against  $\zeta$  seems to yield better results in the case of the Tsimlyansk, LINEX 96/2 and LINEX 97/1 experiments, showing significant correlation to the parameterisations applied. On the other hand, the data obtained during FINTUREX and EBEX-2000 show a better correlation coefficient when scaling them against  $\ln[f(z-d)/u^*]$ . The correlation between the observed and predicted values is significant for the Tsimlyansk, FINTUREX, LINEX 96/2 and EBEX-2000 data when plotting

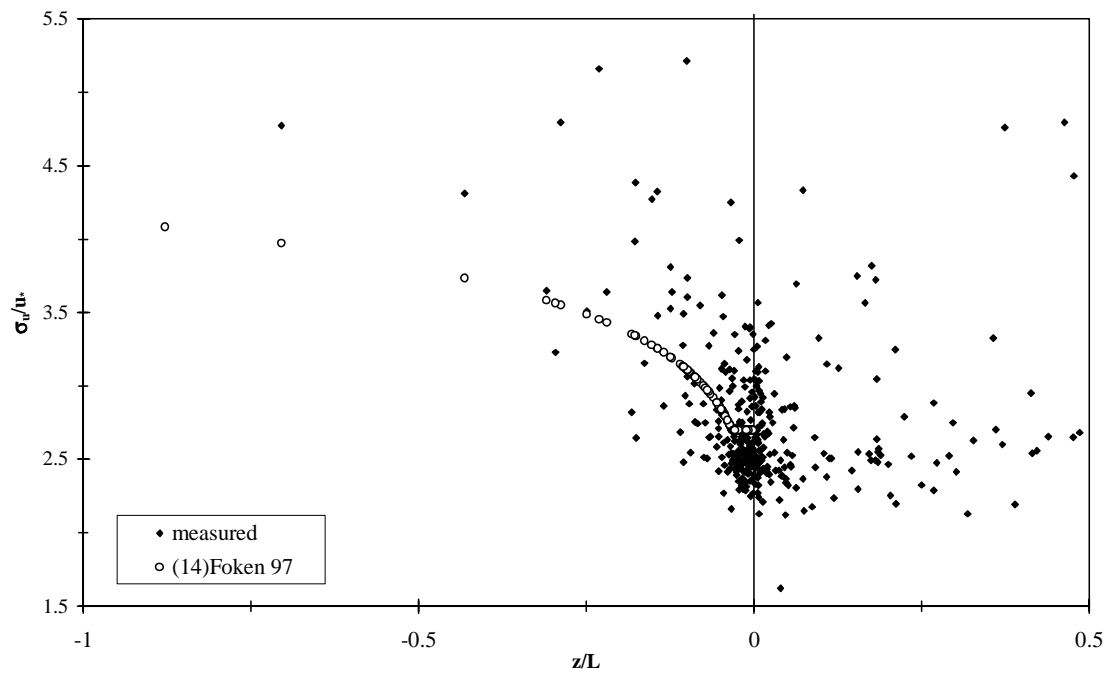


**Figure 21:** The observed nondimensional horizontal velocity standard deviation of the LINEX 96/2 experiment as a function of  $\zeta$ .

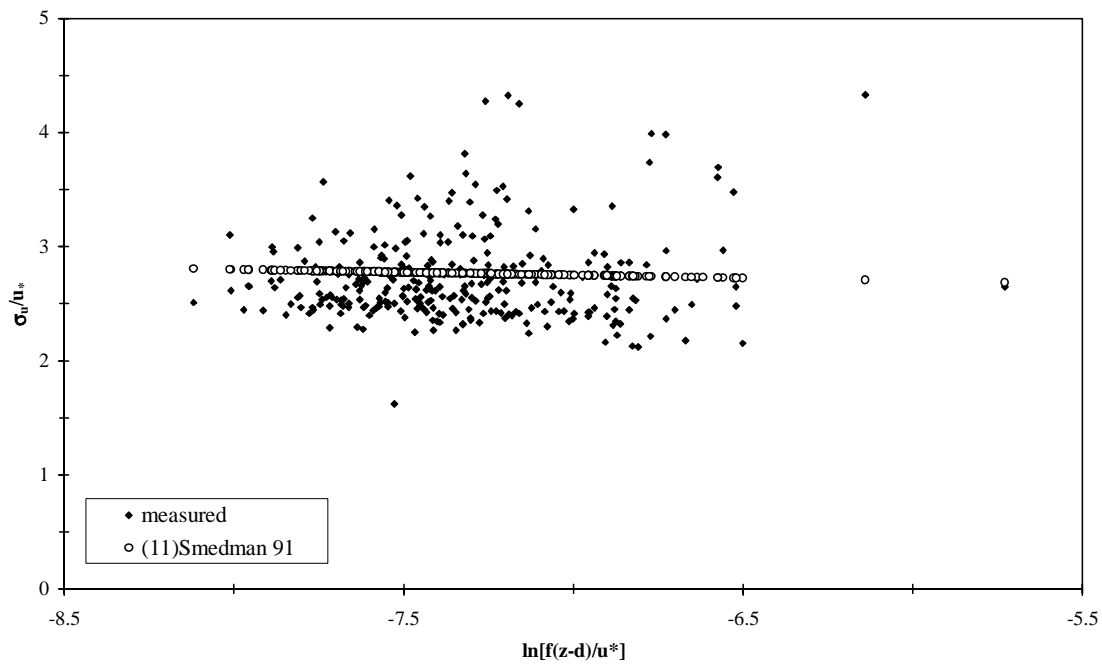


**Figure 22:** The observed nondimensional horizontal velocity standard deviation of the LINEX 96/2 experiment as a function of  $\ln[f(z-d)/u_*]$ .

them as a function of  $\ln[f(z - d)/u_*]$  (Figure 22, Table 12). Thus, a discussion of this scaling factor will follow now. The  $\ln[f(z - d)/u_*]$  scaling factor was decomposed, as described in the previous section, and the resulting parameters were applied to the combined dataset including all experiments. A linear regression and correlation analysis were performed for the near neutral stability range with  $-0.2 < \zeta < 0.1$  on one hand, and for the expanded near neutral range with  $-0.2 < \zeta < 0.4$  on the other hand (Table 13). Figure 23 illustrates the combined dataset with  $-0.2 < \zeta < 0.1$  as a function of  $\ln[f/u_*]$ .

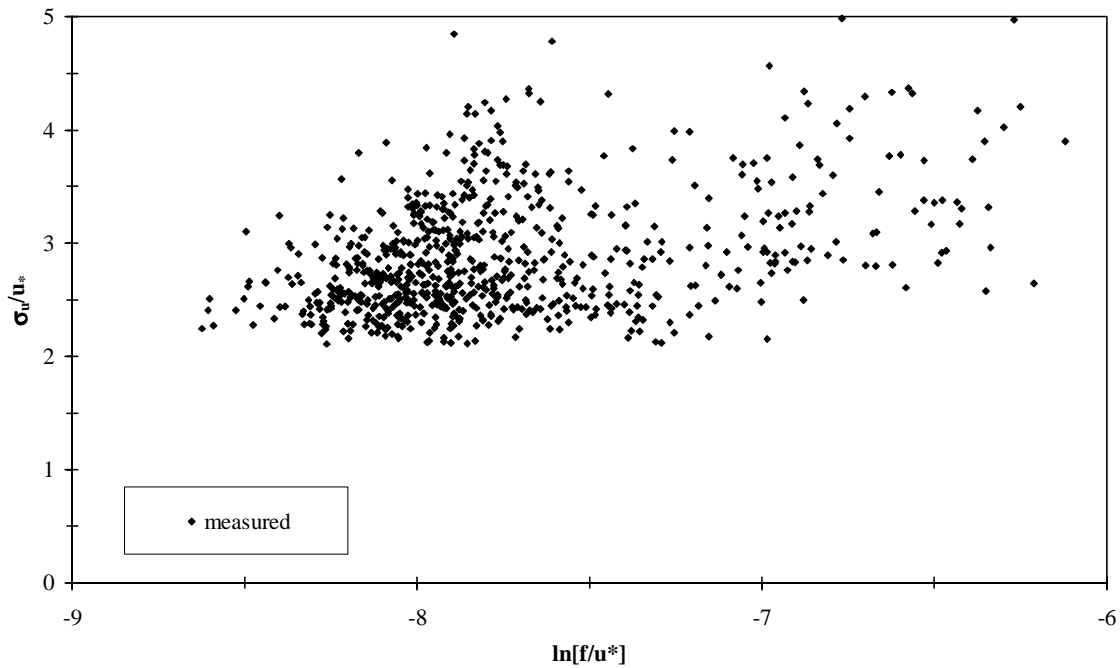


**Figure 23:** The nondimensional horizontal velocity standard deviations of all experiments as a function of  $\ln[f/u_*]$ . Data were selected for  $-0.2 < \zeta < 0.1$ .

**Table 13:** Results of the linear regression using the least squares method and correlation analysis for the observed  $\sigma_w/u_*$  data of all experiments. The near neutral range with  $-0.2 < \zeta < 0.1$  and the expanded range with  $-0.2 < \zeta < 0.4$  were considered.

stability range	considered scale <sup>1</sup>	linear regression $f(x) = ax + b$		correlation coefficient
	x	a	b	R
$-0.2 < \zeta < 0.1$	$-\ln[u_*]$	0.69	2.0	0.45
	$\ln[f/u_*]$	0.53	7.0	0.45
	$\ln[(z-d)/u_*]$	0.29	2.3	0.22
	$\ln[f(z-d)/u_*]$	0.39	5.6	0.32
$-0.2 < \zeta < 0.4$	$-\ln[u_*]$	0.51	2.2	0.37
	$\ln[f/u_*]$	0.44	6.3	0.40
	$\ln[(z-d)/u_*]$	0.22	2.4	0.17
	$\ln[f(z-d)/u_*]$	0.33	5.2	0.28

<sup>1</sup>: Resulting units:  $u_* = [\text{ms}^{-1}]$ ,  $f/u_* = [\text{m}^{-1}]$ ,  $(z-d)/u_* = [\text{s}]$ ,  $f(z-d)/u_* = [1]$

The calculated correlation coefficients for the horizontal wind velocity are lower compared to those for the vertical wind velocity. All R values indicate a significant correlation except predicting  $\sigma_w/u_*$  by  $0.22\ln[(z-d)/u_*] + 2.4$  in the range  $-0.2 < \zeta < 0.4$ . A maximum of 20% of the observed scatter can be explained using an expression derived from the decomposed pressure gradient length scale. The  $-\ln[u_*]$  and the  $\ln[f/u_*]$  scaling factors yield the largest R values (Table 13).

Concluding the findings for the near neutral and stable range, the parameterisations derived from the pressure gradient length scale seem to explain the observed scatter of  $\sigma_w/u_*$  better than those dependent on the atmospheric stability. The best overall correlation to the observed integral turbulence characteristic of the horizontal wind velocity can be obtained using the expression  $\sigma_w/u_* = 0.44\ln[z_+/u_*] + 6.3$  in the stability interval  $-0.2 < \zeta < 0.4$ .

So far, the range with  $\zeta > -0.2$  has been discussed. Now the discussion will deal with data for  $\zeta$  below this boundary. According to Chapter 3, the atmospheric stability and the dimensionless ratio  $|z_i/L|$  were proposed as scaling factors for the fluctuations of the horizontal wind velocity

under unstable conditions. The  $\ln[f(z-d)/u_*]$  length scale is invalid in this stability interval and thus excluded from discussion.

The observed  $\sigma_u/u_*$  data of all experiments is shown as a function of  $\zeta$  with  $\zeta$  ranging from -3 to -0.2 (Figure 24). The correlation coefficient for the parameterisation given in Equation ( 15 ) with the coefficients by Foken et al. (1997a) equals 0.35. The data with  $\zeta < -1$  reflect the conditions of free convection and are not expected to have large influence on the goodness of fit due to their small amount.

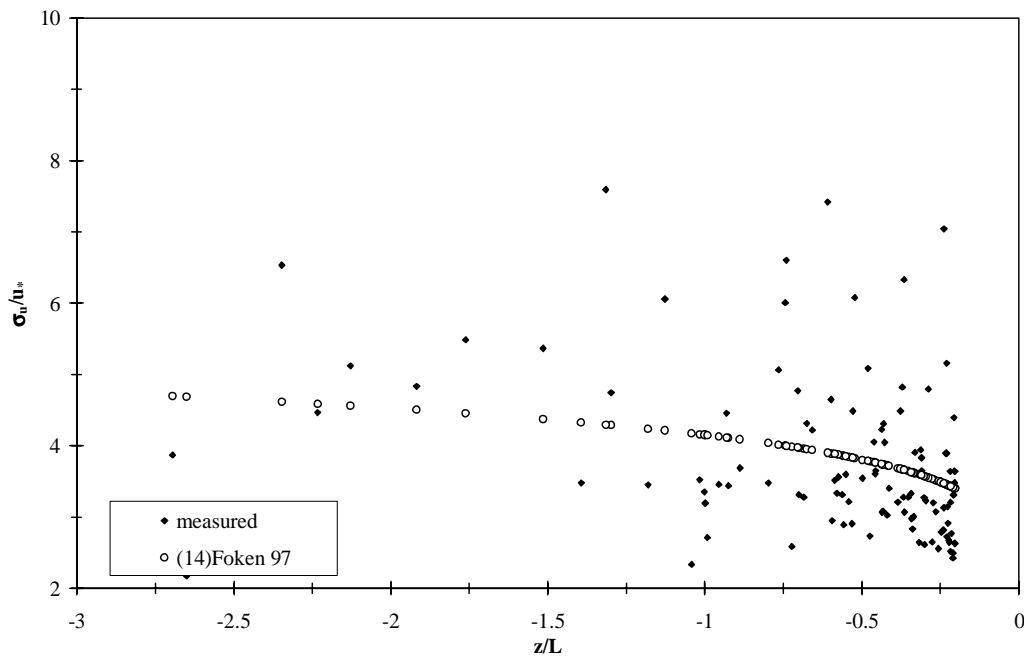


**Figure 24:** Measured nondimensional horizontal velocity standard deviations as a function of  $\zeta$  for  $-3 < \zeta < -0.2$ . The figure contains data of all experiments.

Panofsky et al. (1977) predicted  $\sigma_u/u_*$  to be dependent on the scaling factor  $|z_i/L|$  involving the mixing layer height (Chapter 3). Figure 25 plots the measured integral turbulence characteristic of the horizontal wind velocity of all experiments and the corresponding parameterisation against  $|z_i/L|$  for  $\zeta < -1$ . The correlation coefficient for the parameterisation by Panofsky et al. (1977) is 0.30.

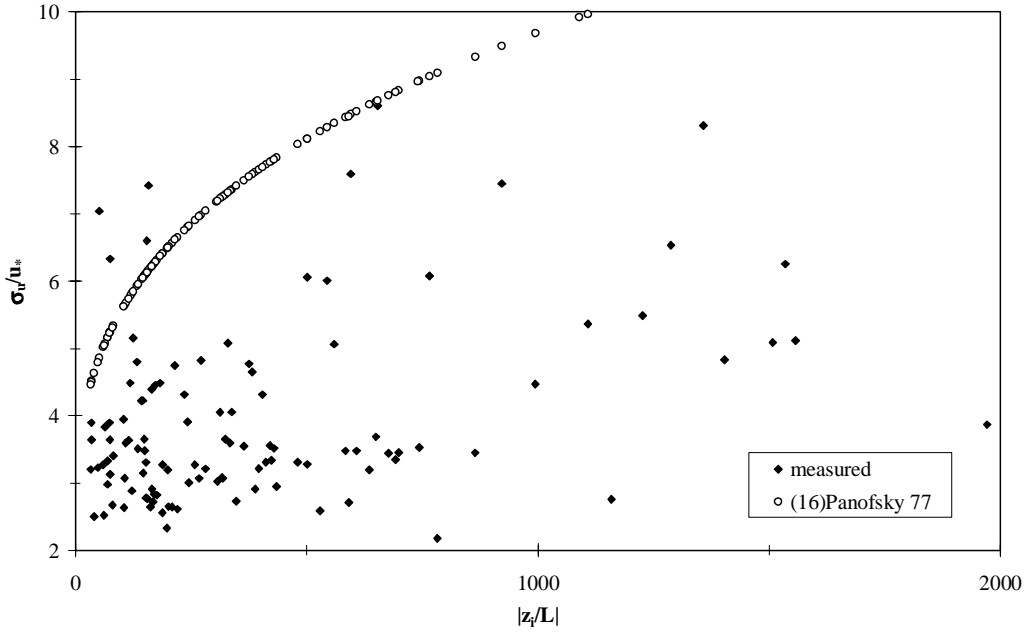


**Figure 25:** Observed nondimensional horizontal velocity standard deviation as a function of  $|z_i/L|$  for  $\zeta < -1$ . The figure contains data of all experiments.

The following conclusions can be drawn for the unstable range: firstly, the scatter of the measured data is large. Secondly, the discussed parameterisations show low, but significant correlation to the observed values of the nondimensional horizontal velocity standard deviation. No significant difference could be found comparing the goodness of fit between parameterisations using the scaling factor  $\zeta$  and  $|z_i/L|$ .

## 6.2 Temperature

In this section, the integral turbulence characteristic of the temperature will be discussed. The datasets obtained using the turbulence measurements complexes described in Chapter 4 provide different temperatures, resulting in different integral turbulence characteristics. On one hand, the acoustic temperature  $T_a$ , determined using the density fluctuations recorded by sonic anemometers, can be used to determine the integral turbulence characteristic  $\sigma_{T_a}/T_{a*}$ . In this case, the normalising factor  $T_{a*}$  will be calculated from the buoyancy flux. On the other hand, the fluctuations of the temperature  $T_p$ , derived from measurements using a fast response platinum probe, can be taken to determine the integral turbulence characteristic  $\sigma_{T_p}/T_{p*}$ . Here, the sensible heat flux will be used to determine the corresponding normalising factor  $T_{p*}$ .

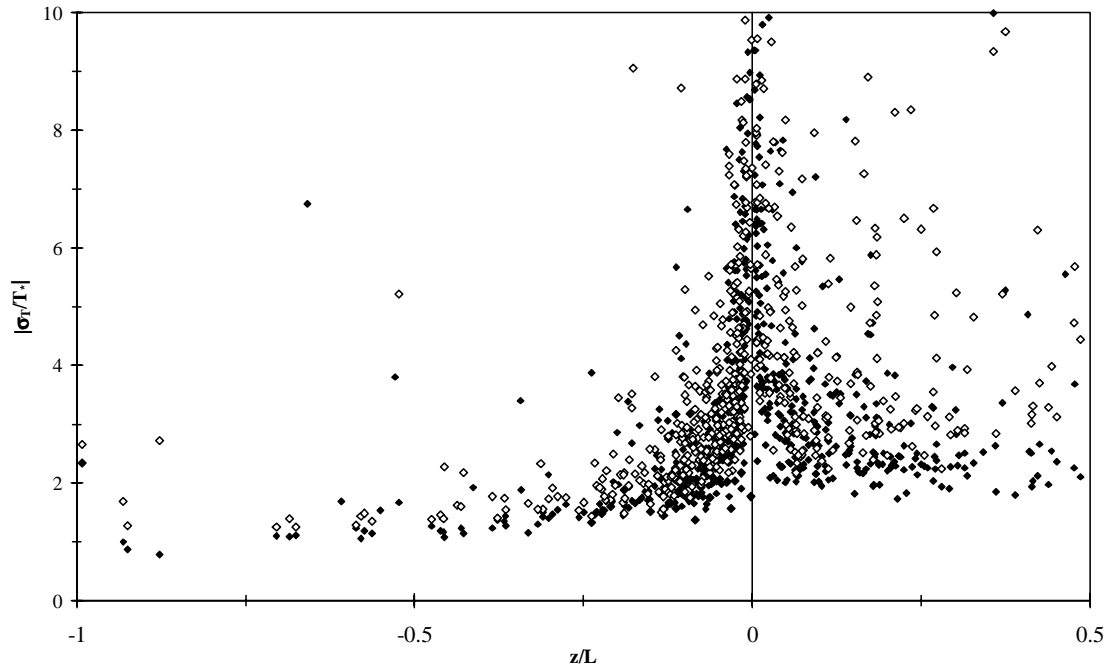


**Figure 26:** The nondimensional temperature standard deviation observed during the considered experiments. Solid rhombi depict  $\sigma_{T_a}/T_{a^*}$ , unfilled rhombi  $\sigma_{T_p}/T_{p^*}$ .

Comparing the integral turbulence characteristics of the different temperatures, one finds that  $\sigma_{T_p}/T_{p^*}$  is systematically higher than  $\sigma_{T_a}/T_{a^*}$  (Figure 26). The magnitude of the normalising factor  $T_{a^*}$  is greater than the magnitude of  $T_{p^*}$  (Liu et al., 2000). Assuming that the standard deviation of the acoustic temperature  $\sigma_{T_a}$  is equal or only little greater than the standard deviation of the platinum temperature  $\sigma_{T_p}$ , it follows that  $\sigma_{T_a}/T_{a^*} < \sigma_{T_p}/T_{p^*}$ . The observed scatter of  $\sigma_{T_p}/T_{p^*}$  increases significantly under stable conditions (Figure 26). This scatter is caused by hardware limitations of the data collector used, giving an insufficient resolution of very little temperature fluctuation under stable conditions. In contrast, the  $\sigma_{T_a}/T_{a^*}$  values seem to follow a decreasing non-linear trend with increasing stability. Thus, further analysis of  $\sigma_{T_a}/T_{a^*}$  was performed, as these data are more likely to obey a functional relationship than the data derived from the platinum temperature.

$\zeta$  is the only possible scaling factor for the integral turbulence characteristic of the temperature as proposed by various authors. The data seem to show a uniform pattern (Figure 27): under unstable conditions, the non-dimensional temperature standard deviation seems to follow a non-

linearly increasing trend with increasing stability. The data exhibit a maximum at neutrality and decrease non-linearly with increasing stability under stable conditions. The plot shows smaller scatter under unstable conditions than under stable conditions. The scatter of the unstable data is mainly caused by data obtained during FINTUREX, while values from both LINEX 96/2 and FINTUREX contribute to the scatter observed under stable conditions. No distinct group could be found, differing from the general trend by showing comparatively small fluctuations, as observed in the  $\sigma_w/u_*$  and  $\sigma_u/u_*$  data. Comparing the chosen y-axis intercept for  $\sigma_T/T_*$  with those chosen for  $\sigma_w/u_*$  and  $\sigma_u/u_*$ , the observed dispersion of  $\sigma_T/T_*$  is found to be much larger.

The nondimensional temperature standard deviation observed during LINEX 96/2 is plotted against the atmospheric stability with  $\zeta$  ranging from -1 to 0.5 (Figure 28). Under unstable and neutral stratification, the prediction by Foken et al. (1991) seems to follow the observed data well, the graph predicted by Tillmann (1972) matches the shape of the values but systematically overestimates the fluctuations of the normalised acoustic temperature. In the stable interval, the prediction by Foken et al. (1991) does not match the measured values beginning at  $\zeta \approx 0.04$  with increasing stability. The prediction by Wesely (1988) assumes  $\sigma_T/T_*$  to be constant at 1.85 for  $\zeta > -0.31$ . It seems obvious that this assumption is not suited to describe the behaviour of  $\sigma_T/T_*$  sufficiently in the considered stability interval. The data of the other experiments support the findings described above.

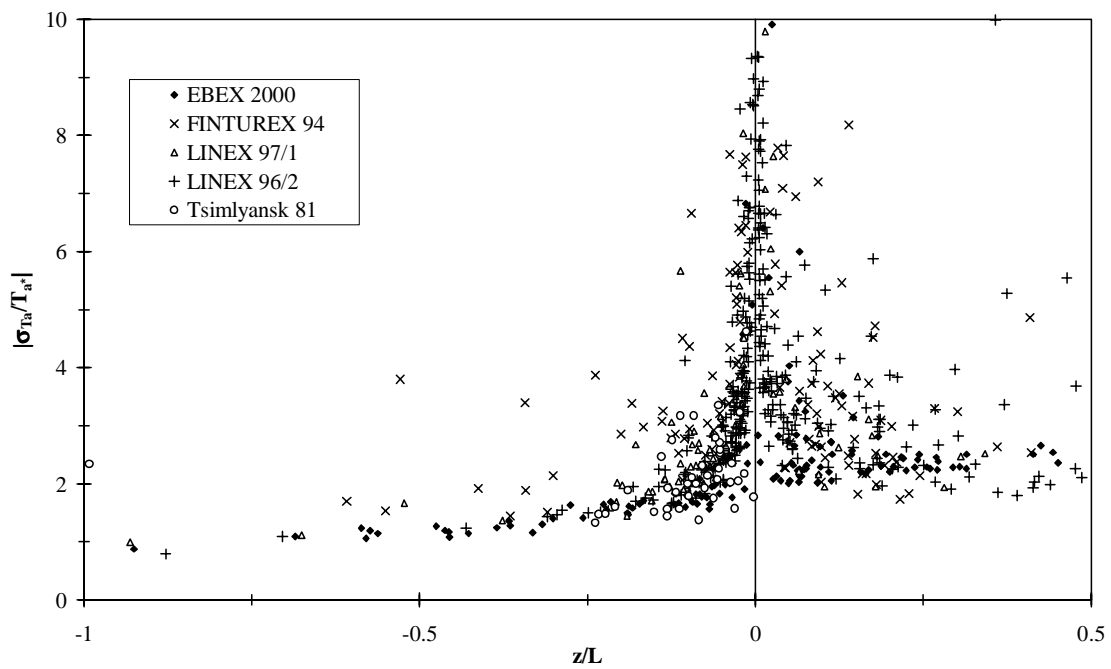


Figure 27: The nondimensional temperature standard deviation  $\sigma_{Ta}/T_{a^*}$  as a function of  $\zeta$ . The plot contains data of all experiments.

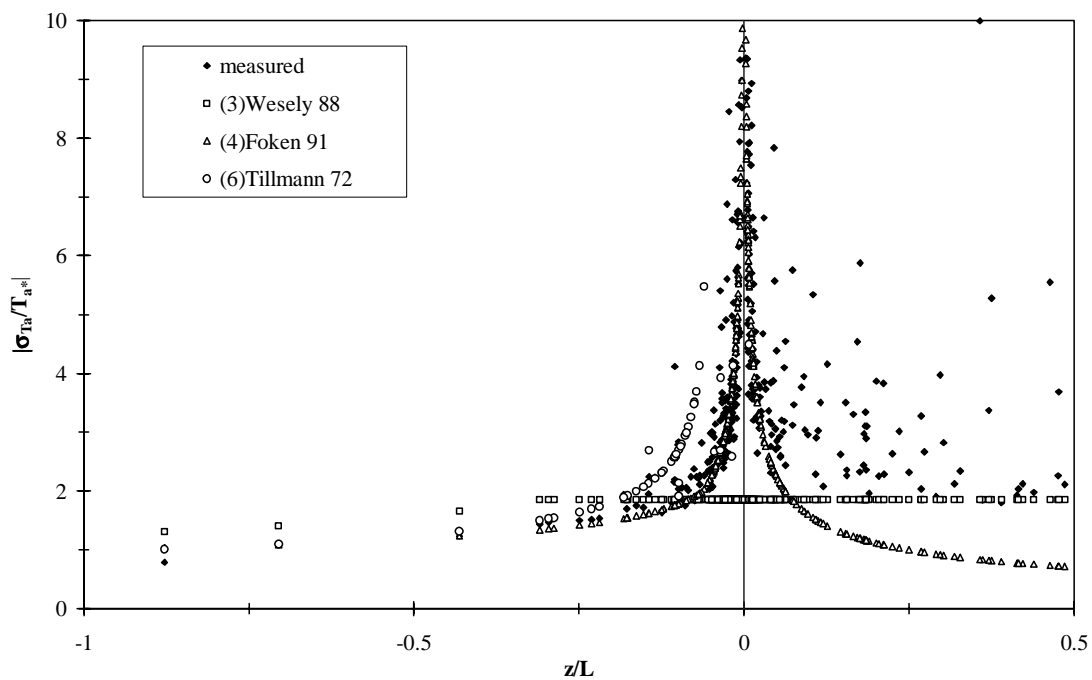


Figure 28: The nondimensional temperature standard deviation  $\sigma_{Ta}/T_{a^*}$  observed during LINEX 96/2 as a function of  $\zeta$ . Coloured symbols depict the predicted values according to parameterisations by various authors.

A correlation analysis of the individual data of all experiments to the predicted values was performed (Table 14). The considered stability range was subdivided into an unstable and a stable interval due to the finding that the predictions seem to match the unstable data better than the stable values. The results support this observation: 50% of the observed variance in Figure 28 can be explained using the parameterisation by Foken et al. (1991) for the unstable data, but only 8% when considering the entire stability interval  $-1 < \zeta < 0.5$ . The other parameterisations were found to yield correlation coefficients of about 0.20 independent on the chosen stability interval.

**Table 14:** Results of the correlation analysis between the combined dataset of all experiments and the predictions according to various authors with  $-1 < \zeta < -0.5$ , subdivided into unstable and stable data. Dashes denote that no correlation factor could be determined or that the parameterisation is invalid in the considered stability interval.

scaling factor	parameterisation	correlation coefficient R		
		$-1 < \zeta < 0$	$0.5 > \zeta > 0$	$-1 < \zeta < 0.5$
$\zeta$	(3) Wesely 88	0.25	-	0.20
	(4) Foken 91	0.70	0.20	0.28
	(6) Tillmann 72	0.22	-	0.22

The stable data of the combined dataset were found to follow a uniform, non-linearly decreasing trend with increasing stability (Figure 27). The prediction by Foken et al. (1991) was observed to miss these stable data. Modifying the coefficients and their validity intervals of this parameterisation by fitting visually, yields that 42% of the variance can be explained in the entire stability range of  $-1 < \zeta < 0.5$  (Table 15, Figure 29).

**Table 15:** The modified coefficients and validity intervals of the parameterisation based on Foken et al. (1991) using the parameterisation given by Equation ( 15 ).

variable x	stability $\zeta$	$C_1$	$C_2$	in Fig. referred to as
T	$0.02 \leq$	1.4	-1/4	(4) modified prediction
	$0.02 > \zeta \geq -0.0625$	0.5	-1/2	
	$-0.0625 > \zeta > -1$	1	-1/4	
	$< -1$	1	-1/3	

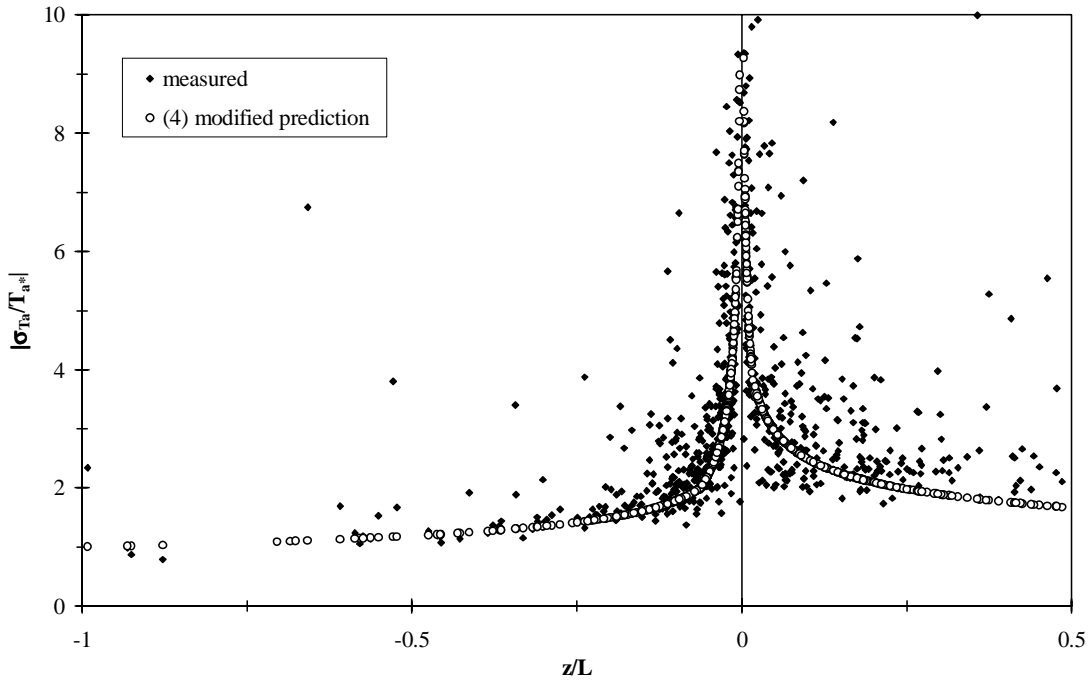


**Figure 29:** The nondimensional temperature standard deviation of the combined dataset as a function of  $\zeta$  with  $-1 < \zeta < 0.5$ . Dots depict the modified parameterisation based on Foken et al. (1991).

From this observations, we can conclude that the observed normalised temperature standard deviations of all experiments were found to show a clear dependency on the atmospheric stability  $\zeta$ . A modified prediction based on the parameterisation by Foken et al. (1991) was found to explain the observed variance best.

### 6.3 Comparison with results from other authors

In this chapter, the findings reported in the previous chapter will be compared to the results obtained by other authors. Additionally, the combined dataset of the five experiments according to Table 6 will be compared to two further datasets, namely the Kansas experimental data used by Wyngaard et al. (1971) and a dataset obtained at Cabauw, Netherlands published by Beljaars et al. (1983) and other experimental results by other authors. The comparison will deal with the vertical wind velocity first, before discussing the results for horizontal wind and temperature.

The combined  $\sigma_w/u^*$  dataset used in this thesis and the observed values of the additional datasets are plotted as a function of  $\zeta$  (Figure 30). The Kansas data and the Cabauw data fit the overall shape observed in the combined dataset used in this study. The findings reported in the previous chapter are thus assumed to be also valid for these additional data.

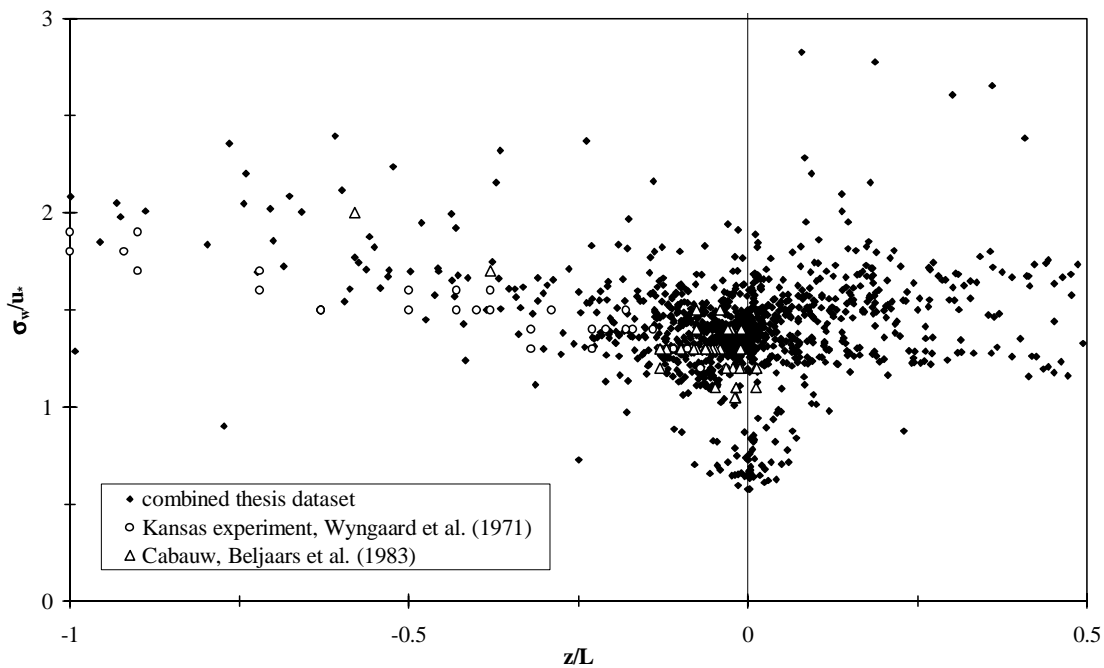


**Figure 30:** The nondimensional vertical velocity standard deviations of the dataset including all experiments (see Chapter 4) and the datasets used by Wyngaard et al. (1971) and Beljaars et al. (1983) as a function of  $\zeta$ .

The scaling factors derived from the pressure gradient length scale were found to be most appropriate for near neutral and stable nondimensional vertical velocity standard deviations in

the stability range with  $-0.2 < \zeta < 0.4$  (Section 6.1.1). This finding is in accordance with the results published by Högström (1990), who analysed near neutral  $\sigma_w/u_*$  data obtained at Lövsta, Sweden. Scaling the observed values with the stability and the pressure gradient dependencies, he found that only about 15% of the variance could be explained when using the scaling factor  $\zeta$ , whereas about 55 % of the dispersion could be explained when scaling with  $\ln[f(z - d)/u_*]$  in the stability interval with  $-0.2 < \zeta < 0.1$ . The dependency of the vertical wind velocity fluctuations on the geographical latitude found here is thus supported.

In this study, the dimensionless vertical velocity standard deviation was found to be invariant with height, as shown by the FINTUREX dataset. In contrast, Högström (1990) found  $\sigma_w/u_*$  to be dependent on the measurement height in neutral conditions, observing increasing values with increasing height. Wind tunnel measurements, as carried out by Mulhearn and Finnigan (1978), also suggest the nondimensional vertical velocity standard deviation to increase with height. As the amount of data in the FINTUREX dataset is small, further investigations are needed to solve this question and to provide possible explanations for the described discrepancy.

For the unstable  $\sigma_w/u_*$  data of the five considered experiments, parameterisations including dependencies on  $\zeta$  were found to yield the highest correlation coefficients. This result supports the findings of the authors (Section 3.1), who proposed the applied parameterisations. The goodness of fit of the correlation of the observed data to the predicted values was not improved including terms that involve the mixing layer height, in the stability range with  $-3 < \zeta < -0.2$ . This finding contradicts the results of Peltier et al. (1996) and Johansson et al. (1999), who recommended to include a  $z/z_i$  term into their parameterisation. However, due to the prevailing effect of free convection with  $\zeta < -3$ , parameterisations involving the mixing layer height are expected to yield better results in this stability range. Figure 31 plots the observed data of all experiments and the predicted values using parameterisations by various authors against the dimensionless height  $\zeta$  with  $\zeta$  ranging from -4.5 to -1. The prediction by Peltier et al. (1996), which uses a  $z/z_i$  dependency, reflects the behaviour of the observed values well. All other predictions seem to underestimate the observed data. Unfortunately, however, statistical analysis of  $\sigma_w/u_*$  values with  $\zeta < -3$  could not be performed in this study due to the small amount of data in this range of free convection.

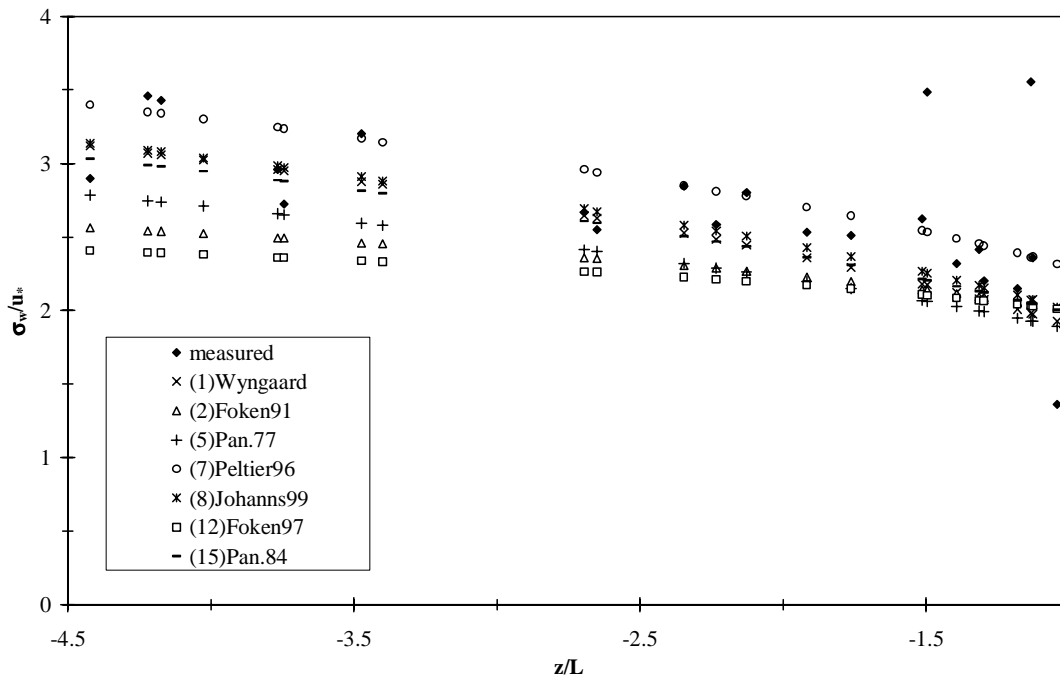


**Figure 31:** The nondimensional vertical velocity standard deviations of the dataset including all experiments (see Chapter 4) as a function of  $\zeta$  with  $-4.5 < \zeta < -1$ .

The observed nondimensional horizontal velocity standard deviations of the Tsimlyansk, FINTUREX, LINEX 96/2 and EBEX-2000 datasets could be explained using  $\ln[f(z-d)/u_*]$  as scaling factor (Section 6.1.2). This finding is in agreement with the results given by Smedman (1991), who found the data obtained at different Swedish sites to exhibit a linear dependency on  $\ln[f(z-d)/u_*]$ . Here, a significant correlation to the datasets of all 5 experiments (see Table 6) could only be found when predicting  $\sigma_u/u_*$  by linear equations, which involve  $-\ln[u_*]$  or  $\ln[f/u_*]$ . According to Smedman (1991), the slope of the linear expression has a negative sign, implying a decreasing trend with increasing stability. In contrast, all expressions derived by regression analysis in this study were observed to have a positive slope. However, as the slope of the found linear expressions is not significantly different from zero (see Appendix C), a direct comparison of the results is not possible.

Plotting the combined  $\sigma_u/u_*$  data of all experiments as a function of  $|z_i/L|$  did not yield a high correlation coefficient between the measured and the predicted values. However, the correlation coefficient was observed to be significantly different from zero. This result does not support the

findings of Panofsky et al. (1977) and Johansson et al. (1999), who found a clear dependence of the non-dimensionalised horizontal standard deviation on this scaling factor.

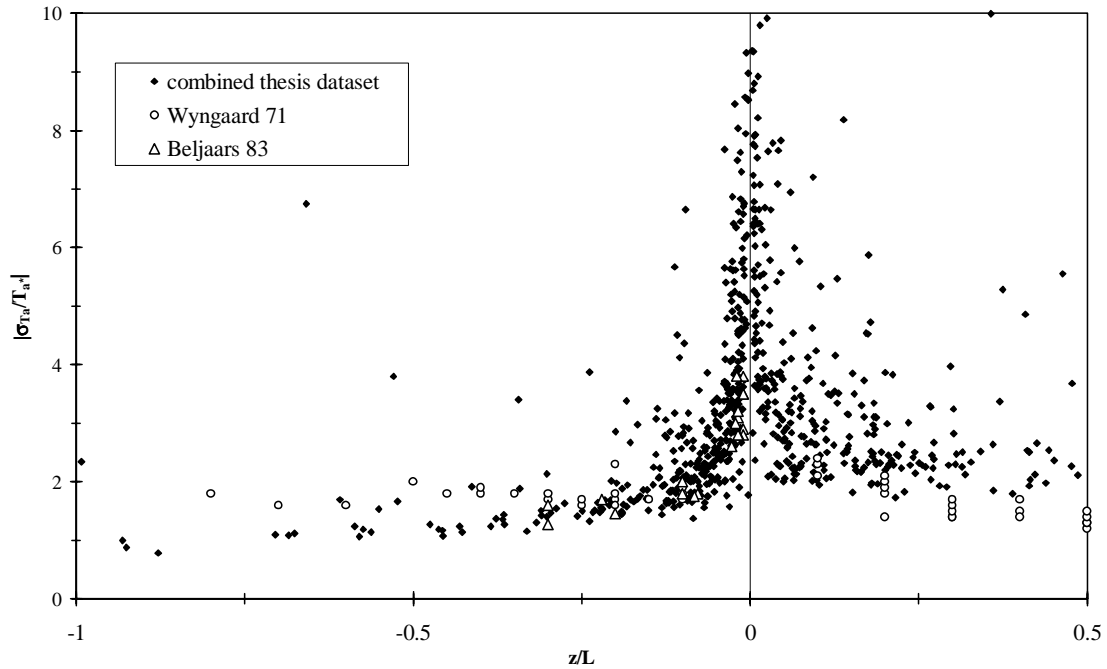


**Figure 32:** The dimensionless temperature standard deviations of the combined dataset and the datasets used by Wyngaard et al. (1971) and Beljaars et al. (1983) as a function of  $\zeta$ .

The  $\sigma_T/T_*$  values of the Cabauw dataset used by Beljaars et al. (1983) seem to agree with the behaviour observed in the datasets of the five experiments according to Table 6 used here (Figure 32). In contrast, the Kansas data show a different behaviour, suggesting  $\sigma_T/T_*$  to be rather constant over the entire stability range of  $-1 < \zeta < 0.5$ . The stable values of the Kansas experiment dataset are generally lower than those of the combined dataset. The strongest non-linear dependency on  $\zeta$  is supposed to occur around neutrality, however, where values are missing in this dataset. This fact complicates a direct comparison of the datasets.

The nondimensional temperature standard deviation was observed to be significantly dependent on atmospheric stability. This finding supports the generally accepted parameterisations given by various authors (Section 3.1). According to the findings reported in Section 6.2, the stability

---

range  $\zeta > -0.0625$  was subdivided into the intervals  $-0.0625 < \zeta < 0.02$  on one hand, and  $0.02 < \zeta$  on the other hand. This suggested subdivision reflects the changing turbulence regime, as the magnitude of turbulence decreases with increasing stability. This procedure is analogous to the analyses given by Skeib (1980) and Foken et al. (1991), according to Obukhov (1946).

## 7 Conclusions and recommendations

The main objective of this study was to re-evaluate parameterisations from literature of integral turbulence characteristics of wind velocity components and temperature in the surface layer. This re-evaluation was performed by applying the parameterisations reported in Chapter 3 to five datasets presented in Chapter 4, representing a great range of local and non-local parameters possibly influencing atmospheric turbulent flow quantities. In summary, we come to the following conclusions and recommendations (Table 16):

The nondimensional vertical velocity standard deviation was found to be significantly dependent on the expression  $f(z-d)/u_*$  under near neutral and slightly stable conditions with  $\zeta$  ranging from -0.2 to 0.4. Thus, the integral turbulence characteristic of the vertical wind velocity reflects an influence of the geographical latitude in this stability range. The dependency on  $f(z-d)/u_*$  was found to be equal to or stronger than the dependency on atmospheric stability in almost all experiments. The linear expression  $\sigma_w/u_* = 0.21 \ln[z_+ \cdot f/u_*] + 3.1$  explains the observed variance best in this stability range. As stratification becomes more unstable, the normalised vertical wind velocity fluctuations were found to scale with the atmospheric stability. The parameterisations involving  $\zeta$  proposed by various authors were found to predict the observed values well in the stability interval  $-3 < \zeta < -0.2$ . The best correlation was obtained using the expression  $\sigma_w/u_* = 1.3(1 - 2\zeta)^{1/3}$  given by Panofsky et al. (1977). Parameterisations including the mixing layer height were not found to improve the prediction of the integral turbulence characteristic of the vertical wind velocity in this stability range. Nevertheless, the dependency on the mixing layer height is supposed to increase under conditions of free convection with  $\zeta < -3$ .

The integral turbulence characteristic of the horizontal wind velocity was also found to be significantly dependent on  $f(z-d)/u_*$  under near neutral and slightly stable conditions in almost all experiments. Here, this dependency is of the same order of magnitude as the dependence on atmospheric stability, however. The best fit for all experimental data was obtained using the linear expression  $\sigma_u/u_* = 0.44 \ln[z_+ \cdot f/u_*] + 6.3$  for values with  $\zeta$  ranging from -0.2 to 0.4. For the unstable range with  $\zeta < -0.2$ , the parameterisation  $\sigma_u/u_* = 4.15(|\zeta|)^{1/6}$  by Foken et al. (1997a) can be recommended. The use of the scaling factor  $|z_i/L|$  as done by Panofsky et al. (1977) yields correlation coefficients significantly different from zero, but was found to overestimate  $\sigma_u/u_*$  and can therefore not be recommended.

The nondimensional temperature standard deviation was found to show a clear dependency on the atmospheric stability over the entire stability range. The parameterisation given by Foken et al. (1991) yields a good overall fit to the experimental data, but is recommended to be modified to  $\sigma_T/T_* = 1.4(|\zeta|)^{-1/4}$  for stable stratification with  $\zeta > 0.02$ .

To our current understanding, the findings of this study represent the most appropriate parameterisations of integral turbulence characteristics of wind velocity components and temperature. Hopefully, these results will improve the quality of applications using integral turbulence characteristics.

**Table 16: Recommendations for the parameterisations of the integral turbulence characteristics of the vertical and horizontal wind velocity components and temperature**

integral turbulence characteristic	stability range			
	$-3 < \zeta < -0.2$	$-0.2 < \zeta < 0.4$		
$\sigma_w/u_*$	$1.3(1 - 2\zeta)^{1/3}$ (1) by Panofsky et al. (1977)	$0.21 \ln \left[ \frac{z_+ \cdot f}{u_*} \right] + 3.1$ (2)		
$\sigma_u/u_*$	$4.15( \zeta )^{1/8}$ by Foken et al. (1991), Foken et al. (1997a)	$0.44 \ln \left[ \frac{z_+ \cdot f}{u_*} \right] + 6.3$ (2)		
integral turbulence characteristic	stability range			
	$\zeta < -1$	$-1 < \zeta < -0.0625$	$-0.0625 < \zeta < 0.02$	$0.02 < \zeta$
$ \sigma_T/T_* $	$( \zeta )^{-1/3}$	$( \zeta )^{-1/4}$	$0.5( \zeta )^{-1/2}$	$1.4( \zeta )^{-1/4}$
by Foken et al. (1991)				

(1) Other parameterisations reported in Chapter 3 were not found to yield significantly different results.

(2)  $z_+ = 1\text{m}$  (see Section 6.1)

## 8 References

- Arya, S.P., 2001. Introduction to micrometeorology. International Geophysics Series, 79. Academic Press, San Diego, San Francisco, New York, Boston, London, Sydney, Tokyo, 2nd, 420 pp.
- Beljaars, A.C.M. and Betts, A.K., 1992. Validation of the boundary layer representation in the ECMWF model, ECMWF Seminar Proceedings: Validation of models over Europe, Reading (UK).
- Beljaars, A.C.M., Schotanus, P. and Nieuwstadt, F.T.M., 1983. Surface layer similarity under nonuniform fetch conditions. *J. Climate & Appl. Meteorol.*, 22: 1800-1810.
- Blackadar, A.K., 1997. Turbulence and Diffusion in the Atmosphere. Springer-Verlag Berlin Heidelberg New York, Berlin Heidelberg, 185 pp.
- Bruckmeier, C., 2001. Die Auswirkung von Gerätekorrekturen auf die Schließung der Energiebilanz am Erdboden. Diploma Thesis, Universität Bayreuth, Bayreuth, 98 pp.
- Bruckmeier, C., Foken, T., Gerchau, J. and Mauder, M., 2001. Documentation of the experiment EBEX-2000., University of Bayreuth, Department of Micrometeorology, Arbeitsergebnisse, 13, 21 pp.
- Businger, J.A., 1982. Equations and concepts. In: F.T.M. Nieuwstadt and H. Van Dop (Editors), Atmospheric turbulence and air pollution modelling. D. Reidel Publishing Company, Dordrecht, Boston, London, pp. 1-36.
- Businger, J.A. and Oncley, S.P., 1990. Flux Measurement with Conditional Sampling. *J. Atmosph. & Oceanic Techn.*, 7: 349-352.
- DeBruin, H.A.R., Bink, N.J. and Kroon, L.J., 1991. Fluxes in the surface layer under advective conditions. In: T.J. Schmugge and J.C. André (Editors), Workshop on Land Surface Evaporation, Measurement and Parametrization. Springer, New York, pp. 157-169.
- Foken, T., 1990. Turbulenter Energieaustausch zwischen Atmosphäre und Unterlage - Methoden, meßtechnische Realisierung sowie ihre Grenzen und Anwendungsmöglichkeiten, Ber. Dt. Wetterdienstes, 180, 287 pp.

- Foken, T., 1998. Ergebnisse des LINEX-97/1 Experimentes., Deutscher Wetterdienst, Forschung und Entwicklung, Arbeitsergebnisse, 53, 38 pp.
- Foken, T., 1999. Der Bayreuther Turbulenzknecht., University of Bayreuth, Department of Micrometeorology, Arbeitsergebnisse, 1, 40 pp.
- Foken, T., 2002. The turbulence experiment FINTUREX at the Neumayer-Station/Antarctica., Deutscher Wetterdienst, Forschung und Entwicklung, Arbeitsergebnisse, in prep.
- Foken, T. and Baum, W., 1994. FINTUREX - Technische Dokumentation., Deutscher Wetterdienst Meteorologisches Observatorium Lindenberg, Berlin, Potsdam, 60 pp.
- Foken, T. and Haake, R. (Editors), 1984. International Turbulence Comparison Expedition "ITCE 1981" Tsimlyansk, USSR. Geodätische und geophysikalische Veröffentlichungen, Reihe II, Heft 26. Nationalkomitee für Geodäsie und Geophysik bei der Akademie der Wissenschaften der DDR, Berlin, 100 pp.
- Foken, T., Jegede, O.O., Weisensee, U., Richter, S.H., Handorf, D., Görsdorf, U., Vogel, G., Schubert, U., Kirzel, H.-J. and Thiermann, V., 1997a. Results of the LINEX-96/2 Experiment., Deutscher Wetterdienst, Forschung und Entwicklung, Arbeitsergebnisse, 48, 75 pp.
- Foken, T., Richter, S.H., Weisensee, U., Görsdorf, U., Pohl, H., Niesche, S. and Dereszynski, P., 1996. LINEX 96/2 Technische Dokumentation., Deutscher Wetterdienst Meteorologisches Observatorium Lindenberg, Berlin, Potsdam, 50 pp.
- Foken, T., Richter, S.H., Weisensee, U., Schmdtke, E., Christoph, A. and Niesche, S., 1997b. LINEX 97/1 Technische Dokumentation., Deutscher Wetterdienst Meteorologisches Observatorium Lindenberg, Berlin, Potsdam, 60 pp.
- Foken, T., Skeib, G. and Richter, S.H., 1991. Dependence of the integral turbulence characteristics on the stability of stratification and their use for Doppler- Sodar measurements. *Z.Meteorologie*, 41: 311- 315.
- Foken, T. and Wichura, B., 1996. Tools for quality assessment of surface-based flux measurements. *Agric. & Forest Meteorol.*, 78: 83-105.
- Haugen, D.A., Kaimal, J.C. and Bradley, E.F., 1971. An experimental study of Reynold stress and heat flux in the atmospheric surface layer. *Quart. J. Roy. Meteor. Soc.*, 97: 168- 180.

- Högström, U., 1990. Analysis of turbulence structure in the surface layer with a modified similarity formulation for near neutral conditions. *J. Atm. Sci.*, 47: 1949- 1972.
- Holtstag, A.A.M., De Bruin, E.I.F. and Pan, H.-L., 1990. A high resolution air mass transformation model for short range weather forecasting. *Mon.Wea. Rev.*, 118: 1561-1575.
- Holzworth, C.G., 1964. Estimates of mean maximum mixing depths in the contiguous United States. *Mon.Wea. Rev.*, 92: 235- 242.
- Hupfer, P., 1996. *Unsere Umwelt: Das Klima*. Teubner-Reihe Umwelt. B.G. Teubner Verlagsgesellschaft, Stuttgart Leipzig, 336 pp.
- Jegade, O.O. and Foken, T., 1999. A study of the internal boundary layer due to a roughness change in neutral conditions observed during the LINEX field campaigns. *Theor. & Appl. Climatol.*, 62: 31-41.
- Johansson, C., Smedman, A.-S. and Högström, U., 1999. Critical test of the validity of Monin-Obukhov similarity during convective conditions, 13<sup>th</sup> Symposium on Boundary Layer and Turbulence. *Am. Meteorol. Soc.*, Dallas, TX, pp. 686-689.
- Kaimal, J.C. and Finnigan, J.J., 1994. *Atmospheric boundary layer flows: their structure and measurement*. Oxford University Press, New York, 289 pp.
- Köhler, W., Schachtel, G. and Voleske, P., 1996. *Biostatistik*. Springer Verlag, Berlin, Heidelberg, New York, 2nd, 285 pp.
- Lehner, I., 2001. *EBEX 2000 (Energy Balance Experiment): Description and analysis of the wind field - with main focus on SODAR measurements*. Semester Thesis, University of Basel, Basel, 44 pp.
- Liu, H., Peters, G. and Foken, T., 2001. New equations for sonic temperature variance and buoyancy heat flux with an omni-directional sonic anemometer. *Boundary-Layer Meteorol.*, 100: 459-468.
- Mangold, A., 1999. *Untersuchung der lokalen Einflüsse auf Turbulenzmessungen der Station Weidenbrunnen*. Diploma Thesis, University of Bayreuth, Bayreuth, 175 pp.

- Monin, A.S. and Obukhov, A.M., 1954. Osnovnye zakonomernosti turbulentnogo peremesivaniya v prizemnom sloe atmosfery. Trudy geofiz. inst. AN SSSR, 24 (151): 163-187.
- Moore, C.J., 1986. Frequency response corrections for eddy correlation systems. *Boundary-Layer Meteorol.*, 37: 17-35.
- Mulhearn, P.J. and Finnigan, J.J., 1978. Turbulent flow over a very rough, random surface. *Boundary-Layer Meteorol.*, 15: 109-132.
- Obukhov, A.M., 1946. Turbulentnost v temperturnoj-neodnorodnoj atmosfere. Trudy Inst. Teoret. Geofiz. AN SSSR, 1.
- Oncley, S.P., Foken, T., Vogt, R., Bernhofer, C., Liu, H., Sorbjan, Z., Pitacco, A., Grantz, D. and Riberio, L., 2000. The EBEX 2000 field experiment, 14th Symposium on Boundary Layer and Turbulence. American Meteorological Society, Boston, Aspen CO., pp. 322-324.
- Panofsky, H.A. and Dutton, J.A., 1984. Atmospheric turbulence, models and methods for engineering applications. Wiley, New York.
- Panofsky, H.A., Tennekes, H., Lenschow, D.H. and Wyngaard, J.C., 1977. The characteristics of turbulent velocity components in the surface layer under convective conditions. *Boundary-Layer Meteorol.*, 11: 355- 361.
- Peltier, L.J., Wyngaard, J.C., Khanna, S. and Brasseur, J.G., 1996. Spectra in the unstable surface layer. *J.Atm.Sci.*, 53: 49- 61.
- Rotach, M.W., 1992. Determination of the zero plane displacement in an urban environment. *Boundary-Layer Meteorol.*, 67: 187- 193.
- Rotach, M.W., 1993. Turbulence close to a rough urban surface part II: variances and gradients. *Boundary-Layer Meteorol.*, 66: 75- 92.
- Schmid, H.P., 1994. Source areas for scalars and scalar fluxes. *Boundary-Layer Meteorol.*, 67: 293-318.
- Seibert, P., Beyrich, F., Gryning, S.-E., Joffre, S., Rasmussen, A. and Tercier, P., 2000. Review and intercomparison of operational methods for the determination of the mixing height. *Atmos. Environm.*, 34: 1001- 1027.

- Seibert, P., Beyrich, F., Gryning, S.-E., Sylvain, J., Rasmussen, A. and Tercier, P., 1998. Mixing height determination for dispersion modelling. In: B.E.A. Fisher et al. (Editors), EUR 18195- COST Action 710 - Final report: Harmonisation of the pre-processing of meteorological data for atmospheric dispersion models. Office for Official Publications of the European Communities, Luxembourg, pp. 431.
- Skeib, G., 1980. Zur Definition universeller Funktionen für die Gradienten von Windgeschwindigkeit und Temperatur in der bodennahen Luftschicht. *Z.Meteorologie*, 30: 23- 32.
- Smedman, A.-S., 1991. Some turbulence characteristics in stable atmospheric boundary layer flow. *J.Atm.Sci.*, 48: 856- 868.
- Stull, R.B., 1988. *An Introduction to Boundary Layer Meteorology*. Kluwer Acad. Publ., Dordrecht, Boston, London, 666 pp.
- Stull, R.B., 2000. *Meteorology for scientists and engineers*. Gary Garlson, Brooks/Cole, 2nd, 502 pp.
- Taubenheim, J., 1969. *Statistische Auswertung geophysikalischer und meteorologischer Daten*. Akad.Verlagsges., Leipzig, 386 pp.
- Tennekes, H., 1982. Similarity relations, scaling laws and spectral dynamics. In: F.T.M. Nieuwstadt and H. Van Dop (Editors), *Atmospheric turbulence and air pollution modelling*. D. Reidel Publishing Company, Dordrecht, Boston, London, pp. 37- 68.
- Tennekes, H. and Lumley, J.L., 1972. *A first course in turbulence*. M.I.T. Press, Cambridge, Mass, 300 pp.
- Thom, A.S., 1971. Momentum absorption by vegetation. *Quart.J.Roy.Meteor.Soc.*, 97: 414- 428.
- Tillmann, J.E., 1972. The indirect determination of stability, heat and momentum fluxes in the atmospheric boundary layer from simple scalar variables during dry unstable conditions. *J. Appl. Meteorol.*, 11: 783- 792.
- Troen, I. and Mahrt, L., 1986. A simple model of the planetary boundary layer: sensitivity to surface evaporation. *Boundary-Layer Meteorol.*, 37: 129- 148.

- Tsvang, L.R., Zubkovskij, S.L., Kader, B.A., Kallistratova, M.A., Foken, T., Gerstmann, W., Przandka, Z., Pretel, J., Zelený, J. and Keder, J., 1985. International turbulence comparison experiment (ITCE-81). *Boundary-Layer Meteorol.*, 31: 325-348.
- Wesely, M.L., 1988. Use of variance techniques to measure dry air- surface exchange rates. *Boundary-Layer Meteorol.*, 44: 13- 31.
- Wichura, B. and Foken, T., 1995. Anwendung integraler Turbulenzcharakteristiken zur Bestimmung von Energie- und Stoffflüssen in der Bodenschicht der Atmosphäre. *Deutscher Wetterdienst, Forschung und Entwicklung, Arbeitsergebnisse*, 29, 51 pp.
- Willis, G.E. and Deardorff, J.W., 1974. A laboratory model of the unstable planetary boundary layer. *J.Atm.Sci.*, 31: 1297- 1307.
- Wyngaard, J.C. and Clifford, S.F., 1978. Estimation momentum, heat and moisture fluxes from structure parameters. *J.Atm.Sci.*, 35: 1204-1211.
- Wyngaard, J.C., Coté, O.R. and Izumi, Y., 1971. Local free convection, similarity and the budgets of shear stress and heat flux. *J.Atm.Sci.*, 28: 1171-1182.
- Yaglom, A.M., 1979. Similarity laws for constant-pressure and pressure-gradient turbulent wall flows. *Ann. Rev. Fluid Mech.*, 11: 505- 540.

## 9 Index of Figures

Figure 1:	Dynamics of the stable nocturnal boundary layer and convectively mixed boundary layer due to cooling and heating processes at the surface. The time indicated is Local Standard Time (Kaimal and Finnigan, 1994).	20
Figure 2:	Typical values of the surface roughness $z_0$ according to different types of terrain [From Tables by the Royal Aeronautical Society (1972), citaded by Arya (2001)].	23
Figure 3:	Geographical position and latitude of the experiments providing data basis for the re-evaluation.	27
Figure 4:	Illustration of the simple (1) and the advanced (2) parcel method used to derive the mixing layer height $z_i$ (Seibert et al., 1998), changed).	39
Figure 5:	Root-mean-square difference as a function of the assumed value of the displacement height $d_*$ for EBEX-2000, wind direction sector 1 - $45^\circ$ . The amount of data for this sector is 41.	43
Figure 6:	Measured $\sigma_w/u_*$ data as a function of $\zeta$ . The Figure contains data of all experiments with $\zeta$ ranging from -1 to 0.5.	46
Figure 7:	Measured $\sigma_w/u_*$ data as a function of $\ln[f(z - d)/u_*]$ . The Figure illustrates data of all experiments selected by $-0.2 < \zeta < 0.1$ .	46
Figure 8:	The nondimensional vertical velocity standard deviation of the LINEX 96/2 experiment as a function of $\zeta$ with $-0.2 < \zeta < 0.1$ . The coloured curves are predicted values of $\sigma_w/u_*$ according to parameterisations by various authors (see Section 3.1).	48
Figure 9:	The nondimensional vertical velocity standard deviation of the LINEX 96/2 experiment as a function of $\ln[f(z - d)/u_*]$ . The coloured lines depict the predictions of $\sigma_w/u_*$ given by various authors. For details of the parameterisations see Section 3.1.	48
Figure 10:	The nondimensional vertical velocity standard deviation over the entire stability range observed during EBEX-2000 plotted against $\ln[f(z - d)/u_*]$ .	50
Figure 11:	The nondimensional vertical velocity standard deviation over the entire stability range observed during LINEX 97/1 plotted against $\ln[f(z - d)/u_*]$ .	50
Figure 12:	The nondimensional vertical velocity standard deviations of all experiments plotted against $\ln[f/u_*]$ . Data was selected with $-0.2 < \zeta < 0.4$ .	52
Figure 13:	The nondimensional vertical velocity standard deviations of all experiments plotted against $\ln[(z - d)/u_*]$ . Data was selected with $-0.2 < \zeta < 0.4$ .	53
Figure 14:	The nondimensional vertical velocity standard deviation observed during LINEX 96/2 plotted against $\ln[f/u_*]$ . The solid line represents $0.21\ln[f/u_*] + 3.1$ with $R = 0.76$ .	54
Figure 15:	The nondimensional vertical velocity standard deviations observed during FINTUREX at three different measuring heights: 2m, 4m and 12m. The individual data and the group mean values are displayed.	56
Figure 16:	The nondimensional vertical velocity standard deviations of all experiments observed with $-3 < \zeta < -0.2$ . The coloured lines depict the predictions according to various authors (see Chapter 3).	57

Figure 17:	$\sigma_w/u_*$ data of EBEX-2000 selected by $-0.2 < \zeta < 0.1$ as a function of $\ln[f(z-d)/u_*]$ .	59
Figure 18:	$\sigma_w/u_*$ data of EBEX-2000 selected by $-0.2 < \zeta < 0.1$ as a function of the observed wind direction.	59
Figure 19:	The observed nondimensional horizontal velocity standard deviation of all experiments plotted against $\zeta$ with $-1 < \zeta < 0.5$ .	62
Figure 20:	The observed nondimensional horizontal velocity standard deviation of all experiments plotted against $\ln[f(z-d)/u_*]$ . Data were selected for $-0.2 < \zeta < 0.1$ .	62
Figure 21:	The observed nondimensional horizontal velocity standard deviation of the LINEX 96/2 experiment as a function of $\zeta$ .	64
Figure 22:	The observed nondimensional horizontal velocity standard deviation of the LINEX 96/2 experiment as a function of $\ln[f(z-d)/u_*]$ .	64
Figure 23:	The nondimensional horizontal velocity standard deviations of all experiments as a function of $\ln[f/u_*]$ . Data were selected for $-0.2 < \zeta < 0.1$ .	65
Figure 24:	Measured nondimensional horizontal velocity standard deviations as a function of $\zeta$ for $-3 < \zeta < -0.2$ . The figure contains data of all experiments.	67
Figure 25:	Observed nondimensional horizontal velocity standard deviation as a function of $ z/L $ for $\zeta < -1$ . The figure contains data of all experiments.	68
Figure 26:	The nondimensional temperature standard deviation observed during the considered experiments. Solid rhombi depict $\sigma_{T_a}/T_{a*}$ , unfilled rhombi $\sigma_{T_p}/T_{p*}$ .	69
Figure 27:	The nondimensional temperature standard deviation $\sigma_{T_a}/T_{a*}$ as a function of $\zeta$ . The plot contains data of all experiments.	71
Figure 28:	The nondimensional temperature standard deviation $\sigma_{T_a}/T_{a*}$ observed during LINEX 96/2 as a function of $\zeta$ . Coloured symbols depict the predicted values according to parameterisations by various authors.	71
Figure 29:	The nondimensional temperature standard deviation of the combined dataset as a function of $\zeta$ with $-1 < \zeta < 0.5$ . Dots depict the modified parameterisation based on Foken et al. (1991).	73
Figure 30:	The nondimensional vertical velocity standard deviations of the dataset including all experiments (see Chapter 4) and the datasets used by Wyngaard et al. (1971) and Beljaars et al. (1983) as a function of $\zeta$ .	74
Figure 31:	The nondimensional vertical velocity standard deviations of the dataset including all experiments (see Chapter 4) as a function of $\zeta$ with $-4.5 < \zeta < -1$ .	76
Figure 32:	The dimensionless temperature standard deviations of the combined dataset and the datasets used by Wyngaard et al. (1971) and Beljaars et al. (1983) as a function of $\zeta$ .	77
Figure 33:	The nondimensional vertical velocity standard deviations of all experiments plotted against $-\ln[u_*]$ . Data was selected with $-0.2 < \zeta < 0.4$ .	96
Figure 34:	The nondimensional vertical velocity standard deviations of all experiments plotted against $\ln[f(z-d)/u_*]$ . Data was selected with $-0.2 < \zeta < 0.4$ .	96
Figure 35:	The unstable nondimensional vertical velocity standard deviation of all experiments plotted against $\ln[f(z-d)/u_*]$ . Data was selected for $\zeta < -0.2$ .	97
Figure 36:	Significance levels ( $R_{\text{significant}}$ ) for correlation coefficients $R$ (Taubenheim, 1969).	99

## 10 Index of Tables

Table 1:	Coefficients used in Equation ( 15 ) as given by various authors _____	14
Table 2:	Coefficients used in Equation ( 16 ) and ( 17 ) as given by various authors _____	15
Table 3:	Coefficients used in Equation ( 23 ) as given by various authors _____	19
Table 4:	Coefficients used in Equation ( 26 ) _____	21
Table 5:	Coefficients used in Equation ( 27 ) as given by various authors _____	22
Table 6:	Overview of basic parameters of the experiments providing the database for this thesis _____	32
Table 7:	Overview of the datasets before and after filtering and application of spectral correction as a function of atmospheric stability classes _____	35
Table 8:	Overview of the initial input data files used for the boundary layer model by Blackadar (1997). Starting time is indicated in Standard Local Time. _____	41
Table 9:	Results of the correlation analysis between the predicted values derived from parameterisations illustrated in Figure 8 and 9 and the observed experimental data of the corresponding experiment. Data were selected for $-0.2 < \zeta < 0.1$ . A dashes denotes that no correlation coefficient R could be determined. _____	47
Table 10:	Results of the linear regression using the least squares method and correlation analysis for the measured $\sigma_w/u_*$ data of all experiments shown in Figure 12, Figure 13 and Appendix C. Data was selected with $-0.2 < \zeta < 0.4$ . _____	53
Table 11:	Results of the correlation analysis between the observed data of all experiments and the predictions according to various authors with $-3 < \zeta < -0.2$ . The total amount of data is 107. _____	57
Table 12:	Results of the correlation analysis between the predicted values derived from parameterisations illustrated in Figure 21 and Figure 22 and the observed experimental data of the corresponding experiment. Data were selected for $-0.2 < \zeta < 0.1$ . _____	63
Table 13:	Results of the linear regression using the least squares method and correlation analysis for the observed $\sigma_w/u_*$ data of all experiments. The near neutral range with $-0.2 < \zeta < 0.1$ and the expanded range with $-0.2 < \zeta < 0.4$ were considered. _____	66
Table 14:	Results of the correlation analysis between the combined dataset of all experiments and the predictions according to various authors with $-1 < \zeta < -0.5$ , subdivided into unstable and stable data. Dashes denote that no correlation factor could be determined or that the parameterisation is invalid in the considered stability interval. _____	72
Table 15:	The modified coefficients and validity intervals of the parameterisation based on Foken et al. (1991) using the parameterisation given by Equation ( 15 ). _____	73
Table 16:	Recommendations for the parameterisations of the integral turbulence characteristics of the vertical and horizontal wind velocity components and temperature _____	80
Table 17:	Significance levels for correlation coefficients (Taubenheim, 1969). _____	98

## 11 Index of the used abbreviations and symbols

$a_1, a_2, B, C$	constant values
$C_{Dg}$	geostrophic drag coefficient
$\overline{x'y'}$	covariance of the fluctuating variables x and y
$c_p$	specific heat at constant pressure for moist air [ $J \cdot kg^{-1} K^{-1}$ ]
CSAT	Sonic anemometer, Campbell Scientific Ltd.
d	displacement height [m]
d*	assumed displacement height [m], see Section 5.2
DAT-310	Sonic anemometer, Kaijo Denki
$dp/dx$	longitudinal pressure gradient [ $hPa \cdot m^{-1}$ ]
E	East
EBEX	Energy Balance Experiment
f	Coriolis parameter [ $s^{-1}$ ]
FINTUREX	Final Turbulence Experiment of the Meteorological Observatory Potsdam
g	acceleration due to gravity [ $ms^{-2}$ ]
$h_c$	average canopy height [m]
K	turbulent exchange coefficient
KH20	Krypton Hygrometer, Campbell Scientific Ltd.
L	Obukhov-length [m]
LAI	Leaf Area Index
LINEX	Lindenberg Experiment
$(\overline{u'w'})^{1/2}$	momentum flux [ $ms^{-1}$ ]
N	North
$p, p'$	mean and fluctuation of the pressure [hPa]

---

$q^*$	normalising factor for the standard deviation of the humidity [hPa]
$q, q'$	mean and fluctuation of the specific humidity [hPa]
$Q_E/\rho, \overline{w'q'}$	latent heat flux [hPa·ms <sup>-1</sup> ]
$Q_H/\rho c_p, \overline{w'T'}$	sensible heat flux [K·ms <sup>-1</sup> ]
R	correlation coefficient
rmsd	root mean square difference
S	South
SLT	Standard Local Time
SODAR	Sound detection and ranging
$T^*$	normalising factor for the standard deviation of the temperature [K]
$T, T'$	mean and fluctuation of the absolute temperature [K]
$T_a^*$	normalising factor for the standard deviation of the acoustic temp. [K]
temp.	temperature
$T_p^*$	normalising factor for the standard deviation of the platinum temp.[K]
$u^*$	friction velocity [ms <sup>-1</sup> ]
$u^*/u$	dimensionless drag coefficient
$u, u'$	mean and fluctuation of the horizontal wind velocity [ms <sup>-1</sup> ]
$u_g$	mean horizontal x-geostrophic wind velocity [ms <sup>-1</sup> ]
UTC	Universal Time Code
$v_g$	mean horizontal y-geostrophic wind velocity [ms <sup>-1</sup> ]
W	West
$w^*$	Deardorff velocity [ms <sup>-1</sup> ]
$w, w'$	mean and fluctuation of the vertical wind velocity [ms <sup>-1</sup> ]
z	geometrical height above ground [m]
(z – d)	aerodynamical height [m]

---

$z_+$	normalising factor with a value of 1, [m]
$z_0$	roughness length [m]
$z_i$	mixing layer height
$\varphi_h$	dimensionless temperature gradient
$\varphi_m$	dimensionless wind shear gradient
$\Theta_v, \Theta_v'$	mean and fluctuation of the virtual potential temperature [K]
$\Omega$	rotational speed of the earth [ $s^{-1}$ ]
$\delta_p$	pressure gradient length scale [m]
$\varepsilon$	dissipation of turbulent kinetic energy
$\phi$	geographical latitude
$\phi_x, \phi_u$	function of the variable x, u
$\kappa$	von-Karman constant
$\theta, \theta'$	mean and fluctuation of the potential temperature [K]
$\rho$	mass density of air [ $kg \cdot m^{-3}$ ]
$\sigma_q/q^*$	integral turbulence characteristics of the specific humidity
$\sigma_T/T^*$	integral turbulence characteristics of the temperature
$\sigma_{T_a}/T_{a^*}$	integral turbulence characteristics of the acoustic temperature
$\sigma_{T_p}/T_{p^*}$	integral turbulence characteristics of the platinum temperature
$\sigma_u/u^*$	integral turbulence characteristics of the horizontal wind velocity
$\sigma_w/u^*$	integral turbulence characteristics of the vertical wind velocity
$\sigma_x$	standard deviation of the variable x
$\sigma_x^2$	variance of the variable x
$\tau_o$	surface drag [ $kg \cdot m^{-1} s^{-2}$ ]
$\tau_o/\rho$	surface shear stress [ $m^2 s^{-2}$ ]
$\zeta = z/L$	dimensionless height, buoyancy parameter

## 12 Appendix A

### Boundary Layer Model

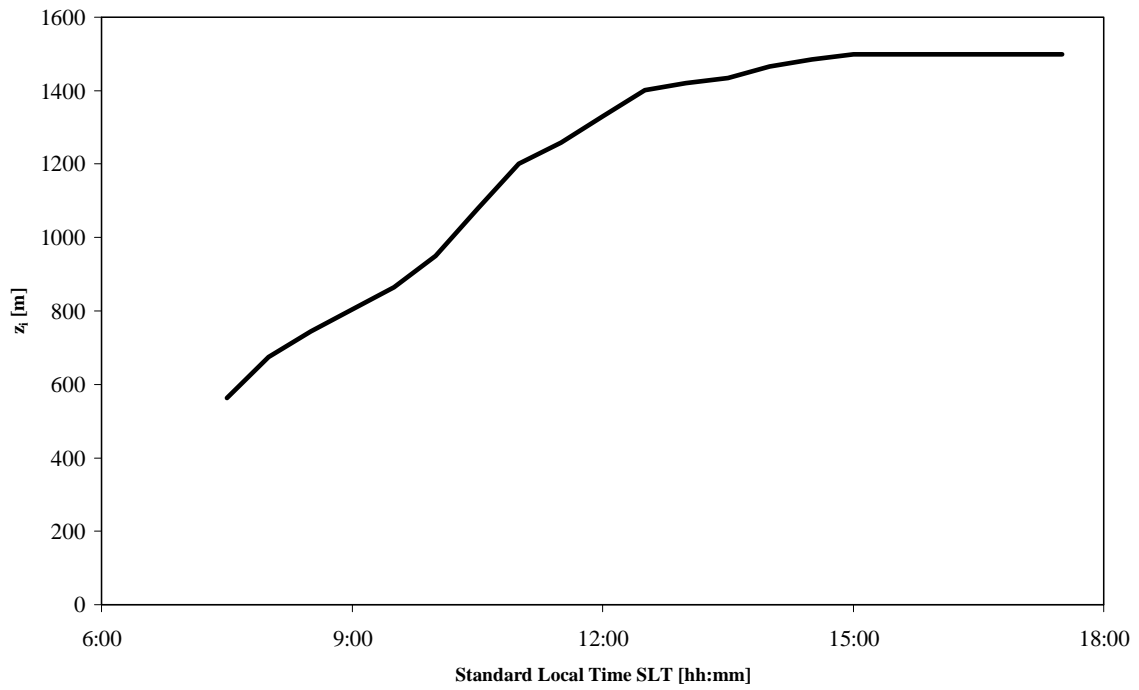
List of variables needed for input of the boundary layer model by Blackadar (1997)

variable	unit	abbrev.	variable	unit	abbrev.
air temperature surface layer	[°C]	ta	2560 m height	[°C]	t26
x- wind velocity surface layer	[m/s]	ua	2660 m height	[°C]	t27
y- wind velocity surface layer	[m/s]	va	2760 m height	[°C]	t28
humidity, mixing ratio surface layer	[1]	qa	2860 m height	[°C]	t29
x- wind geostrophic surface layer	[m/s]	uga	2960 m height	[°C]	t30
y- wind geostrophic surface layer	[m/s]	vga	wind velocity u at 60 m height	[m/s]	u1
latitude	[°]	glatd	160 m height	[m/s]	u2
solar declination	[°]	decltd	260 m height	[m/s]	u3
roughness length	[m]	z <sub>0</sub>	360 m height	[m/s]	u4
cloudiness	[1]	clds	460 m height	[m/s]	u5
sub- soil temperature	[°C]	tm	560 m height	[m/s]	u6
precipitable water	[cm]	prh2o	660 m height	[m/s]	u7
max range for plot	[°C]	tx	760 m height	[m/s]	u8
min range for plot	[°C]	tn	860 m height	[m/s]	u9
time after noon for start	[min]	gotime	960 m height	[m/s]	u10
transmissivity for short wave radiation	[1]	transm	1060 m height	[m/s]	u11
ground surface temperature	[°C]	tg	1160 m height	[m/s]	u12
soil moisture slab field cap.	[1]	rhogx	1260 m height	[m/s]	u13
soil moisture wilt limit	[1]	rhowlt	1360 m height	[m/s]	u14
soil moisture sub soil	[1]	rhom	1460 m height	[m/s]	u15
soil moisture slab	[1]	rhog	1560 m height	[m/s]	u16
heat capacity dry soil	[J/m3]	csd	1660 m height	[m/s]	u17
heat capacity water	[J/m3]	csw	1760 m height	[m/s]	u18
leaf area index	[1]	fn	1860 m height	[m/s]	u19
soil albedo	[1]		1960 m height	[m/s]	u20
vegetation albedo	[1]		2060 m height	[m/s]	u21
vegetated fraction of surface	[1]	sigmaf	2160 m height	[m/s]	u22
potential temperature at 60 m height	[°C]	t1	2260 m height	[m/s]	u23
160 m height	[°C]	t2	2360 m height	[m/s]	u24
260 m height	[°C]	t3	2460 m height	[m/s]	u25
360 m height	[°C]	t4	2560 m height	[m/s]	u26
460 m height	[°C]	t5	2660 m height	[m/s]	u27
560 m height	[°C]	t6	2760 m height	[m/s]	u28
660 m height	[°C]	t7	2860 m height	[m/s]	u29
760 m height	[°C]	t8	2960 m height	[m/s]	u30
860 m height	[°C]	t9	wind velocity v at 60 m height	[m/s]	v1
960 m height	[°C]	t10	160 m height	[m/s]	v2
1060 m height	[°C]	t11	260 m height	[m/s]	v3
1160 m height	[°C]	t12	360 m height	[m/s]	v4
1260 m height	[°C]	t13	460 m height	[m/s]	v5
1360 m height	[°C]	t14	560 m height	[m/s]	v6
1460 m height	[°C]	t15	660 m height	[m/s]	v7
1560 m height	[°C]	t16	760 m height	[m/s]	v8
1660 m height	[°C]	t17	860 m height	[m/s]	v9
1760 m height	[°C]	t18	960 m height	[m/s]	v10
1860 m height	[°C]	t19	1060 m height	[m/s]	v11
1960 m height	[°C]	t20	1160 m height	[m/s]	v12
2060 m height	[°C]	t21	1260 m height	[m/s]	v13
2160 m height	[°C]	t22	1360 m height	[m/s]	v14
2260 m height	[°C]	t23	1460 m height	[m/s]	v15
2360 m height	[°C]	t24	1560 m height	[m/s]	v16
2460 m height	[°C]	t25	1660 m height	[m/s]	v17

variable	unit	abbrev.	variable	unit	abbrev.
1760 m height	[m/s]	v18	960 m height	[m/s]	ug10
1860 m height	[m/s]	v19	1060 m height	[m/s]	ug11
1960 m height	[m/s]	v20	1160 m height	[m/s]	ug12
2060 m height	[m/s]	v21	1260 m height	[m/s]	ug13
2160 m height	[m/s]	v22	1360 m height	[m/s]	ug14
2260 m height	[m/s]	v23	1460 m height	[m/s]	ug15
2360 m height	[m/s]	v24	1560 m height	[m/s]	ug16
2460 m height	[m/s]	v25	1660 m height	[m/s]	ug17
2560 m height	[m/s]	v26	1760 m height	[m/s]	ug18
2660 m height	[m/s]	v27	1860 m height	[m/s]	ug19
2760 m height	[m/s]	v28	1960 m height	[m/s]	ug20
2860 m height	[m/s]	v29	2060 m height	[m/s]	ug21
2960 m height	[m/s]	v30	2160 m height	[m/s]	ug22
mixing ratio q x1000 at 60 m height	[1]	mr1	2260 m height	[m/s]	ug23
160 m height	[1]	mr2	2360 m height	[m/s]	ug24
260 m height	[1]	mr3	2460 m height	[m/s]	ug25
360 m height	[1]	mr4	2560 m height	[m/s]	ug26
460 m height	[1]	mr5	2660 m height	[m/s]	ug27
560 m height	[1]	mr6	2760 m height	[m/s]	ug28
660 m height	[1]	mr7	2860 m height	[m/s]	ug29
760 m height	[1]	mr8	2960 m height	[m/s]	ug30
860 m height	[1]	mr9	wind geostrophic vg at 60 m height	[m/s]	vg1
960 m height	[1]	mr10	160 m height	[m/s]	vg2
1060 m height	[1]	mr11	260 m height	[m/s]	vg3
1160 m height	[1]	mr12	360 m height	[m/s]	vg4
1260 m height	[1]	mr13	460 m height	[m/s]	vg5
1360 m height	[1]	mr14	560 m height	[m/s]	vg6
1460 m height	[1]	mr15	660 m height	[m/s]	vg7
1560 m height	[1]	mr16	760 m height	[m/s]	vg8
1660 m height	[1]	mr17	860 m height	[m/s]	vg9
1760 m height	[1]	mr18	960 m height	[m/s]	vg10
1860 m height	[1]	mr19	1060 m height	[m/s]	vg11
1960 m height	[1]	mr20	1160 m height	[m/s]	vg12
2060 m height	[1]	mr21	1260 m height	[m/s]	vg13
2160 m height	[1]	mr22	1360 m height	[m/s]	vg14
2260 m height	[1]	mr23	1460 m height	[m/s]	vg15
2360 m height	[1]	mr24	1560 m height	[m/s]	vg16
2460 m height	[1]	mr25	1660 m height	[m/s]	vg17
2560 m height	[1]	mr26	1760 m height	[m/s]	vg18
2660 m height	[1]	mr27	1860 m height	[m/s]	vg19
2760 m height	[1]	mr28	1960 m height	[m/s]	vg20
2860 m height	[1]	mr29	2060 m height	[m/s]	vg21
2960 m height	[1]	mr30	2160 m height	[m/s]	vg22
wind geostrophic ug at 60 m height	[m/s]	ug1	2260 m height	[m/s]	vg23
160 m height	[m/s]	ug2	2360 m height	[m/s]	vg24
260 m height	[m/s]	ug3	2460 m height	[m/s]	vg25
360 m height	[m/s]	ug4	2560 m height	[m/s]	vg26
460 m height	[m/s]	ug5	2660 m height	[m/s]	vg27
560 m height	[m/s]	ug6	2760 m height	[m/s]	vg28
660 m height	[m/s]	ug7	2860 m height	[m/s]	vg29
760 m height	[m/s]	ug8	2960 m height	[m/s]	vg30
860 m height	[m/s]	ug9			

### Mixing layer height

Standard development of the mixing layer height assumed for the Tsimlyansk experiment



### 13 Appendix B

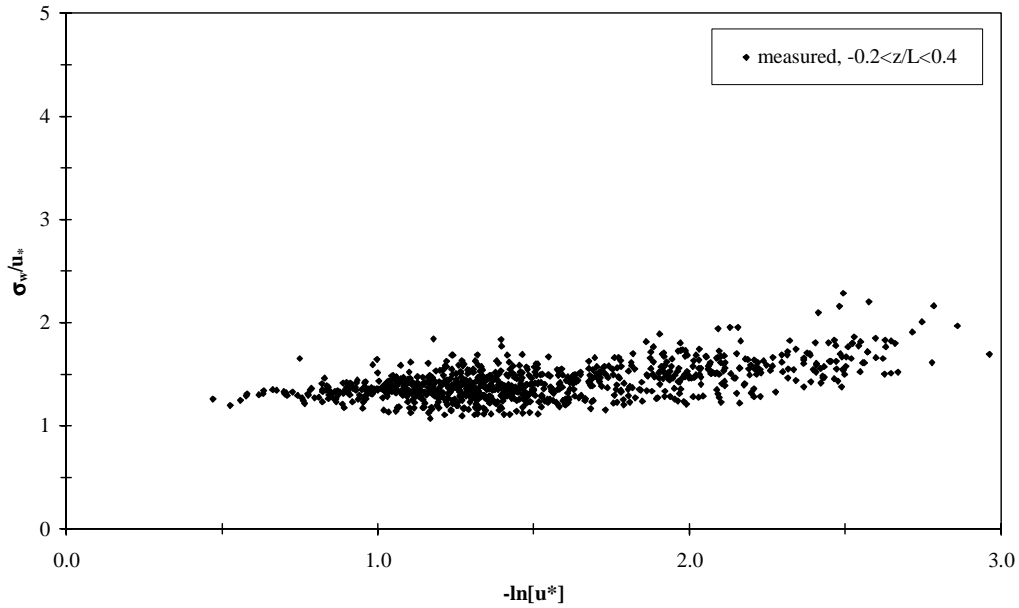


**Figure 33:** The nondimensional vertical velocity standard deviations of all experiments plotted against  $-\ln[u_*]$ . Data was selected with  $-0.2 < \zeta < 0.4$ .

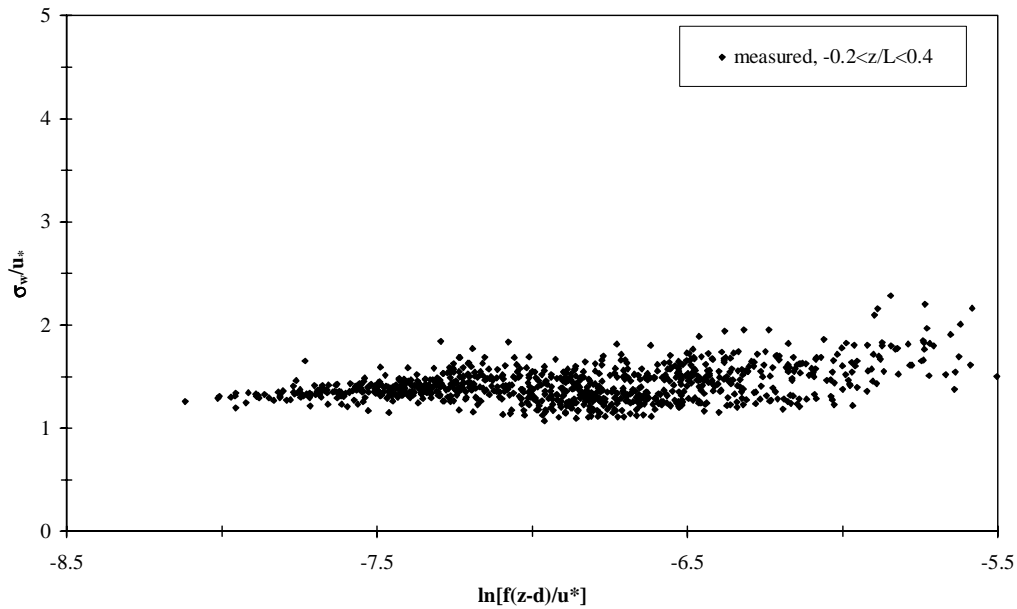


**Figure 34:** The nondimensional vertical velocity standard deviations of all experiments plotted against  $\ln[(z-d)/u_*]$ . Data was selected with  $-0.2 < \zeta < 0.4$ .

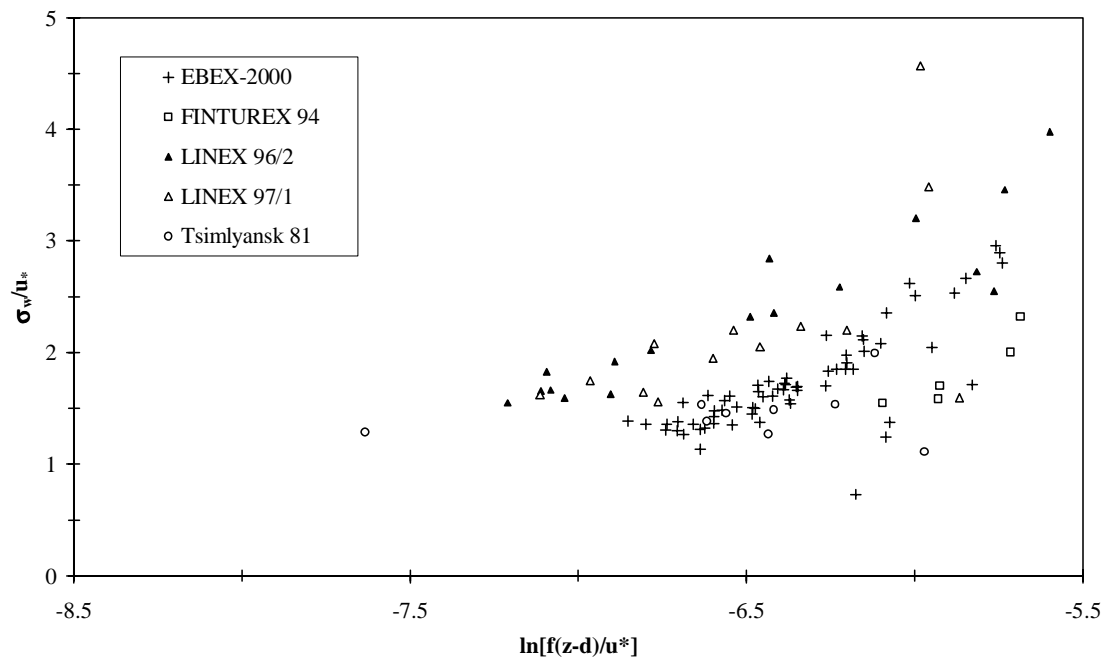


**Figure 35:** The unstable nondimensional vertical velocity standard deviation of all experiments plotted against  $\ln[f(z-d)/u_*]$ . Data was selected for  $\zeta < -0.2$ .

## 14 Appendix C

### Correlation coefficient R

Significance levels for the correlation coefficient R (Taubenheim, 1969): If  $R_{\text{calculated}} > R_{\text{significant}}$  (Table 17, Figure 36), it follows that the correlation coefficient R is significantly different from zero with the selected error of probability.

N Number of values

$n_1$  Number of independent variables (for simple correlation  $n_1 = 1$ )

$n_2$  degrees of freedom;  $n_2 = N - 1 - n_1$

b error of probability

**Table 17: Significance levels for correlation coefficients (Taubenheim, 1969).**

n	R	
	b = 0.05, n = 1	b = 0.01, n = 1
5	0.754	0.875
6	0.707	0.834
7	0.666	0.798
8	0.632	0.765
9	0.602	0.735
10	0.576	0.709
11	0.553	0.684
12	0.532	0.661
13	0.514	0.641
14	0.497	0.623
15	0.482	0.605
16	0.468	0.598
17	0.456	0.575
18	0.444	0.561
19	0.433	0.549
20	0.423	0.537
25	0.381	0.487
30	0.349	0.449
40	0.304	0.393
60	0.250	0.325
120	0.179	0.232

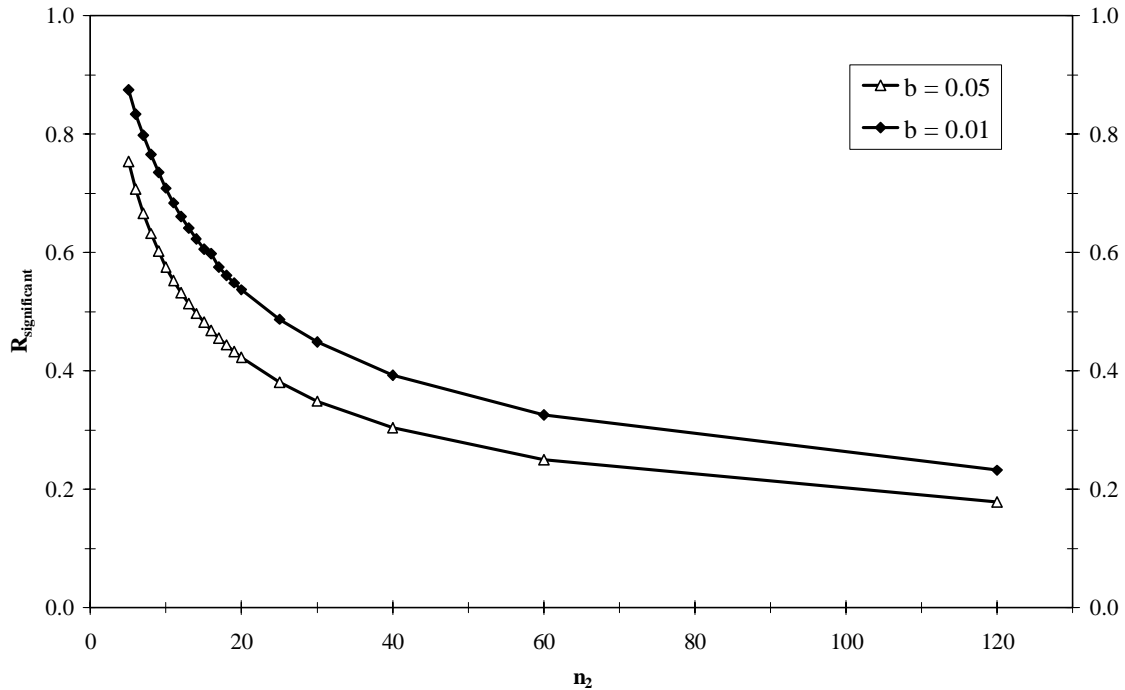


**Figure 36:** Significance levels ( $R_{\text{significant}}$ ) for correlation coefficients  $R$  (Taubenheim, 1969).

### Regression analysis

In this study, a test method for significance of the slope for linear equations was applied (Köhler et al., 1996). If a  $F$ - Test states that MQA is significantly greater than MQU, it follows that the slope of the considered linear regression equation is significantly different from zero.

$$MQA = \frac{\sum_{i=1}^N (\hat{y}_i - \bar{y})^2}{df}, \quad MQU = \frac{\sum_{i=1}^N (y_i - \hat{y}_i)^2}{df}$$

where  $\bar{y}$  = mean of the calculated values using the equation derived from the linear regression

$\hat{y}_i$  = calculated value using the equation derived from the linear regression

$y_i$  = observed/measured value

df = degrees of freedom

N = number of values

## **Acknowledgements**

First of all, I wish to thank Prof. Dr. Thomas Foken for giving invaluable support for this thesis and sharing his time in many discussions.

Wolfgang Adam (German Weather Service) provided radiosonde data from the LINEX experiments, Irene Lehner (University of Basel) shared her semester thesis providing SODAR data from the EBEX-2000 experiment.

I am very grateful to Nele Meckler for the invaluable help she provided, correcting the manuscript and donating her time. Harald Sodemann greatly improved the manuscript, Johannes Ruppert and Claudia Liebenthal provided help and important thoughts in innumerable discussions.

I wish to thank my parents for all their help and encouragement they provided, their financial support made my studies and thus this thesis possible.

Lastly, I wish to thank Gesa, my friends and my room mates for inspiration and understanding.

**Eidesstattliche Erklärung**

Hiermit versichere ich, diese Arbeit selbstständig verfasst und keine anderen als die angegebenen Hilfsmittel und Quellen verwendet zu haben.

Bayreuth, den 28.11.2001

Christoph Thomas